THESIS

MOBILE MEASUREMENTS OF OZONE, ITS PRECURSORS, AND AIR TOXICS AT THE LOCAL AND REGIONAL SCALE DURING THE COLORADO FRONT RANGE OZONE ÉXPERIMENT (FROZÉ 2025)

Submitted by

Jared Stickney

Department of Atmospheric Science

In partial fulfillment of the requirements

For the Degree of Master of Science

Colorado State University

Fort Collins, Colorado

Summer 2026

Master's Committee:

Advisor: Jeffrey L. Collett, Jr.

Emily V. Fischer
Amy P. Sullivan
Ellison M. Carter

Copyright by Jared Stickney 2026

All Rights Reserved

ABSTRACT

MOBILE MEASUREMENTS OF OZONE, ITS PRECURSORS, AND AIR TOXICS AT THE LOCAL AND REGIONAL SCALE DURING THE COLORADO FRONT RANGE OZONE ÉXPERIMENT (FROZÉ 2025)

The Colorado Denver Metro/North Front Range (DMNFR) area has been designated as nonattainment for ozone (O_3) by the Environmental Protection Agency, as this region frequently exceeds the National Ambient Air Quality Standard (NAAQS) for O_3 in the summer. Despite significant reductions in emissions of precursor nitrogen oxides (NO_x = NO + NO_2) and volatile organic compounds (VOCs) in recent years, the area continues to struggle to reach attainment. O_3 and NO_2 are criteria air pollutants, and can both cause significant health concerns. In addition to O_3 nonattainment, the region faces concerns about air toxics exposure to residents. Emissions of air toxics come from many sources, including traffic, oil and gas (O&G) development and production, utilities, manufacturing, and commercial/institutional sectors. With both O&G operations and the region's population growing, air toxics are an increasing concern for the health of residents.

This work focuses on mobile measurements of O_3, NO_2, and VOCs from the Colorado State University (CSU) Plume Tracker during the Colorado Front Range OZone Éxperiment (FROZÉ) in summer 2025. The CSU Plume Tracker completed 13 driving intensives in the Northern Front Range, continuously measuring O_3 and NO_2, and collecting whole air grab canister samples for detailed VOC speciation in 12 disproportionately impacted communities (DICs). We find that air toxics concentrations in DICs were below acute health guideline values at the time of sampling. However, toluene, ethylbenzene, xylenes, and n-hexane were significantly higher in some DICs when compared to the mean value of same-hour measurements in non-DIC communities from stationary monitors. This finding suggests that existing stationary measurements in non-DIC communities do not always reflect air toxics exposures occurring in DICs, and additional monitoring

in these communities should be prioritized. Among criteria air pollutants in DICs, we find that O_3 levels were generally lower, especially during daytime sampling, in DICs when compared to the mean of the stationary sites. Elevated NO_2 levels were also observed in 2 of 12 DICs, relative to the mean value found at stationary monitoring sites. Regional NO_2 hotspots generally aligned with combustion sources near population centers, O&G development, and heavily-trafficked highways, and were highly dependent on meteorological conditions. Finally, we examine the spatial variability in O_3 concentrations across the DMNFR O_3 NAA, finding considerable variability sometimes apparent over relatively short spatial scales. Two distinct O_3 regimes were present: regional O_3 formation, where O_3 concentrations climb steadily throughout the daytime across a broad region, and local O_3 modification, where changes in emissions and/or meteorology can lead to rapid changes in O_3 concentrations over short temporal and spatial scales.

ACKNOWLEDGMENTS

I would like to extend my thanks to all of my collaborators. Without your support, this project would not have been possible.

Funding for FROZÉ 2025, a collaboration between Colorado State University (CSU), the University of Montana, the Colorado Department of Public Health and Environment (CDPHE), and the Regional Air Quality Council, was provided by the Colorado Air Quality Enterprise. The co-PIs of FROZÉ, Emily Fischer, Jeff Collett, and Lu Hu, were instrumental in making the field campaign happen with their valuable expertise and insight. Thank you to CDPHE for teaching us students how to forecast high ozone events in the Front Range, as well as providing input during our daily forecast briefings. Daniela Guevara Proaño, Brandon McGuire, Andrey Marsavin, and Emily Fischer led weather briefings to help make crucial decisions about whether to conduct driving intensives and assisted with drive paths.

Amy Sullivan and Andrey Marsavin helped immensely with setting up the Plume Tracker, from getting instruments running, troubleshooting errors, and assisting with calibrations. Amy's perseverance in getting instruments to work was beyond helpful and inspiring. Lena Low introduced me to the Plume Tracker, assisted with instrument malfunctions, and provided input for data visualization. Special thanks to Andrey, who was present for all of the Plume Tracker driving intensives, has an extensive mechanical aptitude, and was excellent company. I-Ting Ku and Jihee Ban cleaned and prepared all of the whole air grab canisters. I-Ting, Jihee, and Yong Zhou analyzed the VOC grab canisters in gas chromatography systems. Thank you to all three of you for your hard work and patience in teaching me about the GC! I would also like to thank Hannah Grace Marti and Jihee for assisting with the HYSPLIT back trajectories. The City of Broomfield, The City of Longmont, and Boulder Air provided long term VOC data that were used to compare our mobile air toxics measurements to.

Finally, I want to express my deepest gratitude to my advisor, Jeff Collett, for your support, guidance, and mentorship during my time at CSU; to Emily Fischer, Amy Sullivan, and Ellison

Carter for serving on my committee and providing invaluable feedback; to the students of the Collett and Fischer groups for your camaraderie; to my friends at CSU and beyond; and last, but certainly not least, to my amazing partner, Garrett, and my family for all of your love, support, and advice as I navigated living so far from home.

TABLE OF CONTENTS

ABSTRACT ii
ACKNOWLEDGMENTS iv
LIST OF TABLES vii
LIST OF FIGURES viii

1. INTRODUCTION 1

2. METHODS 13
2.1. FROZÉ Field Campaign Overview 13
2.2. CSU Plume Tracker Instruments & Setup Methodology 17
2.2.1. Canister Collection & VOC Speciation Procedure 22
2.3. Instrument Calibrations 23
2.4. Field Deployment Planning & Measurement Strategy 27
2.4.1. Driving Intensives 27
2.4.2. Disproportionately Impacted Communities (DICs) 28
2.5. TEMPO NO_2 Data 32
2.6. HYSPLIT Backward Trajectories 33
2.7. Data Filtering 33
2.7.1. NO_2 Filtering Method 33
2.7.2. O_3 Filtering Method 35
2.8. Statistical Comparison of DICs to Stationary Sites 37

3. RESULTS AND DISCUSSION 39
3.1. DIC Air Quality and Local VOC Plumes 39
3.1.1. Air Toxics & Criteria Air Pollutant Monitoring in DICs 39
3.1.2. Case Studies of Notable Local Plumes 50
3.2. Regional Scale Mobile Measurements 58
3.2.1. Mobile NO_2 Measurements in the Colorado Front Range 58
3.2.2. Mobile O_3 Measurements in the Colorado Front Range 64

4. CONCLUSION 96
4.1. Future Work 98

References 100

APPENDIX 112
A.1. GC VOC Method Detection Limits 112
A.2. POM and EPA O_3 Regulatory Monitor Agreement 114
A.3. Filtered & Unfiltered NO_2 Data for DIC Comparison 116

LIST OF TABLES

Table 2.1: Instrument specifications for the Plume Tracker payload for FROZÉ. 17

Table 3.1: Information on DICs sampled by the Plume Tracker during FROZÉ, as well as legal criteria met for each community, according to Colorado Revised Statute § 24-4-109. 41

Table A.1: Table of the method detection limits (MDLs) for all 51 VOCs analyzed in the GC from October 2024. MDLs represent the mixing ratio required for a peak with a signal-to-noise ratio of 3 from replicate whole air standard analyses, where noise is defined as the standard deviation of the chromatograph baseline adjacent to the peak (Low, 2025). 112

LIST OF FIGURES

Figure 1.1: Spatial extent of the Denver Metro/Northern Front Range O_3 nonattainment area. 2
Figure 1.2: Total NO_x emissions by year in Colorado from 1990-2024. 4
Figure 1.3: Annual anthropogenic (top) and total (bottom) VOC emissions by year in Colorado from 1990-2024. 5
Figure 1.4: Historical record of 8-hour O_3 design values in ppbv for all monitoring sites in Colorado compared to the annual 8-hr NAAQS of 70 ppbv. 6
Figure 1.5: Map of the locations of oil and gas wells in Colorado. 7
Figure 1.6: Time series of the number of producing gas wells (shown in blue) and population growth (shown in orange) per year in Colorado from 1989-2020. 8
Figure 1.7: A pie chart of the contributions of stationary sources from different sectors to the total Colorado air toxics emissions budget for 2024. 11

Figure 2.1: Overview of FROZÉ stationary sites, mobile measurement locations, and canister deployment locations. 14
Figure 2.2: Map of Tahoe driving intensives and both DIC non-DIC air canister deployment locations. 16
Figure 2.3: Photo of the locations of the LI-7810 and Teledyne CAPS instruments in the Plume Tracker. 20
Figure 2.4: Photo of the location of the POM in the Plume Tracker. The device pictured hanging off of the POM is an O_3 scrubber used for zero air tests. 21
Figure 2.5: Photo of the CSU Chevy Tahoe/Plume Tracker. The Airmar can be seen on the roof of the vehicle above the driver's seat and front passenger seat. 21
Figure 2.6: Plot of the instrument concentrations (divided by the maximum value) during a zero air test on the August 14th, 2025 driving intensive. 25
Figure 2.7: 6-panel plot of post-campaign calibration curves for the Plume Tracker instruments. 26
Figure 2.8: Legal criteria that define what a disproportionately impacted community (DIC) is in Colorado. 29
Figure 2.9: Flow chart of the components that go into the calculation of CDPHE's CO Enviroscreen 2.0 percentage for a census block. 30
Figure 2.10: Example drive path from Montbello DIC sampling period. 31
Figure 2.11: Spatial coverage difference between TEMPO NO_2 nominal hourly operations (left) and special operations (right) during FROZÉ. 32
Figure 2.12: Time series plots of raw NO_2 data and filtered NO_2 data using the plume-by-plume and SIBaR methods. 35
Figure 2.13: Time series plots of raw O_3 data and filtered O_3 data using the NO_2 plume-by-plume method plume flags, the O_3 plume-by-plume plume flags, and the SIBaR method plume flags. 36

Figure 3.1: Plot of DICs sampled by the Plume Tracker during FROZÉ and their associated CDPHE Enviroscreen 2.0 percentages. 40
Figure 3.2: Locations of stationary online VOC measurement sites relative to the locations of canisters deployed by the Plume Tracker in DICs. 43
Figure 3.3: Box and whisker plots showing the distribution of hourly VOC stationary measurements at the same date and hour that a mobile canister was collected in a particular DIC (represented by a star). 44
Figure 3.4: Map of O_3 stationary sites (a) and NO_2 stationary sites (b), as well as DIC canister deployment locations. 49
Figure 3.5: Box and whisker plots of hourly stationary site concentrations for O_3 (top) and NO_2 (bottom) compared to the mean concentration of these compounds in DICs measured by the Plume Tracker. 50
Figure 3.6: Map of ethane concentrations from the Longmont DIC plume on August 15, 2025. 52
Figure 3.7: Box and whisker plots of averaged concentrations over the study period (June 1-August 31, 2025) for 51 VOCs from several sites in Broomfield, CO. 53
Figure 3.8: Map of NO_2 concentrations before, during, and after sampling a Fort Lupton DIC on July 31, 2025. 55
Figure 3.9: Map of ethane concentrations from a gas leak on County Road 31, northwest of Greeley, CO on August 1, 2025. 57
Figure 3.10: Map of filtered NO_2 concentrations measured by the Plume Tracker during daytime driving intensives. 59
Figure 3.11: Map of filtered NO_2 concentrations measured by the Plume Tracker during nighttime driving intensives. 60
Figure 3.12: Plots of 1-min rolling-averaged, filtered mobile NO_2 data, as well as TEMPO and stationary site NO_2 data that have been averaged for the duration of each driving intensive. 62
Figure 3.13: Plots of 1-min rolling-averaged, filtered mobile NO_2 data, as well as TEMPO and stationary site NO_2 data that have been averaged for the duration of the Friday, July 25, and Sunday, July 27 driving intensives, respectively. 64
Figure 3.14: Plots of filtered, 10-min rolling-averaged mobile O_3 data for regional O_3 formation (top) and local O_3 modification (bottom) driving intensives during a defined peak photochemical period from 11:00-15:00 MDT. . . 66
Figure 3.15: Maps of the drive paths for regional O_3 formation, or ROF (left), and local O_3 modification, or LOM (right) cases colored by time of day. 67
Figure 3.16: Time series of Plume Tracker/CSU Tahoe O_3, Fort Collins-West (FTCW) O_3, Soapstone Natural Prairie O_3, stationary UM Van O_3 measurements in Bethke, FTCW solar radiation measurements, and CSU Tahoe NO_2 measurements. 69
Figure 3.17: Visible GOES imagery from various times on July 14, 2025 overlaid with the CSU Tahoe O_3 concentrations. 70
Figure 3.18: HYSPLIT back trajectories on July 14, 2025 initiated for 6 hours back in time every 30 minutes of the CSU Tahoe driving intensive overlaid with CSU Tahoe O_3 levels. 71

Figure 3.19: Time series of Plume Tracker/CSU Tahoe O_3 and NO_2 measurements on July 25, 2025. 73
Figure 3.20: Visible GOES imagery from various times on July 25, 2025 overlaid with the CSU Tahoe O_3 concentrations. 74
Figure 3.21: HYSPLIT back trajectories on July 25, 2025 initiated for 6 hours back in time every 30 minutes of the CSU Tahoe driving intensive overlaid with CSU Tahoe O_3 levels. 75
Figure 3.22: TEMPO NO_2 data scans at various times on July 25, 2025 overlaid with semi-transparent mobile O_3 concentrations and hourly NO_2 stationary site measurements. 76
Figure 3.23: Top: Filtered mobile O_3 annotated with times of interest. Bottom: Filtered mobile O_3 and NO_2 concentrations from the July 27, 2025 driving intensive with a 10-min rolling average applied and the NO_2 data have a 1-min rolling average. 79
Figure 3.24: Visible GOES imagery from various times on July 27, 2025 overlaid with the CSU Tahoe O_3 concentrations. 80
Figure 3.25: HYSPLIT back trajectories on July 27, 2025 initiated for 6 hours back in time every 30 minutes of the CSU Tahoe driving intensive overlaid with CSU Tahoe O_3 levels. 81
Figure 3.26: TEMPO NO_2 data scans at various times on July 27, 2025 overlaid with semi-transparent mobile O_3 concentrations and hourly NO_2 stationary site measurements. 82
Figure 3.27: Filtered mobile O_3 concentrations from the August 4, 2025 driving intensive with a 10-min rolling average applied. 84
Figure 3.28: Time series of mobile O_3 and stationary O_3 measurements on August 4, 2025 from: Weld County Tower (WCT), La Salle Tower (LST), and Timnath - Bethke Elementary (TIM). Also shown are mobile NO_2, ethane (C_2H_6), and methane (CH_4) measurements. 85
Figure 3.29: Visible GOES imagery from various times on August 4, 2025 overlaid with the CSU Tahoe O_3 concentrations. 86
Figure 3.30: HYSPLIT back trajectories on August 4, 2025 initiated for 6 hours back in time every 30 minutes of the CSU Tahoe driving intensive overlaid with CSU Tahoe O_3 levels. 87
Figure 3.31: Hourly $PM_{2.5}$ data from the Timnath - Bethke Elementary (TIM) stationary site on August 4, 2025. 88
Figure 3.32: Filtered mobile O_3 concentrations from the August 19, 2025 driving intensive with a 10-min rolling average applied. 90
Figure 3.33: Time series of Plume Tracker O_3, stationary O_3 measurements on August 19, 2025 from the Fort Collins-West (FTCW) site, Plume Tracker NO_2 measurements, and stationary NO_2 measurements from the FCTW, Bethke Elementary (TIM), and Fossil Creek (FOS) sites. 91
Figure 3.34: Visible GOES imagery from various times on August 19, 2025 overlaid with the CSU Tahoe O_3 concentrations. 92
Figure 3.35: HYSPLIT back trajectories on August 19, 2025 initiated for 6 hours back in time every 30 minutes of the CSU Tahoe driving intensive overlaid with CSU Tahoe O_3 levels. 93

Figure 3.36: TEMPO NO_2 data scans at various times on August 19, 2025 overlaid with semi-transparent mobile O_3 concentrations and hourly NO_2 stationary site measurements. 94

Figure A.1: Left: Time series from April 3 - May 7, 2025 of O_3 concentrations from the POM instrument (orange) and EPA O_3 Regulatory Monitor (blue), also referred to as Federal Reference Method (FRM). Right: Comparison of POM and FRM O_3 concentrations during the time of collocation. 115

Figure A.2: Comparison of the mean of filtered (top) vs unfiltered (bottom) NO_2 data in DICs compared to the mean concentration of stationary measurements taken at the same hour. 116

1. INTRODUCTION

The Colorado Front Range faces multiple complex air quality challenges. Of particular concern is the Denver Metro/Northern Front Range ozone (O_3) nonattainment area's (DMNFR O_3 NAA) designation as "Severe" for the 2008 National Ambient Air Quality Standard (NAAQS) of 75 ppbv and "Serious" for the 2015 70 ppbv standard. The DMNFR O_3 NAA, shown in Figure 1.1, extends from the southern Denver Metro area northward up through Weld County and much of Larimer County. Tropospheric O_3 is harmful to human health and has been associated with increased risk of respiratory and cardiovascular mortality (Kim et al., 2020; Lippmann, 1989). In fact, exposure to elevated concentrations of O_3 has been linked to 423,100 deaths annually (Donzelli and Suarez-Varela, 2024). Tropospheric O_3 formation is difficult to mitigate due to its nature as a secondary pollutant, meaning that it is not directly emitted by sources, but instead forms from photochemical reaction of a number of precursor species (Crutzen, 1988). Adding to this challenge is its nonlinear response to precursor emissions. When one group of O_3 precursors, either nitrogen oxides ($NO_x = NO + NO_2$) or volatile organic compounds (VOCs), is present in high concentrations with respect to the other, this can drastically affect O_3 production and which mitigation strategies are effective (Wang et al., 2024; Zhao et al., 2022). Consequently, controlling O_3 levels is a complex challenge that requires knowledge of the emission trends and the spatiotemporal variability of NO_x and VOCs in a particular region.

In Colorado, significant progress has been made to reduce NO_x emissions from the early 2000s to the present, as shown in Figure 1.2. This reflects increasingly fuel-efficient and lower emitting vehicles, including the implementation of catalytic converters (Muzio and Quartucy, 1997) for gas-powered cars and exhaust gas recirculation (EGR) and selective catalytic reduction (SCR) for diesel vehicles. While VOC emissions in Colorado have also been reduced since 2012, the decreases have not been as large, as shown in Figure 1.3. It is important to note, however, that these emission inventories have been known to underrepresent oil and gas (O&G) emissions, so they should be interpreted with caution (Cheadle et al., 2017b). Despite these combined emission reductions,

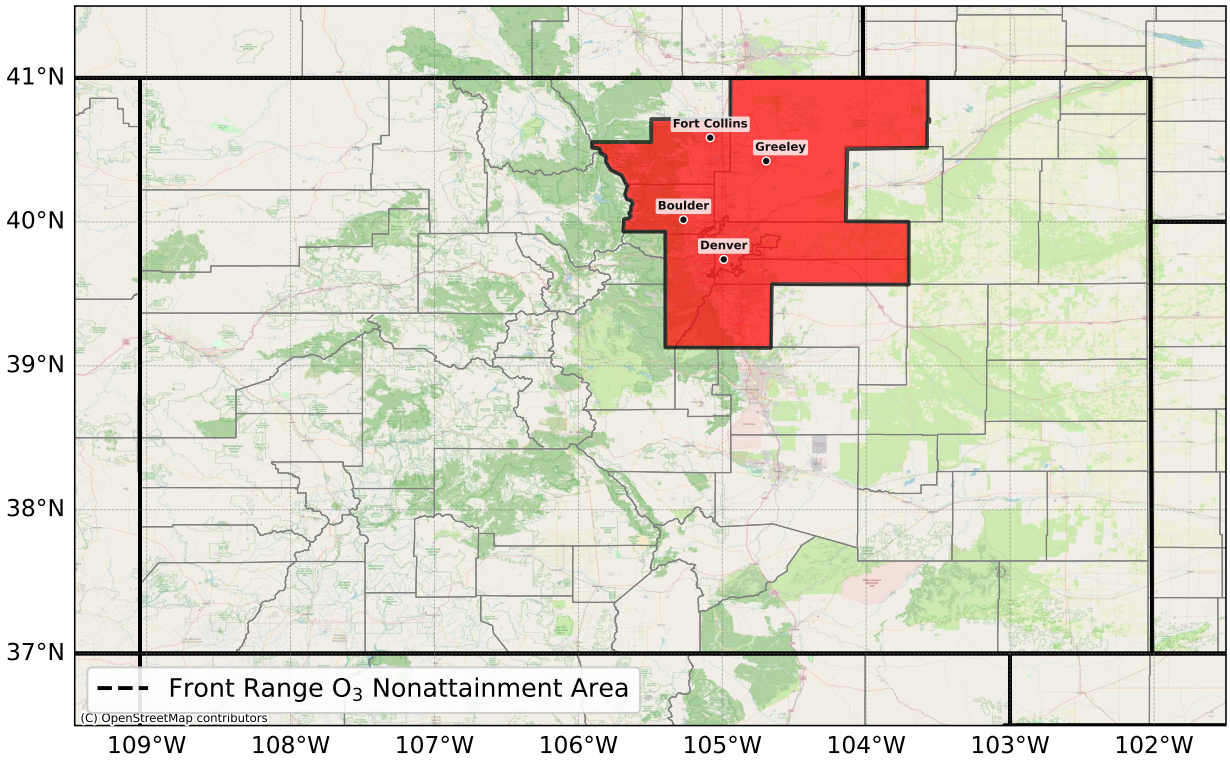


Figure 1.1: Spatial extent of the Denver Metro/Northern Front Range O_3 nonattainment area.

O_3 levels have not decreased proportionately (Figure 1.4). Anthropogenic VOC emissions show a slight decrease in the last decade, assuming emission inventories are correct, with large interannual variability owing to the influence of wildfires. This influence is expected to grow, as wildfires are becoming increasingly common and destructive due to climate change (Di Virgilio et al., 2019; Xu et al., 2020). Beyond detrimental environmental and human health impacts, wildfire smoke has also been shown to enhance O_3 concentrations in the DMNFR O_3 NAA (Lindaas et al., 2017; Pollack et al., 2021b). Another important VOC emission source in this region is O&G production, which is mostly concentrated in the Denver-Julesburg Basin (Pétron et al., 2012). As seen in Figure 1.5, O&G wells are abundant in the DMNFR O_3 NAA, mostly concentrated in the southwestern portion of Weld County. O&G operations in Colorado have surged in the past two decades, as shown in Figure 1.6. From 2017-2020, however, the number of producing O&G wells in the state decreased. This is important because O&G emissions have been found to contribute to O_3 formation (Cheadle et al., 2017b; Evans and Helmig, 2017; Helmig, 2020; McDuffie et al., 2016; Benedict et al., 2019).

Significant progress has been made in studying O_3 formation in the DMNFR O_3 NAA as part of the Front Range Air Pollution and Photochemistry Éxperiment (FRAPPÉ) field campaign in 2014 (Flocke et al., 2020). One major finding of FRAPPÉ was that background O_3 levels in the DMNFR O_3 NAA on a typical summer day are 45-55 ppbv and originate from sources from outside the region and/or residual O_3 from the previous day (Oltmans et al., 2019). The relatively high background levels of O_3 in the region leave less room for local O_3 production before exceeding the 70 ppbv NAAQS, which adds to the challenge of mitigating exceedance events. FRAPPÉ also made important strides in quantifying the impact of O&G emissions on local O_3 production in the DMNFR O_3 NAA, finding that they can contribute to up to 20% of observed O_3 levels (McDuffie et al., 2016). O&G VOC emissions were also found to be a factor of two higher than Colorado state VOC inventories indicated, leading to a historical underrepresentation of these emissions in policy decisions (Cheadle et al., 2017b). The Colorado Front Range also has unique meteorology that affects O_3 production. A thermally-driven circulation develops due to differential heating between the Rockies and High Plains, and FRAPPÉ confirmed with lidar measurements that this circulation is associated with high O_3 events (Sullivan et al., 2016). The easterly upslope flow that results from this circulation causes different air masses rich in O_3 precursors to interact and photochemically react, which leads to increases in O_3 concentrations, often peaking in or near the foothills west of the major urban corridor. While these studies have revealed much about O_3 formation in the DMNFR O_3 NAA, most of these measurements are from over a decade ago and O_3 levels have still not decreased substantially in the face of further emission reductions. Increasing temperatures and wildfire emissions over the past decade have likely impeded progress toward reducing O_3 to protect health.

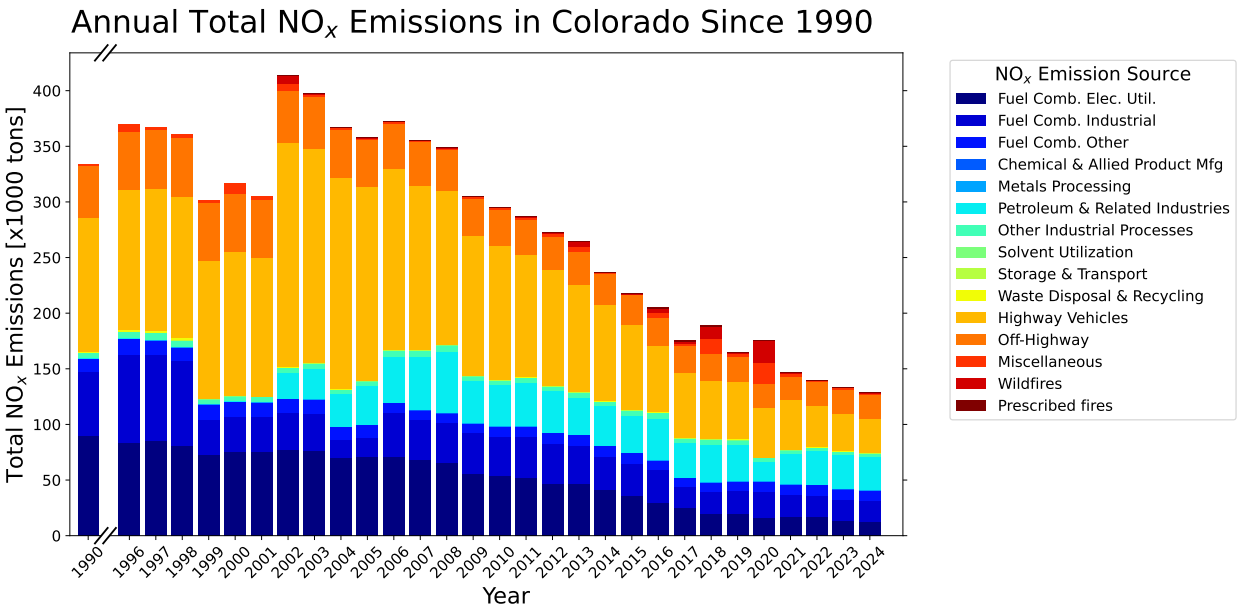


Figure 1.2: Total NO_x emissions by year in Colorado from 1990-2024. The emissions for each year are split into emission source categories, as shown in the legend on the right. There are missing data from 1991-1995, as shown by the break in the x-axis. Data is from EPA EQUATES (Foley et al., 2023).

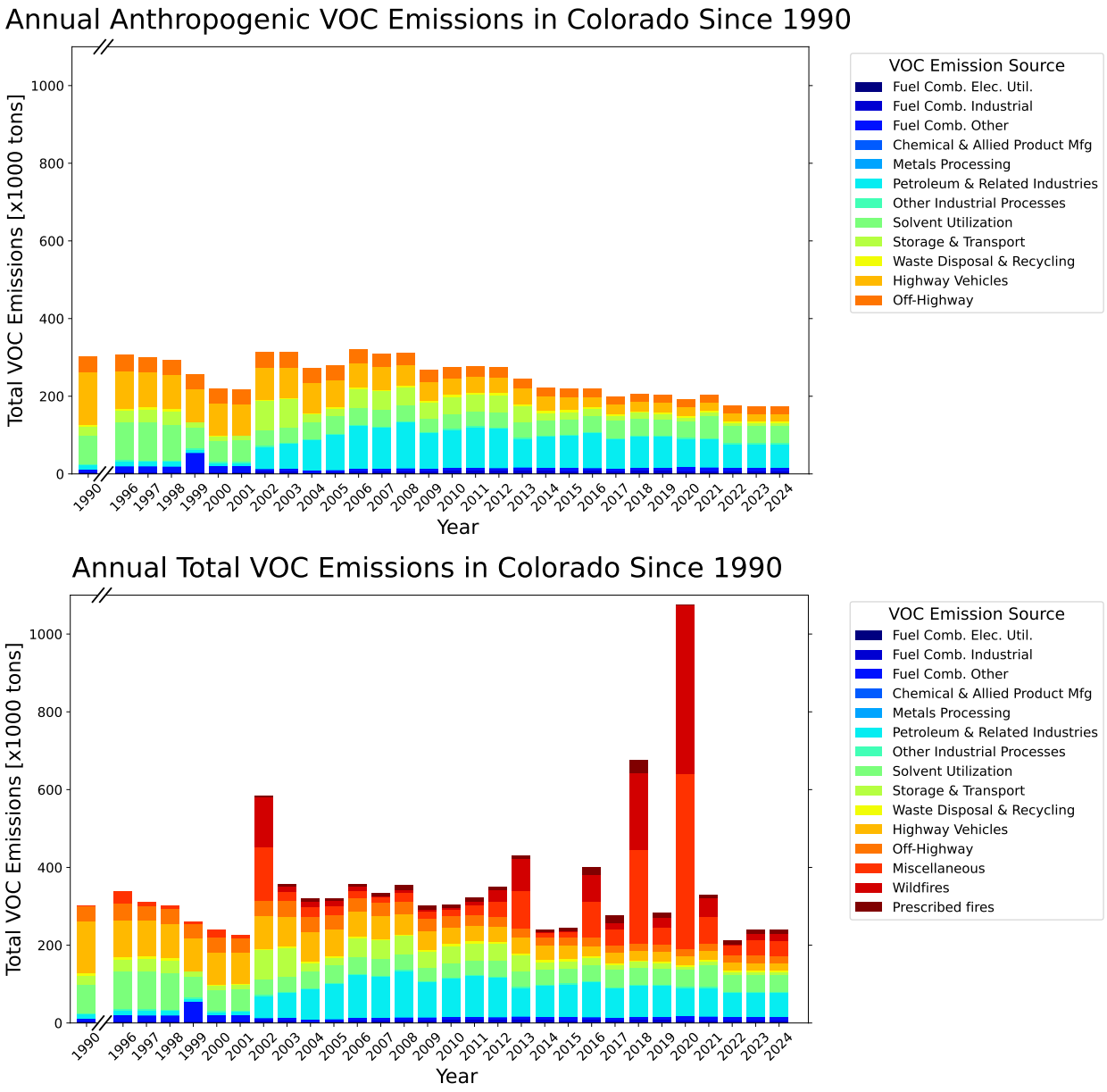


Figure 1.3: Annual anthropogenic (top) and total (bottom) VOC emissions by year in Colorado from 1990-2024. The emissions for each year are split into emission source categories, as shown in the legend on the right. There are missing data from 1991-1995, as shown by the break in the x-axis. Data is from EPA EQUATES (Foley et al., 2023)

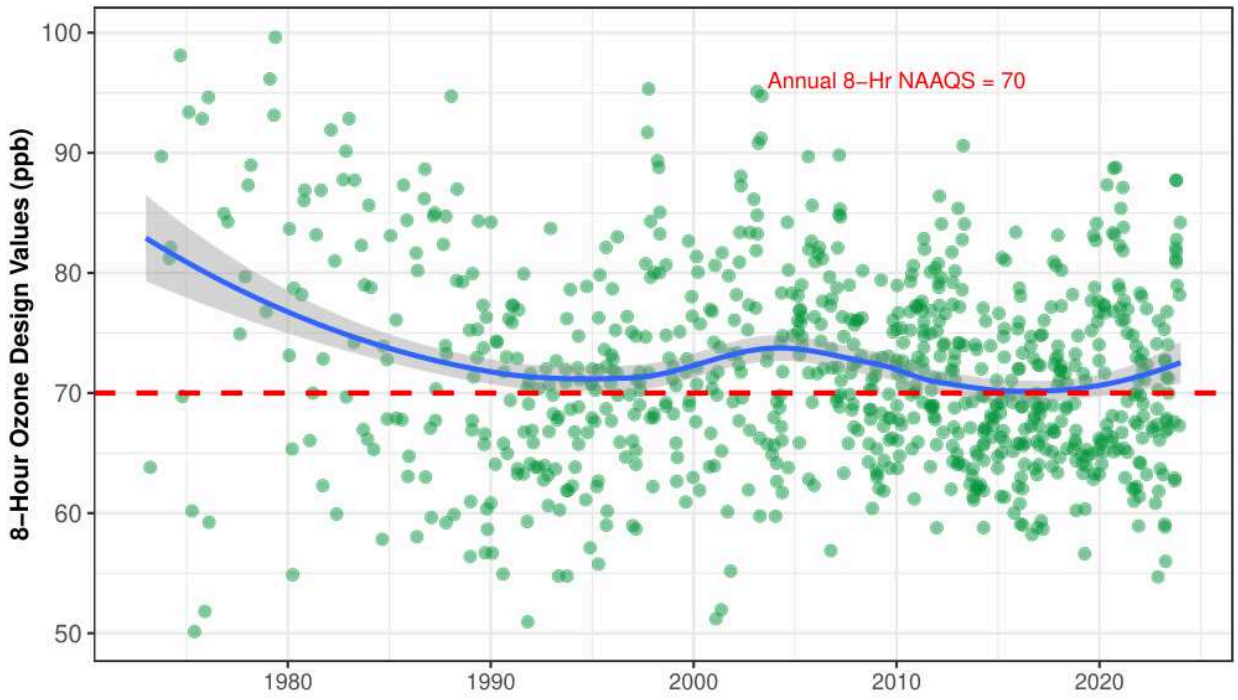


Figure 1.4: Historical record of 8-hour O_3 design values in ppbv for all monitoring sites in Colorado compared to the annual 8-hr NAAQS of 70 ppbv. The mean trend was calculated using a generalized additive model, as shown in the blue line. Figure is from the Colorado Department of Public Health and Environment's 2024 Air Quality Data Report (https://cdphe.colorado.gov/public-information/air-monitoring-data-and-technical-reports).

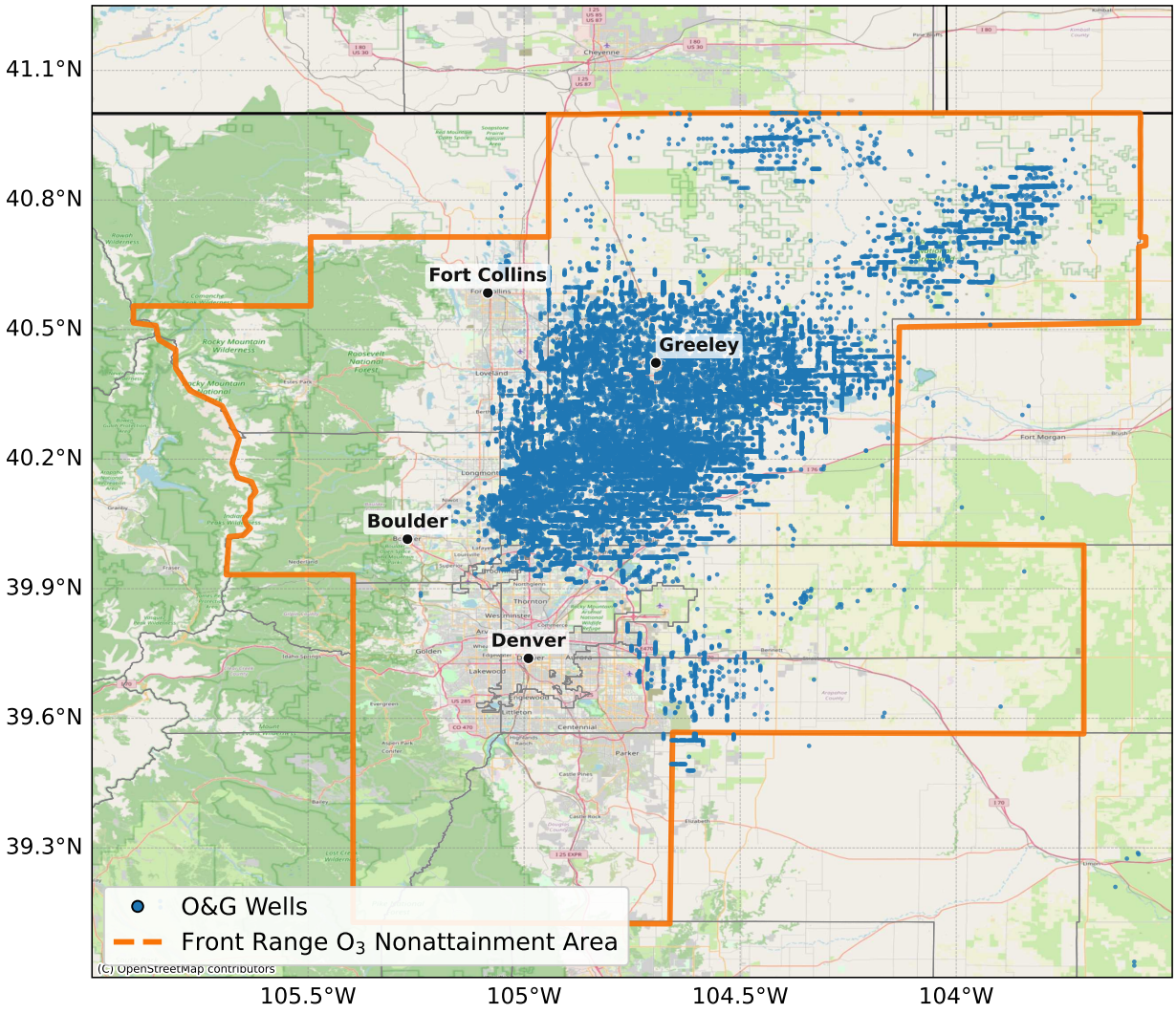


Figure 1.5: Map of the locations of oil and gas wells in Colorado, as shown by the blue dots. The Denver Metro/Northern Front Range O_3 nonattainment area is shown outlined in orange. Well data obtained from the Colorado Department of Natural Resources – Oil & Gas Conservation Commission (https://data.colorado.gov/Environment/Oil-and-Gas-Directional-Well-Actual-and-Planned-Bo/qqfg-3qtd/about_data).

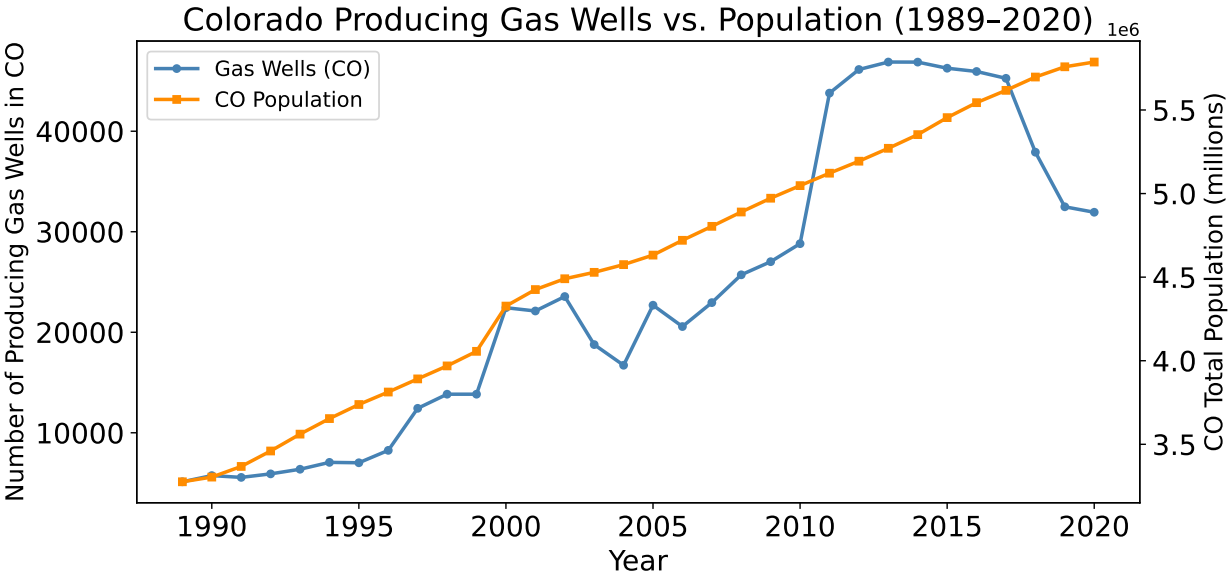


Figure 1.6: Time series of the number of producing gas wells (shown in blue) and population growth (shown in orange) per year in Colorado from 1989-2020. Producing gas well data is from the U.S. Energy Information Administration (https://www.eia.gov/dnav/ng/ng_prod_wells_s1_a.htm). Population data is from the U.S. Census Bureau (https://fred.stlouisfed.org/series/COPOP).

Given the spatial variability in O_3 precursor emissions in the DMNFR O_3 NAA, utilizing mobile measurements methods is a useful method to assess how NO_x, VOCs, and O_3 may vary intraregionally. Mobile measurements of O_3 and NO_x in particular have been shown to agree well with nearby stationary measurements with a bias <10% and can effectively measure local hotspots in gradients as small as 100m (Solomon et al., 2020; Yang et al., 2018). A well-documented finding of mobile O_3 and NO_x measurements is the suppression of O_3 near highways and tunnels due to titration from NO reacting with O_3 to form NO_2 (Oltmans et al., 2019; Yang et al., 2018). Additionally, mobile measurements of NO_2 have shown an enhancement of 210-265% near highways when compared to nearby urban stationary monitors (Levy et al., 2014). This is an important finding, since NO_2 is another one of the defined criteria air pollutants by the EPA and is federally regulated. Many disadvantaged communities are near highways, and if stationary measurements do not accurately represent local NO_2 exposure in these communities, we may not be aware of potential health impacts (Katz, 2015). Exposure to excessive levels of NO_2 has been associated with a 20% increase in

respiratory problems and asthma in the general population of children (Nitschke, 1999). NO_2, therefore, is an important compound that acts both as a respiratory irritant and O_3 precursor. However, as discussed above, NO_x emissions have been decreasing significantly in recent decades. Nevertheless, NO_2 can still contribute greatly to O_3 production, and its health effects close to sources remain underresearched.

In the Colorado Front Range, there have been a few studies leveraging mobile measurements of NO_x, VOCs, and O_3, but these types of observations are rather limited (Cheadle et al., 2017a; McDuffie et al., 2016; Wild et al., 2017). Cheadle et al. (2017a) found that there were variations in O_3 between stationary monitor locations, often finding the highest O_3 levels near O&G operations, corresponding with elevated ethane concentrations. McDuffie et al. (2016) identified significant contributions of O&G to regional O_3 levels in Erie, CO. Wild et al. (2017) focused on titration of O_3 by NO_x in the Denver urban corridor. Only Cheadle et al. (2017a) took measurements in the Northern Front Range. Clearly, significant gaps remain in these limited observations, and there is need for more mobile measurements to assess the spatiotemporal variability of O_3 and its precursors in the DMNFR O_3 NAA.

In addition to O_3 nonattainment and O_3 precursor emissions, the Colorado Front Range is also gaining attention for air toxics exposure in residential communities. Air toxics are classified as hazardous air pollutants (HAPs) by the EPA. Individual HAPs may cause cancer and/or exert adverse cardiological, respiratory, and neurological health effects (Gilman et al., 2013). Some specific compounds of concern are benzene, toluene, ethylbenzene, and xylenes (BTEX), as well as n-hexane, which have sources from O&G, urban, and traffic emissions (Ku et al., 2024; Pollack et al., 2021a). According to the Colorado Department of Public Health and Environment (CDPHE), O&G operations are the largest source fraction of air toxics emissions in Colorado at 60%, followed by utilities at 20% (electricity generation and transmission, gas transmission pipelines, water and wastewater plants, waste management), manufacturing at 16.6% (non-metallic minerals such as cement and glass, as well as the production of ethanol, pharmaceuticals, food, and metal products), and commercial/institutional at 2.6% (gas stations, fuel wholesalers, automotive repair shops), as shown in Figure 1.7. In the Colorado Front Range, the cancer risk associated with benzene exposure

for communities living within 152 m of an O&G facility has been found to exceed the EPA's upper threshold (McKenzie et al., 2018). As shown in Figure 1.6, both the population and O&G activity in the Colorado Front Range have been growing, increasing the risk of air toxics exposure to more people. This is important because communities that are the most environmentally-burdened by these issues are disproportionately impacted communities (DICs) due to placement of large pollution sources near low-income neighborhoods and excessive political influence of emitters (Currit, 2022; Tessum et al., 2019). This is especially true for Colorado, leading to geographic disparities in mortality risk at the county level, as evidenced by higher CO Enviroscreen 2.0 scores, which take into account 35 factors (Pusker et al., 2024). As such, not all counties are subject to the same amount of emissions of air toxics. Weld County represents 80% of the total crude oil production in the state, and is exposed to 45% of the state total of air toxics emissions (U.S. Energy Information Administration, 2025; CDPHE Toxic Air Contaminants Gap Report, 2024). Further, Colorado has one of the highest differences between the minority share of health risk from industrial air toxics and the minority share of the population (Ash et al., 2009). Increased risks in specific areas of the state require continuous monitoring to ensure the safety of residents. Colorado has made progress in addressing some of these concerns with the recent creation of a state air toxics program, increasing source-specific monitoring and public outreach efforts. However, there are still a number of challenges to address regarding data limitations, regulatory compliance efforts, meaningful community involvement, and socioeconomic disparities (Dummer et al., 2025).

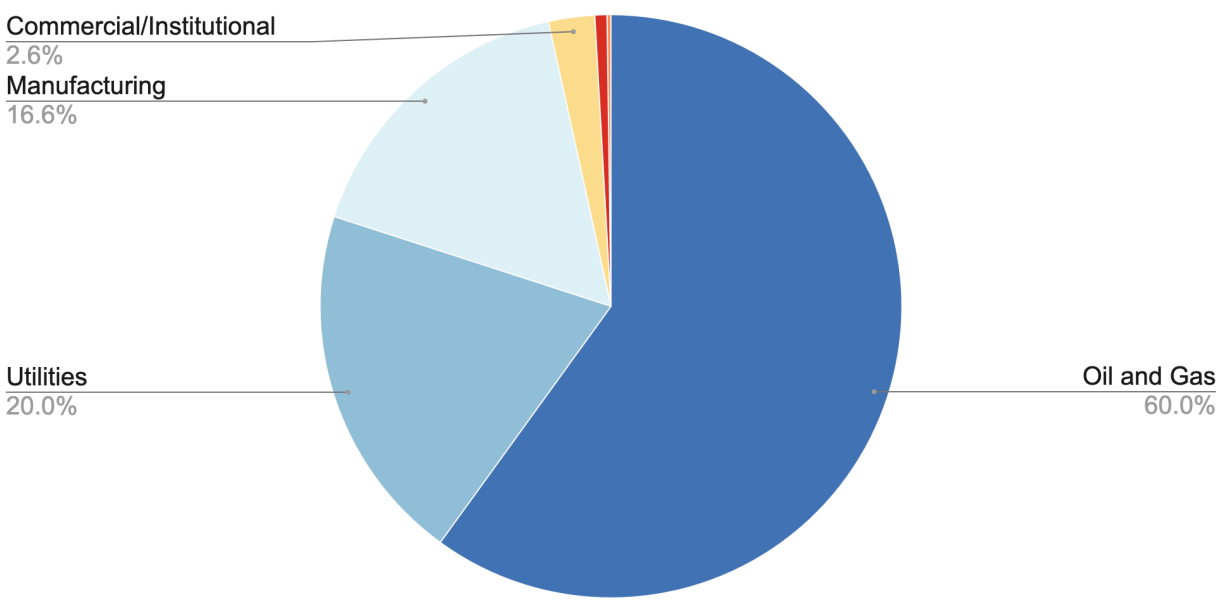


Figure 1.7: A pie chart of the contributions of stationary sources from different sectors to the total Colorado air toxics emissions budget for 2024. Figure is from CDPHE's stationary Air Pollutant Emissions Notice (APEN) website (https://cdphe.colorado.gov/air-toxics/reporting/data). Sectors were assigned based on the North American Industry Classification System (NAICS) code.

There have been several previous studies examining air toxics exposure to residents in the Colorado Front Range (Dummer et al., 2025; Gilman et al., 2013; Hecobian et al., 2019; Helmig, 2020; Low et al., 2026; Macey et al., 2014; Malin et al., 2025; McKenzie et al., 2018; Morgan et al., 2015; Pollack et al., 2021a; Pusker et al., 2024; Weisner et al., 2025). However, only a portion of these studies have focused on DICs specifically, and even less have focused on communities in the Northern Front Range. Most of the existing literature focuses on air toxics from O&G emissions on shorter timescales or one DIC for an extended period of time. Macey et al. (2014) utilized grab and passive air sampling methods to evaluate the concentrations of 75 VOCs in the Northern Front Range, finding that health risks associated with O&G emissions increase with decreasing distance from an O&G facility. Weisner et al. (2025) found that communities in close proximity to O&G well pads were still exposed to acute health risks despite the implementation of practices to reduce emissions. They also found increased risk of cancer, as well as respiratory, neurological, and hematological effects for residents living near O&G well pads from VOCs, including BTEX

(Weisner et al., 2025). Low et al. (2026) presented analysis of whole air canister samples collected at eight locations across the Northern Front Range from 2015-2016 and 2022-2025, finding a strong eastward gradient in light alkanes associated with O&G emissions, as well as strong seasonal trends. However, there is a lack of observations of air toxics exposure in DICs in the Northern Front Range, and a clear bias towards sampling in larger cities, like Denver and Boulder.

In this study, we perform mobile sampling as a part of the Front Range Ozone Éxperiment (FROZÉ) in 12 DICs in the Northern Front Range, measuring criteria air pollutants NO_2 and O_3. We also collect whole air grab canister samples in every DIC to assess the presence of air toxics. Sampling was done during the day and night to account for potential diurnal variability in emissions and weather conditions. Sampling was performed during summer only, so exploring seasonal variation was not possible. These canisters were analyzed in our lab for 51 VOCs. The canister results are then compared to hourly stationary site measurements to assess whether the stationary monitoring sites are representative of the concentration of criteria air pollutants and air toxics we observe in DICs. A particular emphasis was placed on performing observations in communities with no prior monitoring in understudied areas in the Northern Front Range. We also analyze the spatiotemporal distribution of NO_2 along the Front Range using mobile, stationary, and TEMPO measurements to assess how the transport of urban emissions varies from day to day and whether NO_2 concentrations measured in the state monitoring network are representative of levels observed in DICs. This work also introduces novel comparisons of mobile NO_2 data to TEMPO data, contextualizing the benefits and challenges that come with concurrent sampling methods. Finally, we examine O_3 concentrations across the DMNFR O_3 NAA during 11 distinct driving intensives. A main goal is to determine how variable those concentrations are over short distances (e.g., hundreds of meters to kilometers) and what this means for variability in exposure. These results are interpreted alongside stationary measurements, visible satellite imagery, HYSPLIT back trajectories, TEMPO NO_2 data, and mobile methane and ethane data in an attempt to better frame our observations.

2. METHODS

2.1 FROZÉ Field Campaign Overview

The Colorado Front Range OZone Éxperiment (FROZÉ) field campaign took place in the Colorado Front Range from June-August 2025. The FROZÉ field campaign included several elements. One was to measure the spatiotemporal distribution of O_3 and O_3 precursors, namely nitrogen oxides (NO_x) and volatile organic compounds (VOCs), in the Front Range. A second was to measure air pollution levels in several disproportionately impacted communities (DICs) with little or no prior monitoring to assess how levels compared to Front Range locations with more regular monitoring. FROZÉ utilized stationary, mobile, and satellite measurements to accomplish these tasks.

There were 4 supersites for FROZÉ: Fort Collins West (FTCW), La Salle Tower (LST), Rocky Flats North (RFN), and Sheridan/Fort Logan (SHER). The "supersite" designation was made at sites that had continuous, online measurements of O_3, NO_x, and speciated VOCs. FTCW and RFN were located along the base of the foothills, where high O_3 levels are frequently observed (Pfister et al., 2019). LST was a rural oil and gas (O&G)-influenced site in the eastern part of the Denver Metropolitan/Northern Front Range (DMNFR) O_3 nonattainment area (NAA), where a large portion of the Denver-Julesburg Basin is located. The SHER site was the most urban supersite, located 17 km southwest of downtown Denver. In addition to the supersites, there were also numerous sites that measured either both NO_x and O_3 or only O_3, as seen in Figure 2.1. These stationary sites were operated by a joint effort between Colorado State University (CSU), the Colorado Department of Public Health and Environment (CDPHE), and the Environmental Protection Agency (EPA). The strategic locations of the stationary monitoring sites allowed for precise, real-time measurements of O_3 and relevant precursor compounds along the DMNFR O_3 NAA, while also providing crucial contextual data to inform the mobile platform measurements.

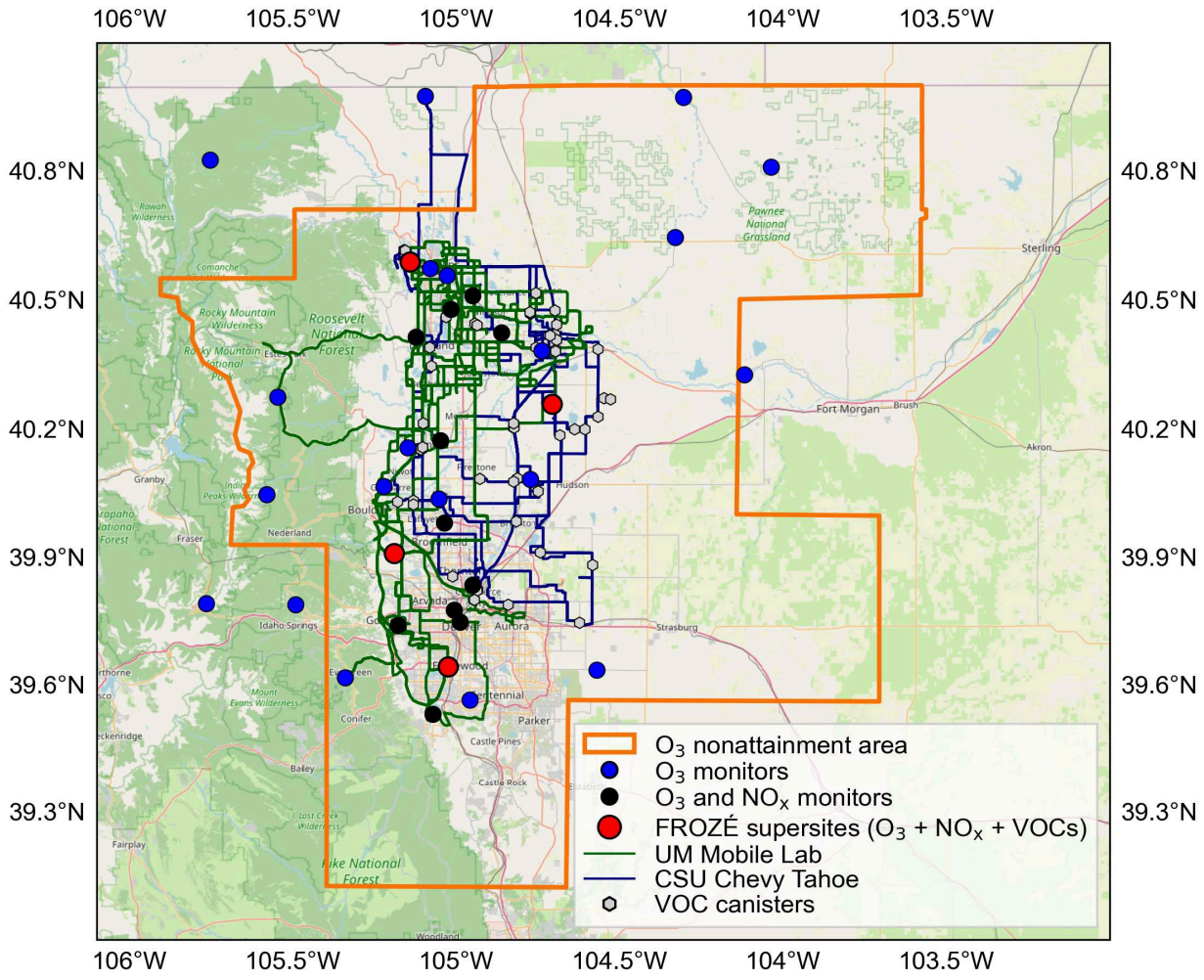


Figure 2.1: Overview of FROZÉ stationary sites, mobile measurement locations, and canister deployment locations. The blue drive tracks are the UM Van, while the green are the CSU Plume Tracker.

There were two mobile measurement platforms operated by the University of Montana (UM) and CSU. The first mobile measurement platform, the UM Van, performed 26 driving intensives, accounting for a total of over 131 hours of mobile measurements between July 9 and August 19. The UM Van had an extensive instrument payload, with online measurements of O_3, NO_x, and speciated VOCs. As seen in Figure 2.1, the UM Van driving intensives were mainly focused closer to the foothills and the Denver metropolitan area. Further discussion of the UM Van is outside of the scope of this analysis, which focuses on the other mobile platform.

The CSU Chevy Tahoe, or "Plume Tracker", completed 13 driving intensives, which resulted in

over 90 hours of continuous measurements between the dates of June 26 and August 19. The Plume Tracker made continuous online measurements of O_3 and NO_2, as well as offline measurements of speciated VOCs using grab canisters for whole air sampling. The driving intensives in this vehicle, as depicted in Figures 2.1 and 2.2, were mostly concentrated in the northern and eastern portions of the DMNFR O_3 NAA, where measurements of O_3 precursors were historically sparse.

In addition to stationary and mobile measurements, TEMPO satellite special operations were requested on select days with favorable meteorology. Special operation requests were required to be made a week in advance, adding a fair amount of uncertainty into the weather forecasts needed to make request decisions. On TEMPO special operation days, nominal temporal resolution of one hour was increased to every 10 minutes over the study domain every other hour. This allows for unprecedented temporal resolution of NO_2 data over the entire DMNFR O_3 NAA. On days when TEMPO special operations were not requested, NO_2 data are available hourly. These satellite data allowed for a third, independent measurement of NO_2 to contextualize both mobile and stationary data.

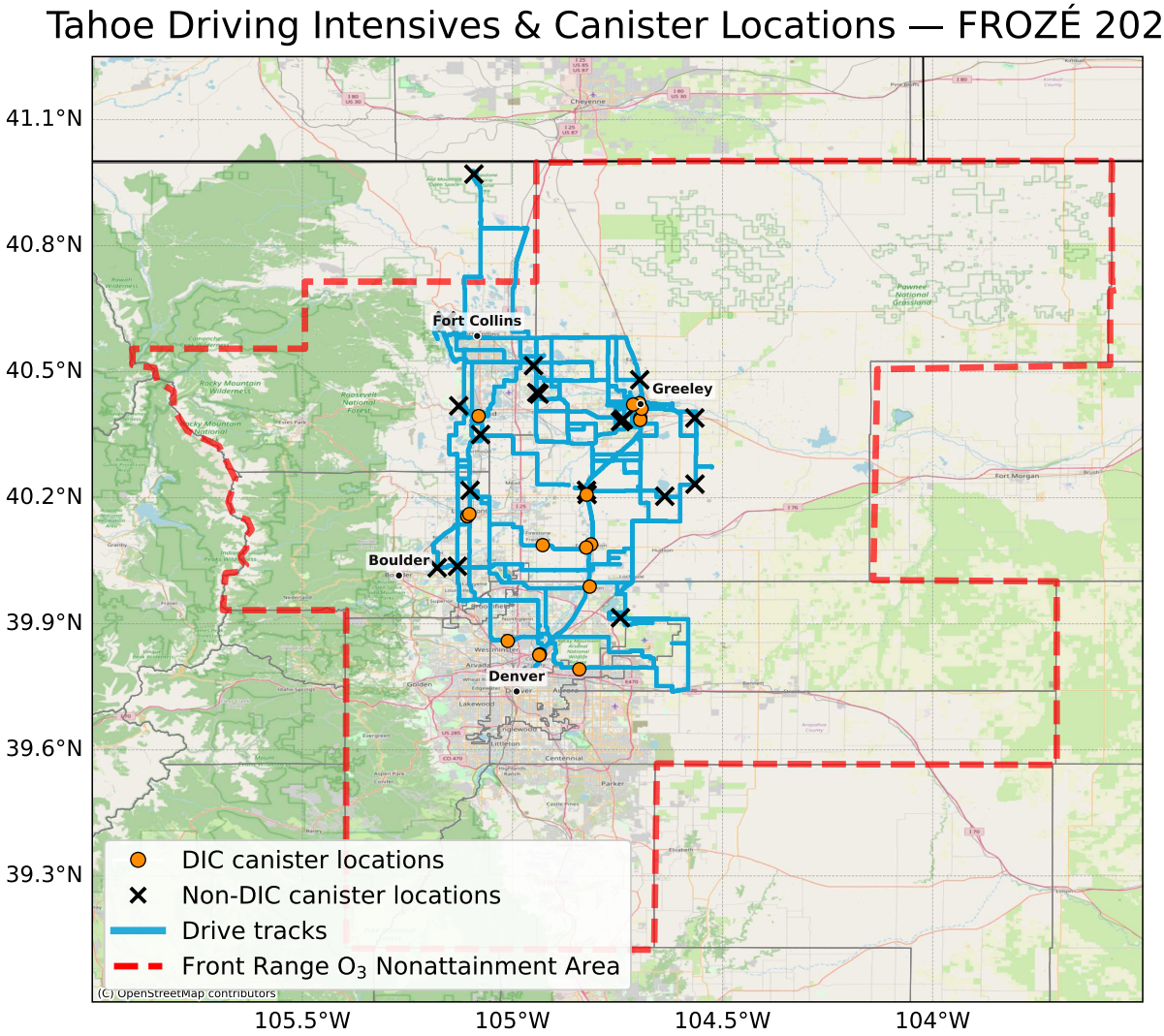


Figure 2.2: Map of Tahoe driving intensives and both DIC & non-DIC air canister deployment locations.

2.2 CSU Plume Tracker Instruments & Setup Methodology

The CSU Plume Tracker featured four instruments used for measuring species of interest during FROZÉ. A quick guide of instrument specifications is shown in Table 2.1. With these instruments, the Tahoe had online sampling of O_3, NO_2, CH_4, C_2H_6, and CO_2. Offline sampling methods involved using 1.4L evacuated whole air canisters to collect air samples that were then brought back to the lab for VOC speciation. Mobile measurement platforms are notoriously difficult for especially sensitive instruments due to vibrations from road surfaces, the vehicle's engine, wind, etc. Precautions were taken when installing the instruments into the Plume Tracker, such as using foam pads to reduce vibration, as well as strapping instruments into place to reduce physical movement due to vehicle motion.

Table 2.1: Instrument specifications for the Plume Tracker payload for FROZÉ. *The AERIS MIRA Ultra Portable instrument was only present for 5/13 driving intensives performed by the Plume Tracker.

Instrument	Species Measured	Sampling Rate	Flow Rate	Response Time	Sampling Method	Reference
Teledyne Model T500U Cavity Attenuated Phase Shift Monitor (CAPS)	NO_2	1s	0.9 LPM	~40s	Online	Birks et al. 2018
AERIS MIRA Ultra Portable*	CH_4, C_2H_6	1s	0.6 LPM	1s	Online	Liu et al. 2026
Li-COR LI-7810 analyzer	CH_4, CO_2, H_2O	1s	0.25 LPM	2s	Online	Irie et al. 2026
2B Personal Ozone Monitor (POM)	O_3	2s	~0.8 LPM	4s	Online	Anderson et al. 2010
Entech 1.4L Silonite-LL MiniCans	VOCs	~30s/can	N/A	N/A	Offline	Russo et al. 2010; Swarthout et al., 2013

The Teledyne Model T500U Cavity Attenuated Phase Shift Monitor (CAPS), referred to as the Teledyne CAPS from this point on, measured NO_2. The Teledyne CAPS uses optical absorption spectroscopy to measure the amount of light that is attenuated by NO_2, which is directly proportional to the path length of the instrument and the concentration of the absorbing gas, according to the Beer-Lambert Law. A more complete description of this instrument and common applications can be found in Birks et al. (2018). This method is faster than the commonly used chemoluminescence method, making the Teledyne CAPS an optimal choice for mobile measurements. One important thing to note about this instrument is that it has a relatively long response time (~40s) when compared to the other three online instruments. When calibrations were completed (see Section 2.3), the instrument response time exhibited an exponential decay with an e-folding time of 5.17s. The total response time in calibrations was measured to be ~30s.

The AERIS MIRA Ultra Portable (MIRA Ultra) measured methane (CH_4) and ethane (C_2H_6). The MIRA Ultra utilizes mid-infrared radiation (MIR), solid-state laser spectroscopy in a temperature and pressure-controlled small volume, with a 13-meter absorption path length. The MIRA Ultra uses multipass cell technology to detect the amount of absorption that occurs at different points in the volume at MIR wavelengths where CH_4 and C_2H_6 strongly absorb. A more detailed treatment of the MIRA Ultra, as well as technical performance evaluations, are outlined in Liu et al. (2026). The MIRA Ultra features a tablet that displays a plot of the C_2H_6/CH_4 ratio updated at a frequency of 1 Hz. When the C_2H_6/CH_4 ratio exceeds a certain threshold, the tablet displays "O&G signature detected!" This was especially useful for driving intensives that sampled DICs and O&G facilities, as it allowed for fast distinguishment between agricultural and O&G-related emissions. Due to the purchasing timeline of the instrument, the MIRA Ultra was only present for 5/13 of the drives.

The Li-COR LI-7810 analyzer (LI-7810) measured CH_4, CO_2, and H_2O on the Plume Tracker. The LI-7810 uses Optical Feedback-Cavity Enhanced Absorption Spectroscopy (OF-CEAS) by shining a laser beam onto a V-shaped mirror, which causes the beam to bounce back and forth, creating a long path for absorption. The LI-7810 utilizes wavelengths where CH_4 and CO_2 absorb strongly; concentrations are determined based on measured absorption. A more comprehensive

overview can be found in Irie et al. (2026). It was helpful to have concurrent measurements of CH_4 with both the MIRA Ultra and LI-7810, so that the magnitude of intercepted plumes could be quantified with greater confidence.

O_3 was measured using 2B Technologies' Personal Ozone Monitor (POM). The POM is small, weighing only 0.75 lb. It is intended to be a portable, precise instrument for assessing personal O_3 exposure in a plethora of environments. The POM utilizes the Environmental Protection Agency (EPA) Federal Equivalence Method (FEM) of measuring O_3. This method involves absorption of ultraviolet (UV) light using a low-pressure mercury lamp that emits at 254 nm at one end of the 15-cm optical cell, and a photodiode sensor at the other end. A valve switches air intake between two paths: one that has an O_3 scrubber, and one that does not. Each of these samples is separately injected into the absorption cell, and the O_3 concentration is then derived based on the difference in absorption. For more details on the POM's technical performance, see Andersen et al. (2010). The POM has been used in a variety of settings for O_3 measurements, and its size and precision made it an ideal choice for measuring O_3 in a mobile laboratory (Niu et al., 2018). Another useful component of the POM is that it does not require frequent calibration, as it uses an absolute measurement method that relies on UV absorption, which is an unchanging physical property (Andersen et al., 2010).

These instruments were installed into the Plume Tracker in a way that minimized both the footprints of the instruments due to space constraints, as well as effects from vibrations from the road. As a result, the LI-7810, MIRA Ultra, and Teledyne CAPS were mounted on separate shelves of a custom-made wooden rack. Placement of the LI-7810 and Teledyne CAPS in the Plume Tracker is shown in Figure 2.3. The MIRA Ultra was placed in the middle rack, but was not present at the time that the photo was taken. The instruments were secured into place using two pairs of bungee cords each to minimize movement caused by vehicle motion. These three instruments were connected to a common inlet (Teflon, 64 in. length, 0.25 in. outer diameter, 6.05 LPM total flow) that reached through a hole through the vehicle roof. The common inlet was connected to an auxiliary pump (Barnant Co., model no. 400-1941) to increase the flow. This setup allowed the LI-7810, MIRA Ultra, and Teledyne CAPS to sample outside air concurrently. Flow checks

were performed periodically throughout the field campaign to make sure that the flow rate of the common inlet was more than the sum of the required flow rates for all three instruments, which are shown in Table 2.1.

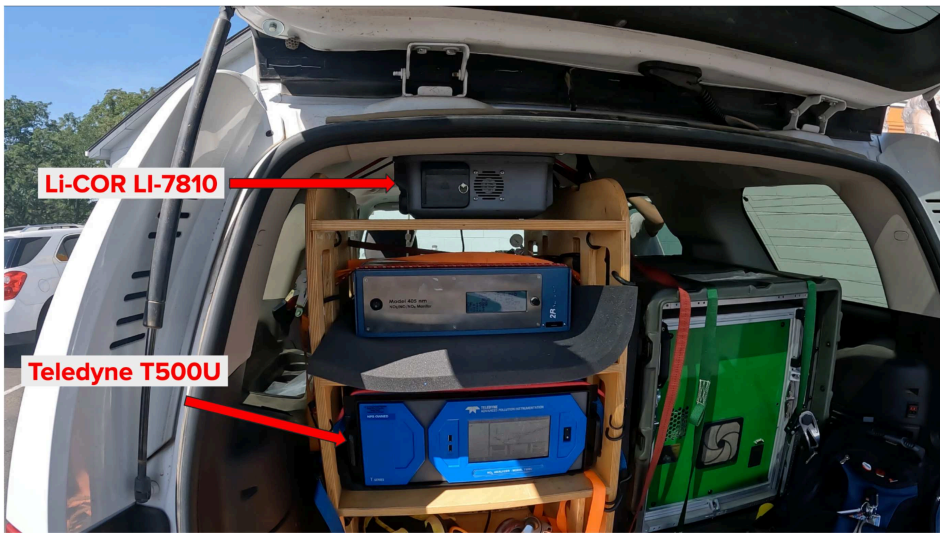


Figure 2.3: Photo of the locations of the LI-7810 and Teledyne CAPS instruments in the Plume Tracker.

The POM was installed separately from the other three instruments to ensure its small pump could handle the inlet pressure drop. The instrument itself is quite small (4 x 3 x 1.5 in), so it was able to be clipped into a groove on the side of the Chevy Tahoe, behind the driver's seat, as can be seen in Figure 2.4. Shorter inlet tubing (Teflon, 42 in. length, 0.25 in. outer diameter) was installed from the POM out the rear left car window and fastened to the roof next to the other common instrument inlet. Since the POM was placed on a separate inlet, it cannot be guaranteed that the same air was sampled across all four instruments, but inlet co-location was intended to minimize sampling differences.

All instruments were connected to a Goal Zero Yeti 6000X portable power station. The battery life when connected to all instruments and computers was approximately 16 hours, well above the drive durations. Also attached to the portable power station were two laptops used to monitor the instruments. The first laptop, located in the back of the vehicle, had the LI-7810 and MIRA

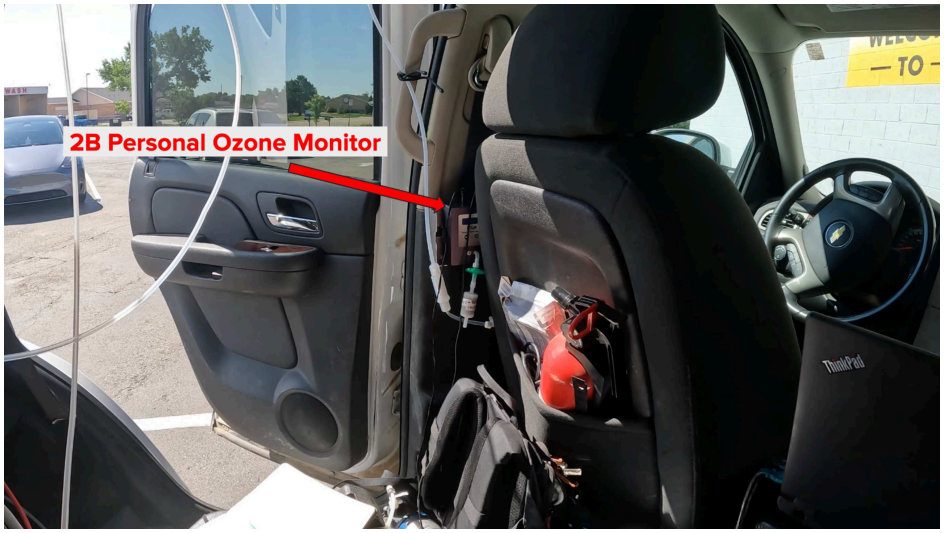


Figure 2.4: Photo of the location of the POM in the Plume Tracker. The device pictured hanging off of the POM is an O_3 scrubber used for zero air tests.

Ultra connected so that methane measurements on both instruments could be compared. The second laptop, located in the front of the vehicle, had the Teledyne CAPS and POM connected to it, allowing for observations of O_3 titration by fresh NO_x plumes from nearby vehicles. Also connected to this computer was an Airmar WeatherStation 220WX, which recorded the vehicle's GPS location, as well as meteorological information. The Airmar WeatherStation was mounted on the roof of the vehicle with suction cups for security, as shown in Figure 2.5.



Figure 2.5: Photo of the CSU Chevy Tahoe/Plume Tracker. The Airmar can be seen on the roof of the vehicle above the driver's seat and front passenger seat.

2.2.1 Canister Collection & VOC Speciation Procedure

The final component of Plume Tracker measurements was offline collection of whole air canister samples at various locations using Entech 1.4L Silonite-LL MiniCans. Canisters were evacuated and cleaned using an Entech 3100D Canister Cleaning System prior to sampling. The canisters were first evacuated to 10^{-2} torr and purged with ultra-high purity nitrogen for 8 cycles at 80 °C (Ku et al., 2024; Weber et al., 2018). A canister was collected in every DIC the Plume Tracker visited, as well as several non-DIC locations, such as in suspected O&G facility plumes or when high O_3 was detected. Every drive, 6 canisters were taken for sampling in DICs and any additional plumes/areas of interest. Canisters were deployed by inserting a compression fitting (Entech SC Female MQT-1/4" Compression Fitting-30-22800S) onto the top of the canister and pulling upwards when sampling. The canisters were held above our heads to avoid contamination from breathing. Canister sampling lasted for ~30 seconds.

Collected canister samples were analyzed within one week and speciated for 51 VOCs using a 5-channel GC with 3 flame ionization detectors (FIDs), an electron capture detector (ECD), and a quadrupole mass spectrometer (MS) (Benedict et al., 2019; Russo et al., 2010; Swarthout et al., 2013; Weber et al., 2018; Zhang et al., 2024). The 5-channel GC system featured a 30 cm stainless steel cryogenic pre-concentration loop with an internal diameter of 0.3175cm containing 1mm diameter glass beads, a splitter box, an excess volume canister, and three GC systems (Weber et al., 2018). A comprehensive description of the 5-channel GC setup and analysis technique can be found in Weber et al. (2018). A list of the 51 VOCs speciated by the GC and their method detection limits (MDL) can be found in Table A.1. The canisters were also analyzed for methane using a Shimadzu GC-8A equipped with a digital temperature programmer and FID. More details on the methane GC are described in detail in Ku et al. (2024). The methane MDL can also be found in Table A.1.

2.3 Instrument Calibrations

Before the field campaign, steps were taken to ensure that the instruments were ready for deployment. The MIRA Ultra was calibrated multiple times while at the Fort Collins West (FTCW) EPA site, and the instrument response was fairly stable between these calibrations. The POM was not directly calibrated before the campaign, but was co-located at the FTCW site with the EPA O_3 regulatory monitor for 2 weeks and exhibited very good agreement (Figure A.1). The Teledyne CAPS manually corrects for drift every time the instrument undergoes a zero air test (discussed below), so calibrations before the campaign were not critical. The Teledyne CAPS was included in the post-campaign calibrations. The LI-7810 had intermittent availability in the weeks leading up to the start of the field campaign due to its shared use for a different project. For this reason, pre-field campaign calibrations were unavailable for this instrument. The LI-7810 was calibrated post-campaign. The LI-7810 manual states that the maximum drift is less than 1 ppb for every 24 hours of continuous monitoring for CH_4. Therefore, any drift that may have occurred before/during FROZÉ would likely be inconsequential, especially given that the Plume Tracker had concurrent CH_4 measurements with the MIRA Ultra.

During the field campaign, zero air tests were performed at the start of every drive. This procedure involved connecting the common inlet for the LI-7810, MIRA Ultra, and Teledyne CAPS to a zero air cylinder (Airgas Ultra Zero Grade Air, Size 80 High Pressure Steel, CGA 590). The point of using this cylinder was so the instruments sample "clean" air that has no pollutants in order to assess baseline response. This also allowed for the time to be aligned for all instruments. The cylinder was strapped to the back of the front passenger seat of the Chevy Tahoe so that a zero air test could be performed at any location. At the start of the test, zero air was injected into the common inlet at a high flow rate to overflow the inlet. Zero air flowed through the inlet for 10 minutes to allow for the instrument readings to stabilize. During this period, the LI-7810, MIRA Ultra, and Teledyne CAPS sampled clean air, so their values should read zero, assuming no baseline drift. At the same time that this test was happening, the POM was disconnected from its separate inlet, and an O_3 scrubber was placed over the POM's inlet. Once 10 minutes had passed, the common inlet was removed from the zero air cylinder, and the O_3 scrubber was removed from

the POM. Once the data were analyzed for these instruments, the baseline offset (i.e. how far away the baseline was from zero) was subtracted/added to the data for the entirety of a driving intensive. An example of what the instruments read when zero air is injected can be seen in Figure 2.6. The manual baseline drift correction for the Teledyne CAPS can be seen in the sudden downward jump of the red line near the end of the test. Also apparent in Figure 2.6 is more noise in the POM O_3 concentrations than the other instruments during the zero air test. This observation was consistent among all zero air tests. Each of the 13 driving intensives had its own zero air test, and consequently, a respective offset value subtracted from the data after each drive was completed. The main goal of these tests was to account for any drift that may occur in the instruments between driving intensives. For two driving intensives, a zero air test was conducted at the beginning and end to check for instrument drift during the sampling periods themselves. Little response drift was found between the zero air tests in a single driving intensive, so only one zero air test was performed subsequently. The zero air tests also provided a way to align the separate instrument clocks, as there were some minor variations between them.

After the field campaign was over, multi-point calibrations were performed on all four instruments. This was done to define the full instrument response and, in some cases, to ensure there was no significant drift in instrument response over the course of the summer campaign. The POM was calibrated using a 2B Model 306 Ozone Calibration Source that was diluted with ambient air. The Teledyne CAPS was calibrated using gas-phase titration of NO calibration gas (9.89 ppm NO +/- 1% in N_2, Airgas) with O_3 generated by a Teledyne T700U dilution calibrator (zero air source: Teledyne T701H zero air generator). For CH_4 and C_2H_6 for the MIRA Ultra and LI-7810, a multi-point calibration was performed using a diluted air stream from a Linde cylinder with 10.2 ppm CH_4 +/- 5% and 1.00 ppm C_2H_6 +/- 5% in N_2. Finally, CO_2 for the LI-7810 was calibrated using dilutions from an Airgas cylinder with 5% CO_2 +/- 0.5% in N_2 (zero air source: Airgas UZA cylinder). The results of these calibrations are shown in Figure 2.7, and indicate a linear response with strong agreement between the expected and measured concentrations.

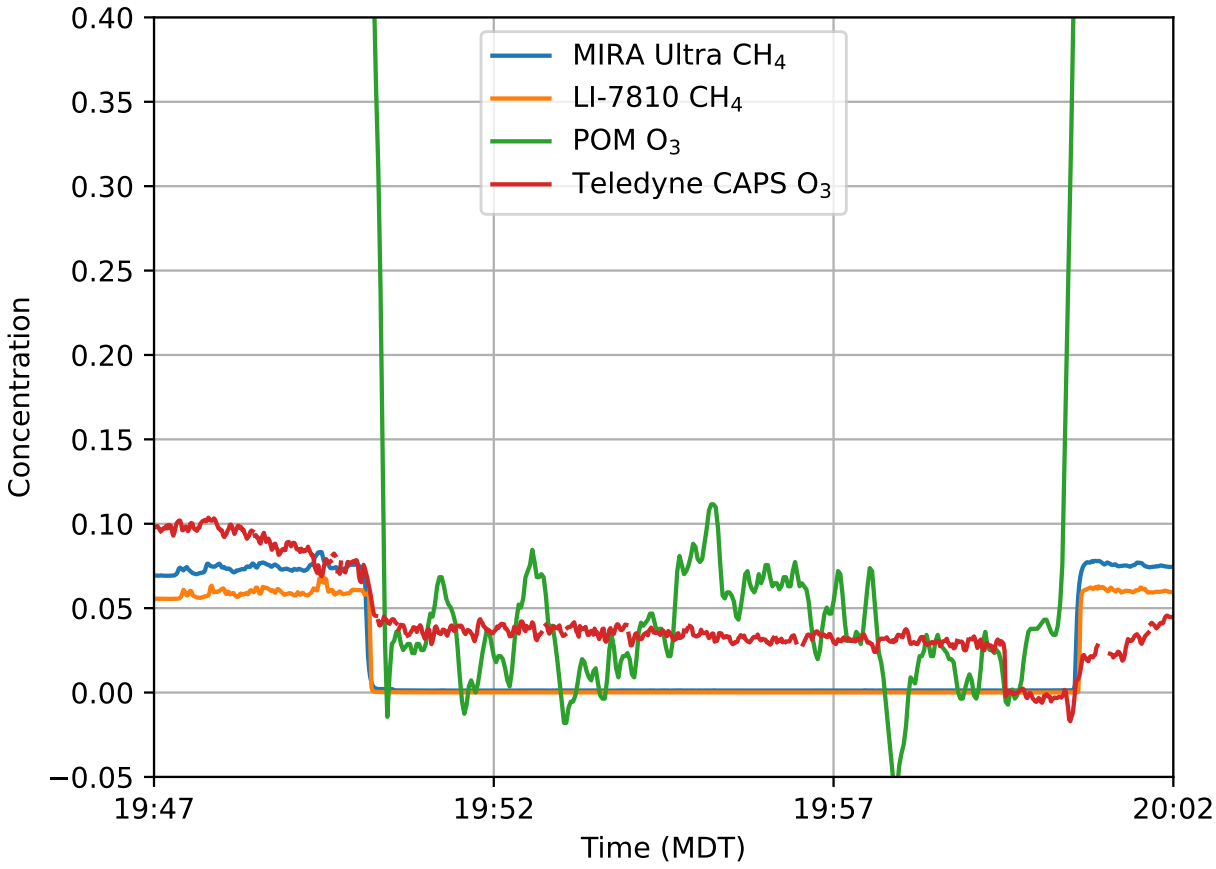


Figure 2.6: Plot of the instrument concentrations (divided by the maximum value) during a zero air test on the August 14th, 2025 driving intensive. The y-axis values are normalized by the maximum value for each instrument for comparison.

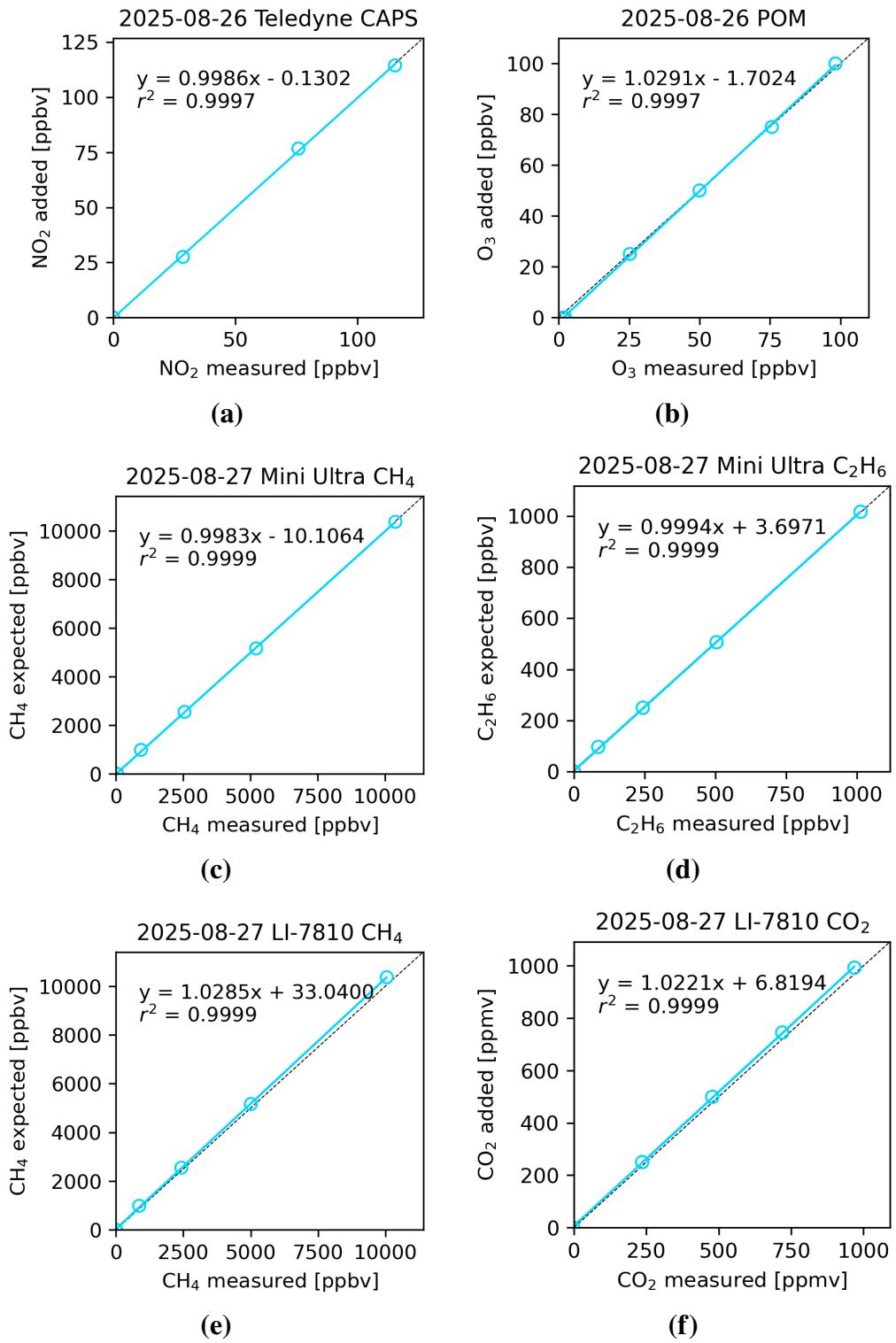


Figure 2.7: Post-campaign calibration curves for the Teledyne CAPS NO_2 (a), POM O_3 (b), Mini Ultra CH_4 (c), Mini Ultra C_2H_6 (d), LI-7810 CH_4 (e), and LI-7810 CO_2 (f).

2.4 Field Deployment Planning & Measurement Strategy

2.4.1 Driving Intensives

Planning driving intensives was a joint effort by Colorado State University, University of Montana, the Colorado Department of Public Health and Environment (CDPHE), and the Regional Air Quality Council (RAQC). Weather forecast briefings were held daily at 3 PM MDT. These briefings were led by Colorado State University professors and graduate students, with significant input from CDPHE's air quality meteorologists. The goal of the briefings was to discuss whether meteorology was favorable enough to deploy the UM Van or CSU Chevy Tahoe, as well as look at long range forecasts to decide when to request TEMPO special operations. Key meteorological factors that were supportive of high O_3, as instructed by CDPHE, were establishment of the Denver cyclone in the overnight/morning hours, light/sustained upslope flow (less than 10 knots) or stagnant winds, sunny skies/limited cloud cover, and hot (but not excessively hot) temperatures (80-95 degrees Fahrenheit). The Denver cyclone, an orographically-induced mesoscale vortex, has previously been found to increase aerosol mass loading in the Colorado Front Range, leading to deterioration in air quality (Vu et al., 2016; Wilczak and Christian, 1990). In the context of high O_3 forecasting, the Denver cyclone's ability to transport and concentrate O_3 precursors in the eastern High Plains before the initiation of upslope flow has implications for increased O_3 formation (Reddy and Pfister, 2016). Other more unique factors monitored by CDPHE and the forecast team for high O_3 were stratospheric intrusions (less common in the summertime), long range pollution transport, and wildfire smoke. Meteorological factors that CDPHE has found to be less supportive of high O_3 events were strong winds (greater than 15-20 knots), clouds, rain/thunderstorms and associated outflow, cool temperatures (less than 80 degrees Fahrenheit), cold fronts/syntoptic disturbances, westerly winds (induces mixing), and extreme heat (100+ degrees Fahrenheit). CDPHE also looked at overnight drainage and clean transport off of the Cheyenne Ridge, which can also decrease the likelihood of high O_3. It is important to note that every day there was a combination of these factors present and no single meteorological factor listed above was likely to lead to a high O_3 event alone.

When a decision was made to perform a driving intensive the next day, KMZ route files were

drawn for the UM Van (and sometimes the Plume Tracker). Drive planning for the UM Van was more detailed due to the more extensive instrument payload and specific emission sources intended to be sampled. For the Plume Tracker, however, there was an emphasis on sampling the Front Range more regionally, as well as prioritizing at least one DIC sampling period within each driving intensive. For this reason, the Plume Tracker driving paths were often more fluid, and were easily changed in the field if there were afternoon clouds developing, for example. On days when there were more specific objectives for the Plume Tracker, such as sampling around Denver International Airport, KMZ route files were drawn by the lead forecaster. The general strategy for the Plume Tracker driving intensives was to start sampling early in the morning before the initiation of upslope flow, usually around 7-8 AM MDT. While the specific drive pattern changed from day to day, one of the main objectives was to head west after the initiation of upslope flow, which is thermally-driven and usually started around 11 AM. The vehicle's speed was moderated (typically 35-40 mph) to reduce the distance between measurement points. However, often this was not possible when needing to cross highways and other congested roads. Care was taken to avoid highways and roads with lots of traffic to reduce contamination from fresh NO_x plumes from nearby vehicles. Sampling ended in the late afternoon/early evening, after O_3 concentrations typically had peaked.

2.4.2 Disproportionately Impacted Communities (DICs)

Colorado is one of the only states in the U.S. to have a legal definition of disproportionately impacted communities (DIC), per Colorado Revised Statute § 24-4-109. Defining criteria can be found in Figure 2.8. and include demographic, socioeconomic, environmental burden, and other factors. If any of the criteria are met, the community is classified as a DIC. In choosing which communities to sample, particular emphasis was placed on the Colorado EnviroScreen score. EnviroScreen 2.0 is a tool developed by CDPHE and CSU to assess the amount of environmental burden a specific census block has. A schematic of how this score is calculated by CDPHE can be found in Figure 2.9. The EnviroScreen score is a percentage, with higher numbers signifying increased environmental burden. All of the communities chosen for sampling in FROZÉ had an EnviroScreen score above 80%, meaning that they represent some of the

most environmentally-burdened communities in Colorado due to pollution, proximity to emission sources, and other factors. In addition to the EnviroScreen score, special care was taken to ensure that every DIC sampled in the field campaign also met at least one of the DIC demographic criteria: >40% low-income households, >40% of population identifies as people of color, >50% housing cost burdened households, or >20% linguistically isolated households. Often, communities met at least 2-3 of these. The goal in choosing DICs that met multiple legal criteria was to assess communities that experience intersectionality. In an environmental justice context, "intersectionality" means communities that are burdened by multiple, compounding socioeconomic and environmental factors, making them more vulnerable to harmful environmental effects and natural disasters (Ryder, 2017). It was important to our study that the communities sampled for air toxics were among the most vulnerable and had little to no prior monitoring.

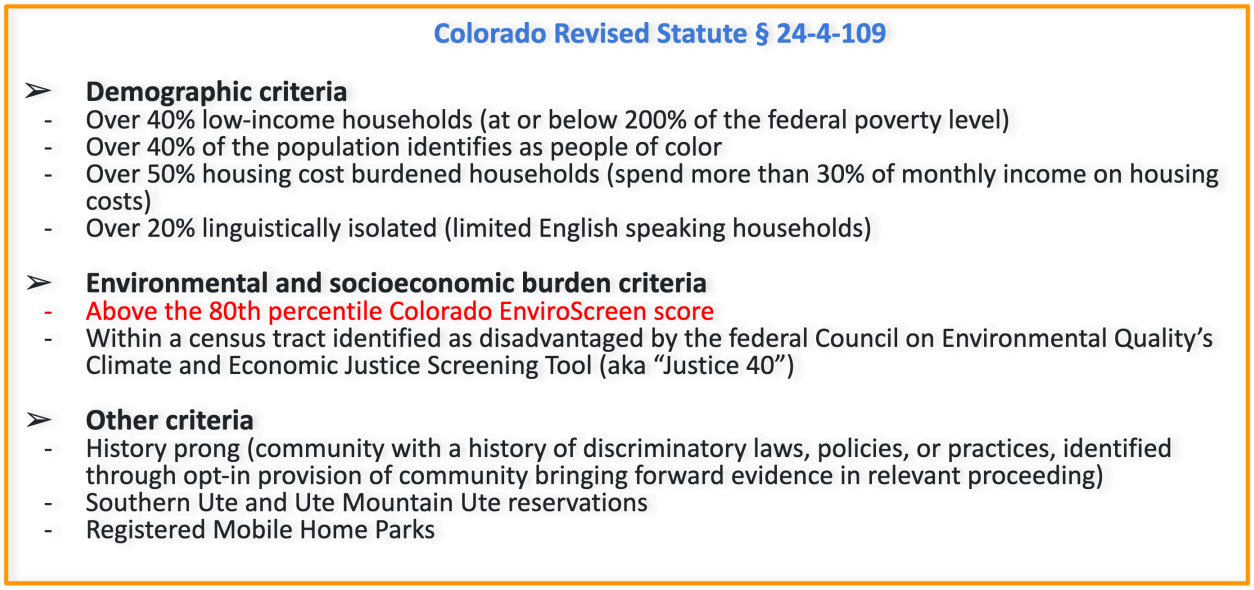


Figure 2.8: Legal criteria that define what a disproportionately impacted community (DIC) is in Colorado. Adapted from CDPHE's Environmental Justice Mapping Tools training presentation.

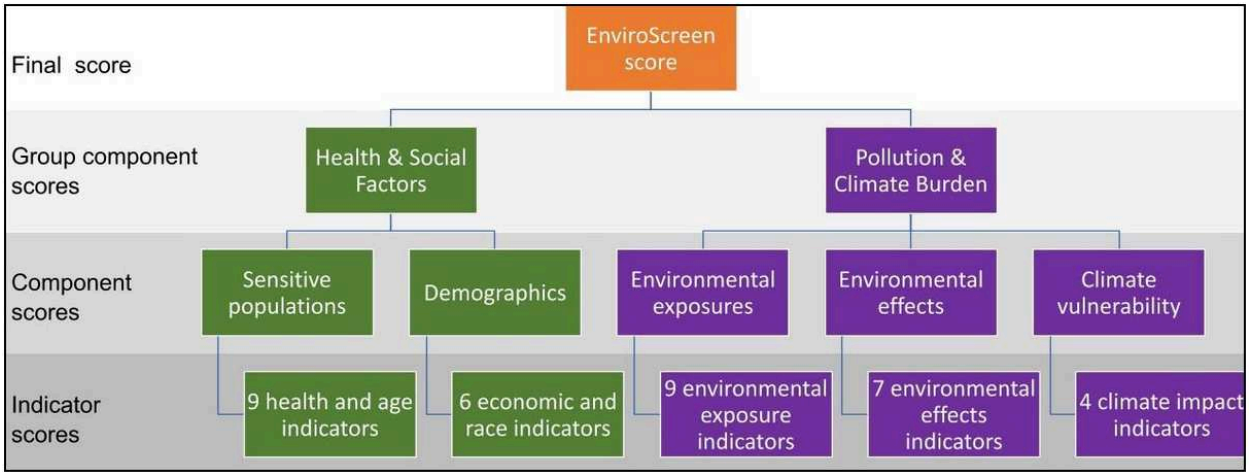


Figure 2.9: Flow chart of the components that go into the calculation of CDPHE's CO Enviroscreen 2.0 percentage for a census block (Source: https://cdphe.colorado.gov/user-guide-colorado-enviroscreen-20).

DICs were selected using the above process, as well as trying to maximize the spatial extent of communities sampled in the DMNFR O_3 NAA. Once the driving intensive plans were formulated, a DIC was selected, and the drive path for that day was adjusted as needed to incorporate DIC sampling. Balancing the need to sample the Front Range on a regional scale, while also including local scale sampling periods in DICs, meant that most communities were visited during the daytime. While O_3 is higher in daytime, NO_2 and VOC concentrations are often higher at night when the surface mixed layer is shallower. Two nighttime driving intensives were added to take measurements in multiple DICs when the boundary layer was lower and surface emissions were likely less diluted. Once the Plume Tracker actually entered a DIC, a special measurement strategy was employed, shown in Figure 2.10. This zigzag pattern was used to maximize the area of the DIC sampled by the vehicle, as well as attempt to capture any variability that might be present in the community. The typical time spent sampling in DICs was on the order of 30-45 minutes, depending on the size of the community. Canister samples were taken at the end of the DIC sampling period unless there was a plume intercepted along the drive.

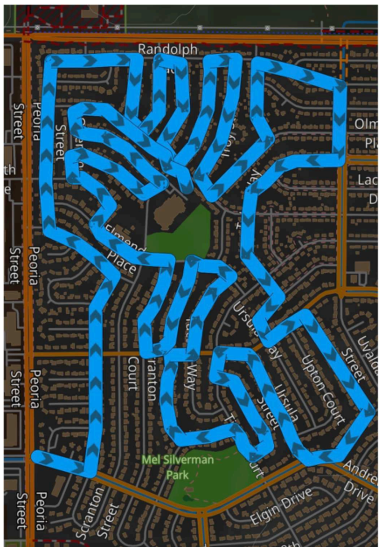


Figure 2.10: Example drive path from Montbello DIC sampling period.

2.5 TEMPO NO_2 Data

TEMPO is a relatively new NASA geostationary satellite, launched in 2023, with high resolution (2.21 x 4.97 km footprint) that provides hourly monitoring of NO_2. TEMPO NO_2 data have been proven to be accurate at a scale that was not possible with prior satellites (Nowlan et al., 2025). On special operation days, scans were increased to every 10 minutes every other hour over the Rocky Mountain region. The difference between nominal operations and special operations is illustrated in Figure 2.11. TEMPO special operations were requested a week in advance for select days where the forecast indicated minimal cloud cover and meteorological support for high O_3. TEMPO data allowed for extensive monitoring of NO_2 in the entire Front Range, and provided qualitative context for mobile and stationary NO_2 data from FROZÉ. We used L2 (Level 2) data for this analysis, which represent geophysical parameters derived from processed sensor radiance data (Level 1), at the original resolution and orbital path of the satellite (Nawaz et al., 2025). For the driving intensives when TEMPO special operations were not requested, L2 scans were retrieved for every hour. On driving intensives when special operations were requested, scans were retrieved every 10 minutes every other hour, with hourly scans retrieved in between these hours. These data were not regridded, but rather, the raw L2 data were used for visualization purposes. TEMPO pixel sizes are not consistent among the swaths in L2 data.

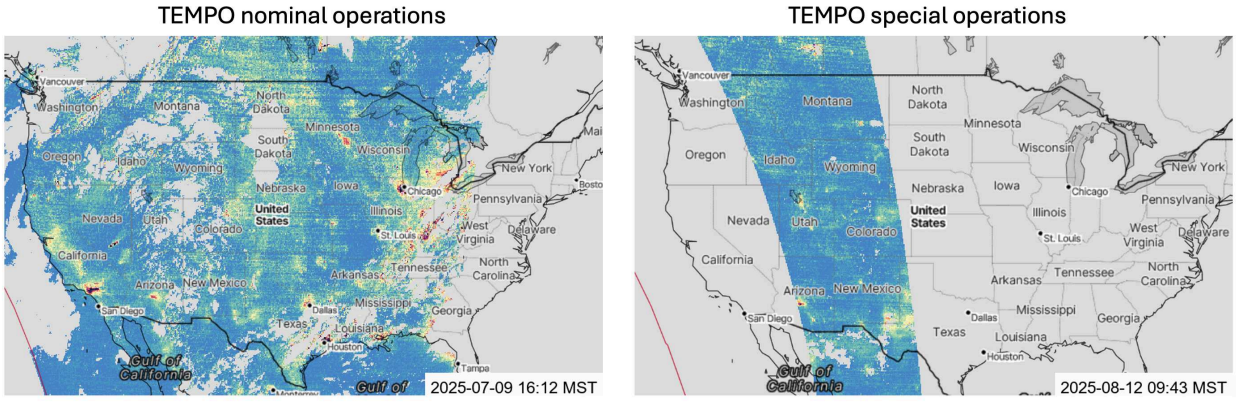


Figure 2.11: Spatial coverage difference between TEMPO NO_2 nominal hourly operations (left) and special operations (right) during FROZÉ.

2.6 HYSPLIT Backward Trajectories

Air mass backward trajectories were calculated for each of the mobile O_3 case studies using NOAA's HYSPLIT atmospheric transport and dispersion modeling system (Rolph et al., 2017; Stein et al., 2015). Six-hour backward trajectories were initiated every 30 minutes along the drive path for each of the five case studies. For meteorological reanalysis, we used NOAA's High-Resolution Rapid Refresh (HRRR) model, which has 3 km grid spacing and is convection-allowing. To prevent interference from the surface on trajectory paths, parcels were initiated at 300 m agl, which is the same height used in previous work (Cheadle et al., 2017b).

2.7 Data Filtering

2.7.1 NO_2 Filtering Method

Mobile measurements of NO_2 (and, more broadly, NO_x) are susceptible to interference from fresh tailpipe emissions emanating from vehicles immediately in front of the sampling vehicle, leading to overestimated measurements of typical local conditions (Whitehill et al., 2020; Wild et al., 2017; Woo et al., 2016). As a result, the raw measurements of NO_2 collected by the Plume Tracker are not likely representative of regional patterns in the DMNFR O_3 NAA. Therefore, a method of filtering fresh plumes from proximate vehicles must be employed to isolate data more broadly indicative of regional patterns of NO_2.

For this study, two filtering methods were attempted. The first was a plume-by-plume method, developed by Zuraski et al. (2025). This method identifies vehicle plumes as discrete NO_2 spikes above a local baseline (calculated by the algorithm). In order for the algorithm to correctly identify a plume, the user must specify a derivative threshold and fallback threshold manually. The derivative threshold is used to identify when a peak is beginning. The fallback threshold tells the algorithm when a plume has ended once the concentration falls to a set value above the peak start value. NO_2 peaks identified by these two thresholds are flagged. The method's efficacy in removing vehicle plumes depends on the values chosen for thresholds. If the derivative threshold is set too low, the algorithm becomes too aggressive and removes data that are likely not vehicle plumes, and vice

versa. The values that filtered out vehicle plumes most effectively, while also retaining regional trends, for this dataset were 0.25 ppbv/s for the derivative threshold, and 2.75 ppbv for the fallback threshold. It is important to note that these values are much lower than those used in Zuraski et al. (2025), as they were filtering for NO_x, which is present at much larger concentrations than NO_2 in fresh NOx emissions.

The second filtering method tested in this study was the State-Informed Background Removal (SIBaR) method, developed by Actkinson et al. (2021). SIBaR uses Hidden Markov models to classify each observation as either "background" or "source-influenced" by detecting changes in the time series. A natural spline is fit through the background-assigned points to generate a continuous, time-varying background signal, which is then subtracted from the full time series to yield local source contributions. For a more comprehensive description of this method, see Actkinson et al. (2021). An advantage of SIBaR is that it is more objective, as it does not require manual selection of thresholds. However, SIBaR also places a strong emphasis on having well-defined background values, especially near the beginning of the time series. This is not always realistic, as traffic was quite variable from day to day during the driving intensives.

A comparison of raw NO_2 data from the Plume Tracker and the filtered data using the plume-by-plume and SIBaR methods is shown in Figure 2.12. The raw data is quite noisy due to many local vehicle plumes. An interesting feature is found in the raw data between 10:00-11:00 MDT, indicating a period of extended elevated NO_2 concentrations not due to individual vehicle plumes. The plume-by-plume method does not completely eliminate local NO_2 variability/noise, but mutes the intensity of the vehicle plumes. It also preserves the elevated NO_2 feature. When looking at data filtered with SIBaR, the results look much different. While SIBaR gets rid of much of the noise caused by vehicle plumes, it is clearly too aggressive for this dataset. The elevated NO_2 feature is completely removed, and no large variations in concentration can be found throughout the entire driving intensive. Neither of these methods perfectly filters vehicle plumes from the raw data. The plume-by-plume method, however, dampens influence of local vehicle plumes while preserving more regional concentration variability patterns as opposed to the SIBaR method which

removes nearly all sources of variability in the data set. For these reasons, the plume-by-plume method was chosen to filter the Plume Tracker NO_2 data for all driving intensives.

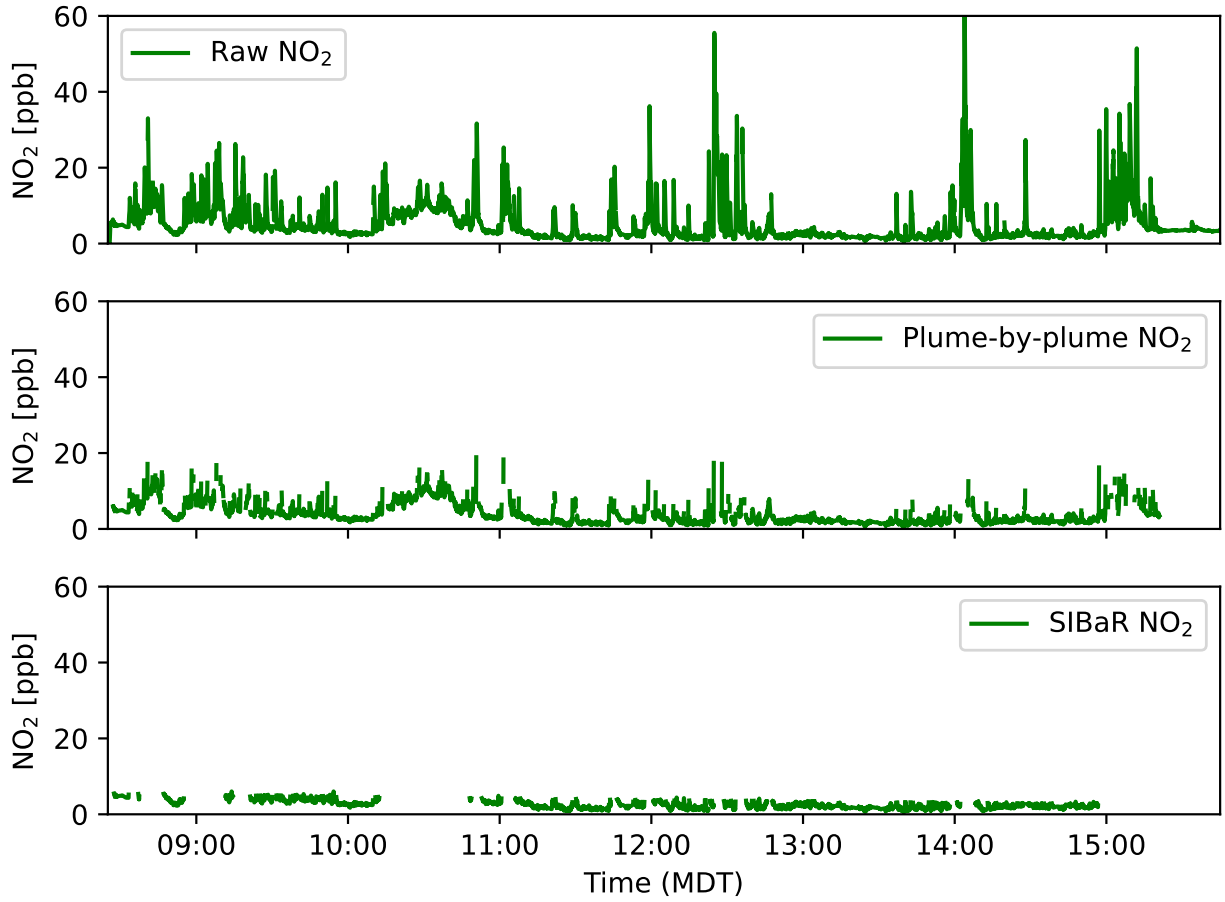


Figure 2.12: Time series plots of raw NO_2 data and filtered NO_2 data using the plume-by-plume and SIBaR methods.

2.7.2 O_3 Filtering Method

O_3 concentrations measured by the Plume Tracker also experienced contamination due to local titration from fresh vehicle NO_x emissions. When vehicles directly in front of the Plume Tracker release fresh NO_x, NO from these plumes reacts with O_3 to yield NO_2. Consequently, every time a vehicle-related spike in NO_2 was observed in the raw data, a corresponding decrease in O_3 was also observed. This poses a challenge for analysis of regional O_3 variability. The filtering process

utilized for O_3 data was rather straightforward. As mentioned above, the plume-by-plume NO_2 filtering method creates data flags for every instance a vehicle plume is identified. Whenever a plume in NO_2 was identified, the corresponding O_3 measurement at the same time step was filtered out. This process successfully removed most of local titration events, but it was not perfect. To remove local O_3 titration events that the NO_2 filtering missed, an adjusted O_3 plume-by-plume filtering method was used. This used the same NO_2 filtration algorithm, except for changing the derivative and fallback thresholds to apply to O_3. Additionally, the algorithm was changed to only identify "negative peaks", or titration events, instead of the usual positive spikes found for NO_2. A range of values was tested for the thresholds for the O_3 plume-by-plume algorithm. The derivative threshold for the O_3 plume-by-plume method was set to -1 ppbv/s, and the fallback threshold was set to -3 ppbv. The sequential plume-by-plume methodology was quite comprehensive and led to increased efficacy in filtering the O_3 data when compared to raw O_3 data, as can be seen in Figure 2.13.

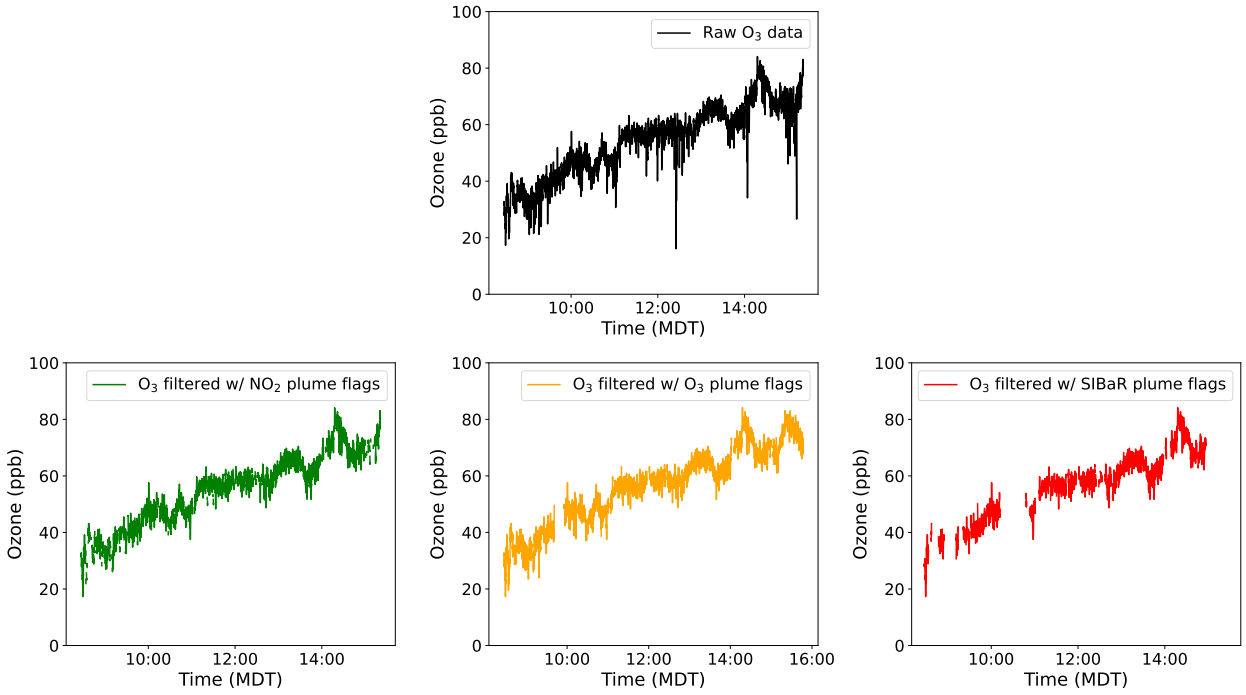


Figure 2.13: Time series plots of raw O_3 data and filtered O_3 data using the NO_2 plume-by-plume method plume flags, the O_3 plume-by-plume plume flags, and the SIBaR method plume flags.

2.8 Statistical Comparison of DICs to Stationary Sites

In each DIC, a canister was collected for VOC speciation. One canister represents a "snapshot" of the concentration of compounds of interest, such as air toxics, in the DICs. This canister was treated as a fixed hypothesized population mean for the community. This single canister measurement was then matched to a single stationary measurement from each of the 6 stationary sites at the same time that the canister was collected. Stationary site measurements were available on an hourly basis, and a strict +/- 1 hr window was used for the stationary site measurements matched to the DIC canister. If a measurement did not exist at a particular stationary site for the time window that the DIC canister was taken, then the site was excluded from the analysis. Once these values were obtained from the stationary sites, the mean (Eq. 2.1), standard deviation (Eq. 2.2), and sample size, n, were calculated for the stationary distribution. For O_3 and NO_2, measurements were taken continuously every 2 seconds during the duration of the DIC sampling periods. As such, a mean was calculated for these compounds for the duration of the time spent in a DIC. For O_3 and NO_2, n=14 and n=13 stationary sites, respectively, were available for the analysis.

$$\bar{y} = \frac{1}{n}\sum_{i=1}^{n} y_i \tag{2.1}$$

where:

$\bar{y}$ = mean concentration across the stationary monitoring sites,
y_i = concentration measured at stationary site i,
n = number of stationary sites included in the comparison.

$$s = \sqrt{\frac{\sum_{i=1}^{n} (y_i - \bar{y})^2}{n-1}} \tag{2.2}$$

where:

s = sample standard deviation of the stationary-site concentrations,
y_i = concentration measured at stationary site i,
$\bar{y}$ = mean stationary-site concentration calculated using Eq. 2.1,
n = number of stationary sites included in the comparison.

In order to examine whether the concentration of a compound measured in a DIC was significantly higher than the mean value measured across the stationary sites, a one-sample t-test was employed, shown in Eq. 2.3. A significance threshold of $\alpha = 0.05$ was chosen. The t-test

used in this analysis is one-tailed for every compound, except for O_3 and the i/n-pentane ratio, where the goal was to assess whether the value measured in the DIC was significantly different (higher or lower) than the mean value measured across the stationary sites. The hypothesis tested for each VOC and NO_2 concentration comparison was that the concentration of that compound was higher at the DIC location (the DIC was more highly burdened) than represented by the mean of the non-DIC stationary site measurements during the same hour. O_3 had a two-tailed t-test applied to examine whether the DIC value was significantly higher or lower than the stationary site mean. For the i/n-pentane ratio, the hypothesis was also that this ratio was significantly different, either higher or lower in DICs than at the stationary sites, because a DIC may be impacted by a multitude of emission sources (e.g., O&G operations, industry, and/or traffic) that may readily push this ratio above (greater combustion influence) or below (greater O&G influence) the mean value measured at non-DIC stationary monitoring sites. One stationary supersite that had online hourly VOC measurements, La Salle Tower (LST), was excluded from comparative analysis due to its very close proximity to O&G operations in a rural area, making it a less representative site for populated areas of the Front Range.

$$t = \frac{\bar{y} - \bar{x}_{\mathrm{DIC}}}{s/\sqrt{n}} \tag{2.3}$$

where:

t = calculated one-sample t-statistic,
$\bar{y}$ = mean concentration across the stationary monitoring sites,
$\bar{x}_{\mathrm{DIC}}$ = mean mobile concentration during the DIC sampling interval,
s = sample standard deviation calculated using Eq. 2.2,
n = number of stationary sites included in the comparison.

3. RESULTS AND DISCUSSION

Analysis of the Plume Tracker measurements during FROZÉ is split into three sections. First, we discuss measurements of air toxics in DICs, as well as plumes encountered at the local scale. Second, mobile NO_2 data will be examined in the context of stationary measurements, satellite observations, and time of day/week at the regional scale. Last, the spatial and temporal variability of O_3 levels measured during Plume Tracker drives will be analyzed to (1) examine whether O_3 variability is important across local to regional scales and (2) assess important factors associated with any observed variability.

3.1 DIC Air Quality and Local VOC Plumes

3.1.1 Air Toxics & Criteria Air Pollutant Monitoring in DICs

A map of DICs visited by the Plume Tracker can be found in Figure 3.1. Information on the Enviroscreen scores, as well as demographic criteria, met by each community are shown in Table 3.1. Three communities were sampled in the northern Denver metropolitan area (Montbello, Adams Heights, Federal Heights). Two communities were located near the foothills (Loveland, Longmont). The remaining seven communities were spread across a region of abundant O&G operations, mostly in Weld County. The southern extent of this area was represented by three communities (Brighton, Fort Lupton, Dacono). There was also a cluster of four sampled communities near Greeley, where Enviroscreen scores were quite high (>95% for most of the area) with little to no prior air toxics monitoring.

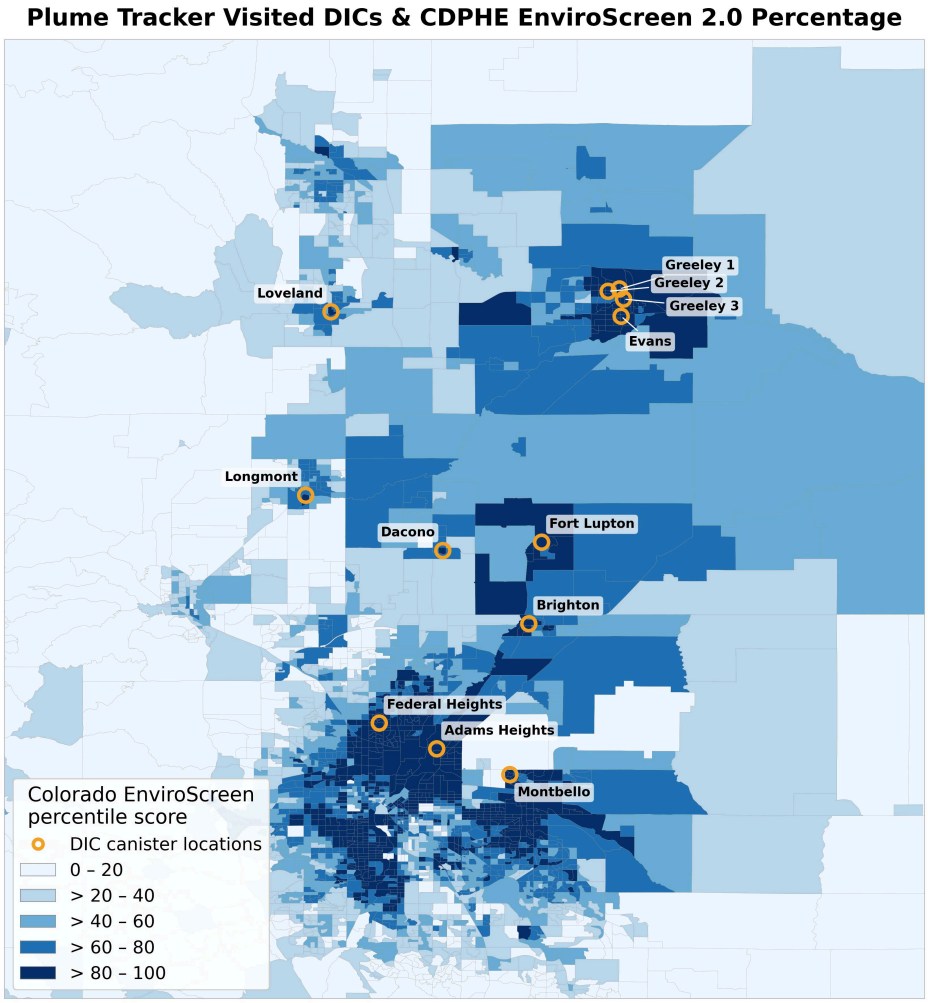


Figure 3.1: Plot of DICs sampled by the Plume Tracker during FROZÉ and their associated CDPHE Enviroscreen 2.0 percentages. Three Greeley DICs sampled are labeled as Greeley 1, 2, and 3.

To provide context, the VOC concentrations in the canisters collected in each DIC were compared to hourly VOC measurements from stationary, online GC systems operated at 6 sites across the Front Range: Fort Collins West (FTCW), Longmont Union Reservoir (LUR), Broomfield Soaring Eagle Park (BSE), Broomfield North Pecos (BNP), Rocky Flats North (RFN), and Sheridan/Fort Logan (SHER). FTCW, RFN, and SHER were all FROZÉ field campaign supersites. LUR, BSE, and BNP are all part of the Boulder Air monitoring network, supported by the City of Longmont and the City and County of Broomfield. The locations of these stationary sites and the canisters collected in DICs are shown in Figure 3.2. Comparison of air toxics observed in DICs

Table 3.1: Information on DICs sampled by the Plume Tracker during FROZÉ, as well as legal criteria met for each community, according to Colorado Revised Statute § 24-4-109.

DIC	Latitude	Longitude	EnviroScreen 2.0 Score (%)	>40% low income households	>40% of population identifies as people of color	>50% housing cost burdened households	>20% linguistically isolated
Adams Heights	39.82548	-104.93625	97.92	✓	✓		
Brighton	39.98855	-104.81618	93.08	✓	✓	✓	
Dacono	40.0873	-104.92798	86.39		✓		
Evans	40.38939	-104.6958	94.10	✓	✓		
Federal Heights	39.85908	-105.01117	96.23	✓	✓	✓	
Fort Lupton	40.08157	-104.82441	95.98	✓	✓		
"Greeley 1"	40.42502	-104.69804	99.60	✓	✓	✓	
"Greeley 2"	40.42192	-104.71274	97.40		✓	✓	
"Greeley 3"	40.41180	-104.69267	97.97	✓	✓		
Longmont	40.16112	-105.1026	81.98	✓	✓		
Loveland	40.39443	-105.08063	80.42	✓		✓	
Montbello	39.79188	-104.84088	94.57	✓	✓		

to simultaneous measurements at the these stationary sites, all located in non-DIC Front Range population centers, is to assess whether the current VOC monitoring network in the Front Range is representative of air toxics concentrations present in DICs where VOC monitoring is scarce or nonexistent. This is important because these DICs are home to vulnerable populations and prior work has attributed higher Enviroscreen 2.0 scores to increased risks of mortality at the county level (Pusker et al., 2024).

Figure 3.3 compares VOC concentrations measured in each DIC with distributions of VOC concentrations measured during the same hour at the 6 stationary monitors. Comparisons are shown for select air toxics and other VOCs of interest, including BTEX (benzene, toluene, ethylbenzene, xylene), n-hexane, ethane, and the i/n-pentane ratio. Each comparison represents a "snapshot" in time for a particular DIC. The DIC canister concentration value is plotted as a star on top of a box plot representing the variability measured during the same hour across the six non-DIC stationary VOC monitors. A same-hour comparison is critical because changes in emissions and meteorology cause substantial changes in VOC concentrations across time (see, for example, Ku et al., 2024). Twelve different DICs were sampled. Fifteen comparisons are presented since the Evans, Fort Lupton, and Longmont DICs were sampled twice (day and night). A t-test (see Section 2.8) was

used to determine the significance of observed DIC canister compound values when compared to the mean of the stationary sites. The concurrent measurements at all 6 stationary sites constituted our samples, and the DIC canister values were treated as the hypothesized population mean. A significance threshold of $\alpha = 0.05$ was chosen. The t-test used in this analysis is one-tailed for every compound, except for O_3 and the i/n-pentane ratio. The hypothesis tested for each compound comparison was that the concentration of a particular compound was higher at the DIC location (the DIC was more highly burdened) than represented by the mean of the non-DIC stationary site measurements during the same hour. O_3 had a two-tailed t-test applied due to the possibility of O_3 titration from fresh NO_x emissions. For the i/n-pentane ratio, the hypothesis was that this ratio was either higher or lower in DICs than at the stationary sites, based on an assumption that each DIC is in proximity to a multitude of emission sources (e.g., O&G operations, industry, and/or traffic) that may readily change this ratio. One more stationary supersite that had online hourly VOC measurements, La Salle Tower (LST), was excluded from comparative analysis due to its very close proximity to O&G operations in a rural area, making it a less representative site for populated areas of the Front Range.

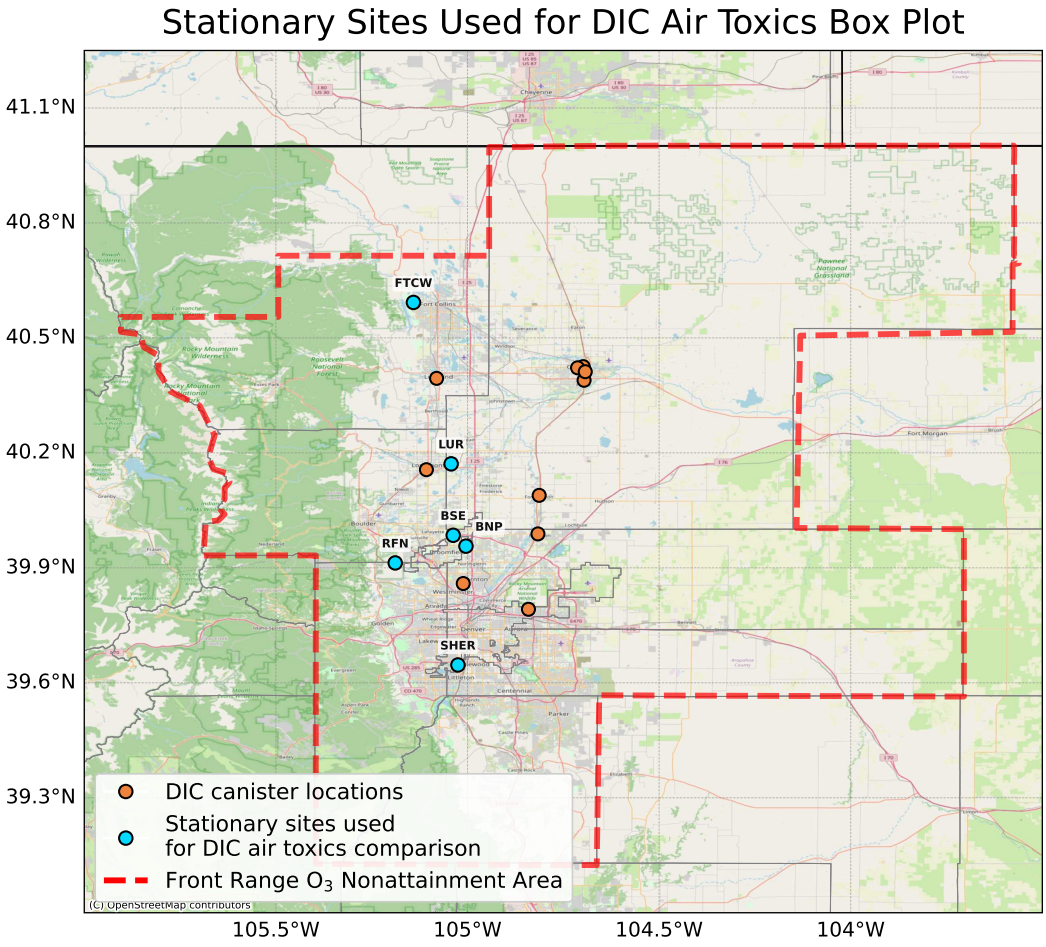


Figure 3.2: Locations of stationary online VOC measurement sites relative to the locations of canisters deployed by the Plume Tracker in DICs.

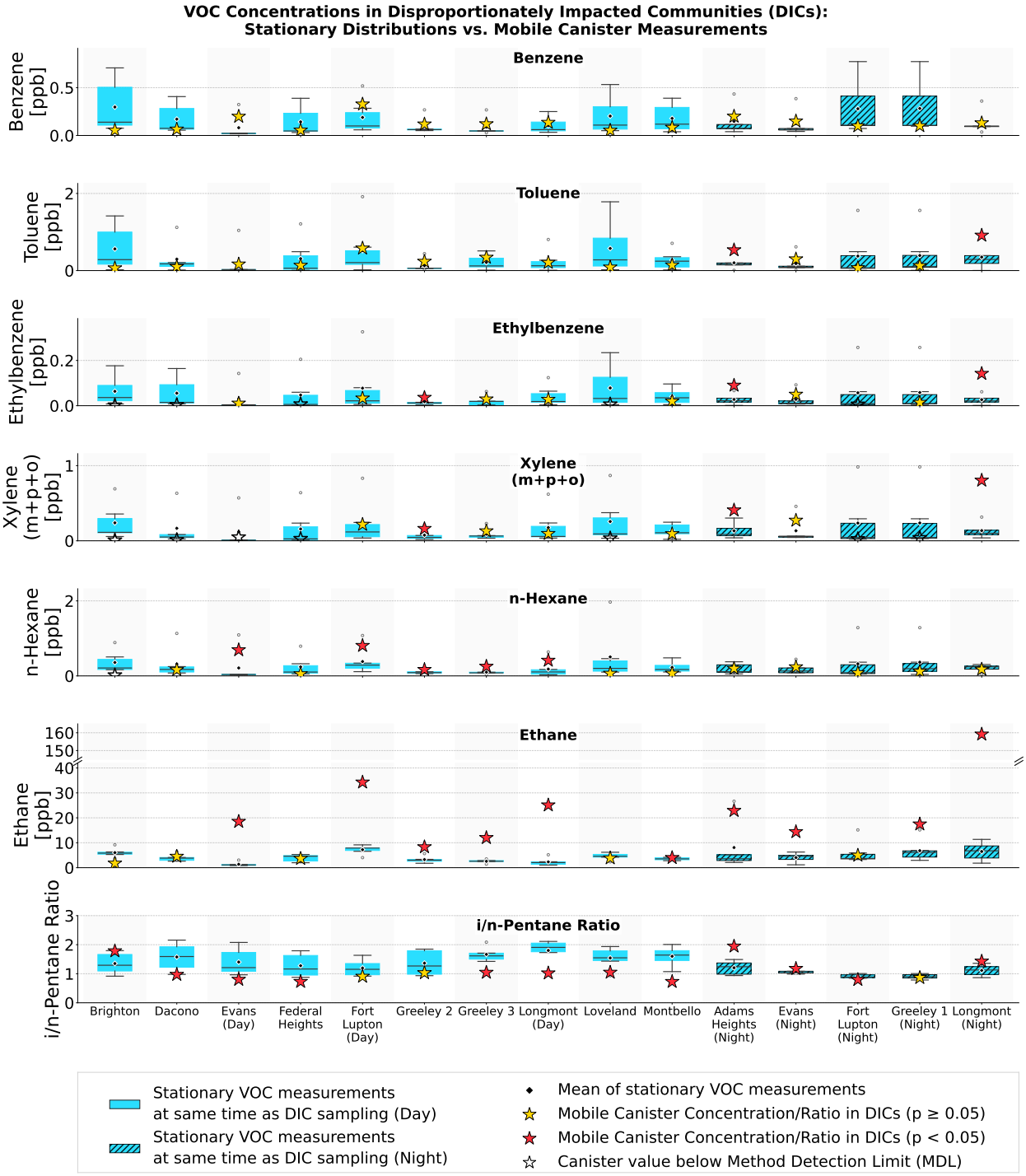


Figure 3.3: Box and whisker plots showing the distribution of hourly VOC stationary measurements at the same date and hour that a mobile canister was collected in a particular DIC (represented by a star). Red (yellow) stars indicate a statistically (in)significant difference between the stationary measurements and DIC canister. The small diamond shape inside the boxes indicates the mean of the stationary sites, while the horizontal line is the median. The whiskers indicate 1.5*IQR. Longmont (Night) and Adams Heights (Night) samples were taken in a plume.

Benzene, a carcinogenic aromatic compound associated with emissions from a variety of sources, including O&G operations, traffic, fueling stations, biomass burning, and solvent evaporation, was the highest priority air toxic to examine since prior work in the region has shown it to approach levels of potential concern with respect to cancer and non-cancer health effects (Kim et al., 2026; Ku et al., 2024) and some DICs examined were close to O&G operations (Chiavarini et al., 2024; Weisel, 2010). Although the sample size here is small, benzene was not found to be significantly higher in any of the sampled DICs than the non-DIC stationary site mean. Measured DIC benzene values were also lower than the benzene U.S. Agency for Toxic Chemicals and Disease Registry (ATSDR) acute health guideline value (HGV) of 9 ppbv.

Toluene is also a carcinogenic aromatic, and emissions come mainly from combustion, petroleum operations, and its use as a cleaning solvent (Cohr and Stokholm, 1979; Fishbein, 1985a). Toluene was significantly elevated in two of 15 sampled DICs, Adams Heights and Longmont. Both of these communities were sampled at night. Adams Heights is in close proximity to a major oil refinery, while the Longmont sampling location has nearby O&G and manufacturing operations. Despite being significantly elevated, the toluene concentrations in these DICs were still below 1 ppbv, well below the ATSDR acute HGV of 2000 ppbv. Ethylbenzene is a carcinogenic aromatic that also irritates the skin and mucus membranes, and can have narcotic effects at high concentrations (Fishbein, 1985b; Saeedi et al., 2024). Ethylbenzene is primarily emitted from vehicle exhaust and solvent use (Das et al., 2025). In our sampling periods, ethylbenzene was found to be significantly elevated in three of 16 DICs: Adams Heights, Longmont, and Greeley 2. Greeley 2 was the only DIC sampled during the day to have significantly elevated ethylbenzene. Similar to toluene, the concentrations of ethylbenzene measured in DICs, as well as from the stationary sites, were low (rarely reaching above 0.2 ppbv) and all well below the ethylbenzene ATSDR acute HGV of 5000 ppbv. Xylene is another aromatic hydrocarbon that poses threats to human health in excess concentrations. While not currently thought to be carcinogenic, xylene can cause health effects via the central nervous system (T. Rajan and Malathi, 2014). Primary emission sources include O&G operations, as well as paints, dyes, varnishes, and medical technology (Niaz et al., 2015). Xylene (m+p+o) was significantly elevated in the same three DICs as ethylbenzene. Especially

notable was the nighttime value measured in Longmont. The concentrations of xylene at both DIC and stationary site locations, however, were very low compared to the ATSDR acute HGV of 2000 ppbv. While none of the DIC measurements indicated the presence of air toxics exceeding acute exposure guidelines, the sample size was limited. Even so, we did find cases where DIC air toxics concentrations significantly exceeded the mean value from non-DIC monitors, pointing to the importance of future DIC representation in Front Range air toxics monitoring.

Concentrations of hexane, ethane, and the i/n-pentane ratio in DIC and non-DIC locations are also shown in Figure 3.3. Hexane is an alkane primarily emitted by O&G operations, as well as industrial processing, due to its ability to thin and dissolve oils (Hamilton and Schaffer, 2026; Li et al., 2017). Hexane can also cause health effects via the central nervous system if inhaled in sufficient amounts (Hamilton and Schaffer, 2026). In the Colorado Front Range, hexane has been measured in enhanced concentrations in residential communities near O&G operations (Thompson et al., 2014). Hexane was found to be significantly elevated in five of 15 sampled DICs when compared to the non-DIC stationary site mean. These five DICs were all sampled during the daytime and were near abundant O&G operations in the Denver-Julesburg Basin. Our results are consistent with previous studies that measured a mean hexane concentration of around 1 ppbv at various locations in the Front Range (Gilman et al., 2013; Swarthout et al., 2013; Thompson et al., 2014). All measured hexane concentrations were below the EPA acute HGV of 5400 ppbv.

Ethane is an alkane primarily emitted by O&G operations, and has been measured at relatively high concentrations in many parts of the Front Range near O&G wells (Gilman et al., 2013; Smith et al., 2015). As such, the presence of elevated ethane can also be used as an indicator of O&G emissions impacts in DICs in our study. Ethane was significantly elevated in 10 of 15 sampled DICs when compared to the non-DIC stationary site mean, revealing a substantial DIC impact from O&G emissions. Measured ethane concentrations varied quite a bit, but were highest in the Longmont DIC at night, where ethane exceeded 159 ppbv. This high concentration was intercepted from a plume that we repeatedly observed in Longmont both during the day and night, to be discussed in more detail further on. The i/n-pentane ratio can help to distinguish emission source contributions. i-pentane is primarily released by gasoline vapors and vehicle exhaust, and n-pentane is more

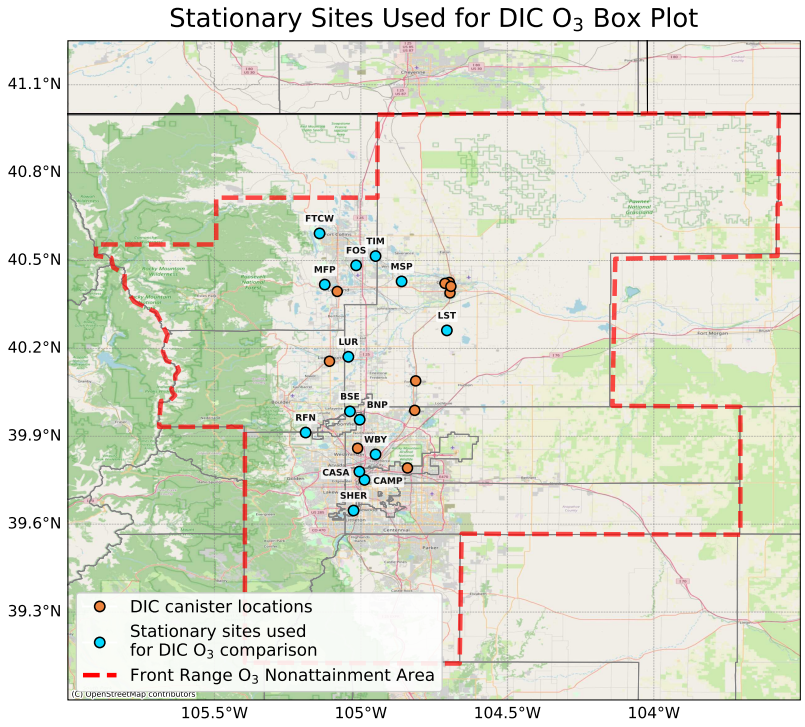
indicative of thermogenic sources (Rossabi and Helmig, 2018). Values of the i/n pentane ratio below 1.0 are typically associated with strong influence from O&G emissions and values near 2.0 are typical of combustion/traffic emissions (Gilman et al., 2013; Johnston et al., 2021; Pollack et al., 2021a; Rossabi et al., 2021). Intermediate values typically reflect a mix of O&G vs. traffic emissions. Nine of the DICs had significantly lower i/n-pentane ratios compared to the stationary sites, while three had significantly higher i/n-pentane ratios. The lowest i/n-pentane ratio measured in DICs was ~0.7 in Montbello. This result was surprising, as Montbello is not as close to O&G sources as some of the other communities we sampled. The highest i/n-pentane ratio measured in DICs was ~2 in Adams Heights, which is in the Denver metro area and in close proximity to the Suncor Energy Refinery in Commerce City, CO. Other than Adams Heights, Brighton, and Longmont (night), most of the DICs had a relatively low i/n-pentane ratio compared to the non-DIC stationary site mean, which increases our confidence that O&G emissions have a disproportionate influence in these already-burdened communities. The overall mean i/n-pentane ratio measured in DICs in our study was 1.08, similar to a previous study that measured a mean i/n-pentane ratio of 1.01 in Northern Colorado communities (Thompson et al., 2014).

O_3 and NO_2 were also measured in the 15 DIC sampling periods to assess whether the stationary sites in the Front Range that measure O_3 and NO_2 are representative of what is observed in all communities. O_3 and NO_2 are both criteria pollutants with well-established health impacts (Pandey and Singh, 2021). Mean O_3 and NO_2 concentration values measured in DICs, typically during 30-45 minute drive periods, were compared to same-hour stationary site measurements. Available stationary site numbers for O_3 and NO_2 totaled 14 and 13 sites, respectively (see Figure 3.4). Box and whisker plots of the distributions of same-hour stationary site O_3 and NO_2 are compared to the mean measured concentrations in DICs in Figure 3.5.

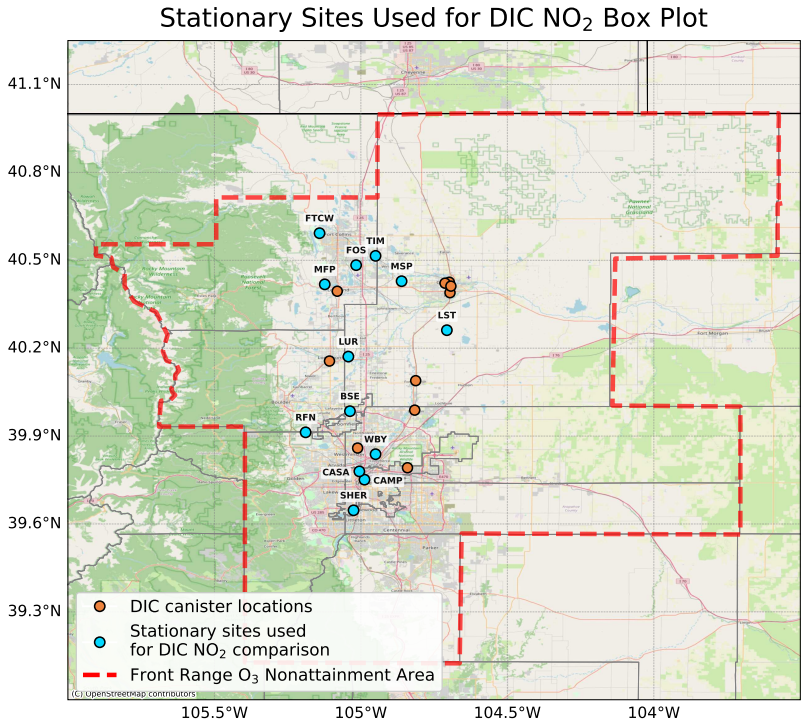
DIC O_3 concentrations were significantly elevated relative to the mean stationary monitoring site concentrations in only 1 of 15 sampling periods. Focusing on daytime samples, when elevated O_3 is likely to be of greatest concern, we see a tendency (7 of 10 cases) for DIC O_3 values to fall below the stationary site mean. While O_3 exposure in DICs is an understudied topic in the literature, a few studies have focused on this issue explicitly. Bravo et al. (2016) found that O_3 scales

positively with increasing racial isolation, while Winter et al. (2019) did not find any significant trend in O_3 across communities. Our measurements represent only short snapshots of O_3 across DIC and non-DIC communities and more extended observations would be valuable. Our initial results, however, indicate that O_3 exposure in DICs in Northern Colorado may be lower than at regional O_3 monitoring sites, suggesting one possible case where the burden of pollution might be reduced relative to other communities.

For NO_2, only 13 sampling periods were available from DICs due to instrument malfunction. NO_2 was significantly elevated in two of 13 DICs (Federal Heights and Longmont, both samples during daytime) when compared to the mean value from stationary sites. All measured values were well below the 1-hour NO_2 NAAQS of 100 ppbv. An important consideration for this analysis is that we used filtered NO_2 data to remove local, on-road plume interference. This may lead to a low bias in measured NO_2 concentration in DICs used for this analysis. The magnitude of the unfiltered NO_2 data in DICs was also checked and can be found in Figure A.2. The fact that NO_2 was observed to be higher in some DICs is consistent with previous work (Houston et al., 2004; Sexton et al., 1993; Su et al., 2011, 2024).



(a)



(b)

Figure 3.4: Map of O_3 stationary sites (a) and NO_2 stationary sites (b), as well as DIC canister deployment locations.

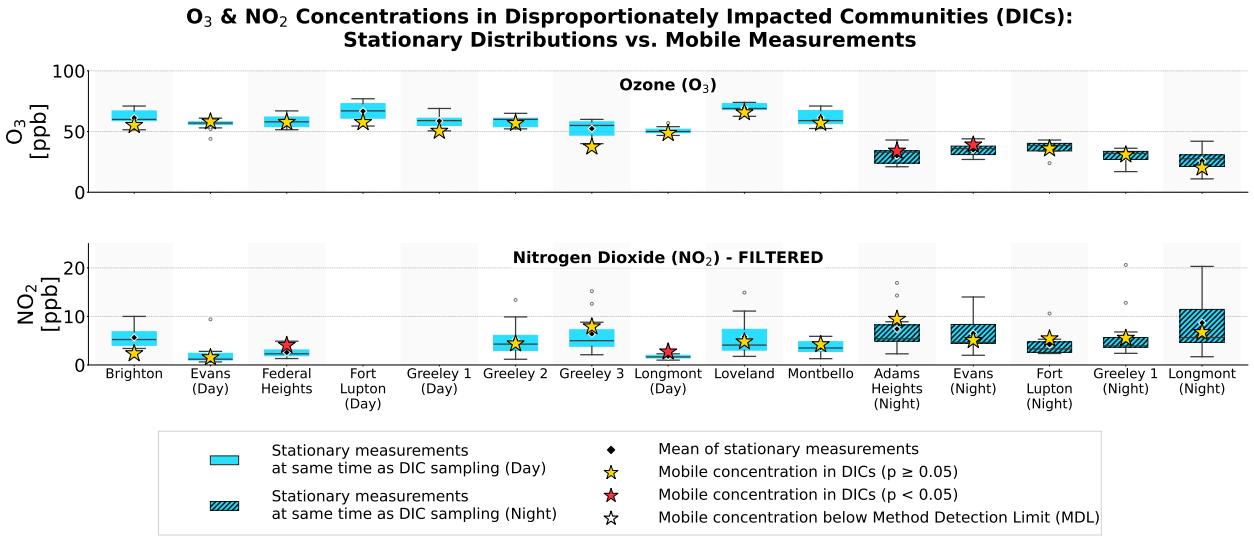


Figure 3.5: Box and whisker plots of hourly stationary site concentrations for O_3 (top) and NO_2 (bottom) compared to the mean concentration of these compounds in DICs measured by the Plume Tracker. Red (yellow) stars indicate a statistically (in)significant difference between the stationary measurements and DIC canister. The small diamond shape inside the boxes indicates the mean of the stationary sites, while the horizontal line is the median. The whiskers indicate 1.5*IQR.

3.1.2 Case Studies of Notable Local Plumes

A substantial VOC plume was intercepted several times in the Longmont DIC during a nighttime drive on August 14-15, 2025. A canister sample from this plume (see Figure 3.3) contains the highest toluene, ethylbenzene, xylene, and ethane concentrations measured in a DIC. This plume was first encountered by the Plume Tracker near several warehouses at 2:05 AM MDT. A map of ethane concentrations from the MIRA Ultra can be seen in Figure 3.6. The plume was intercepted five times, with ethane concentrations exceeding 100 ppbv each time. While the plume was first seen near warehouses, it was also detected near residential duplexes soon afterward. The wind was blowing from the north during sampling, potentially indicating an emission source across the Saint Vrain River, where a number of industrial manufacturing facilities are located. The canister sample included in Figure 3.3 was collected during the final encounter with the plume and analyzed for 51 VOCs. The results of this analysis are shown in Figure 3.7. Also shown in this figure are box and whisker plots of averages for each species over the FROZÉ study period obtained from several weekly VOC measurement sites in Broomfield, CO. In addition to ethane, there were

elevated concentrations of other light alkanes in the Longmont DIC canister when compared to the Broomfield weekly observations. Also of note were elevated levels of alkenes and aromatics, especially toluene, ethylbenzene, and xylene. Benzene, on the other hand, was comparable to the Broomfield weekly observations. The toluene to benzene ratio in the canister was high (~7), suggesting a possible nearby combustion source (Gelencsér et al., 1997). Elevated concentrations of alkenes and aromatics also support the idea that the source may have been combustion-related, while elevated light alkane concentrations suggest an O&G influence (Cardoso-Saldaña et al., 2019). It is possible that this plume was composed of emissions from multiple local sources. While this plume was sampled at night, we are fairly certain that this plume represents an ongoing emission source during the day as well, as it was first identified during a daytime drive on July 27, 2025. Longmont has a number of monitoring sites on the outskirts of the town, but none in the DIC we sampled, where there were numerous residential communities. Our observations highlight the importance of expanding monitoring in DICs where important sources may go undetected and elevated exposures may occur.

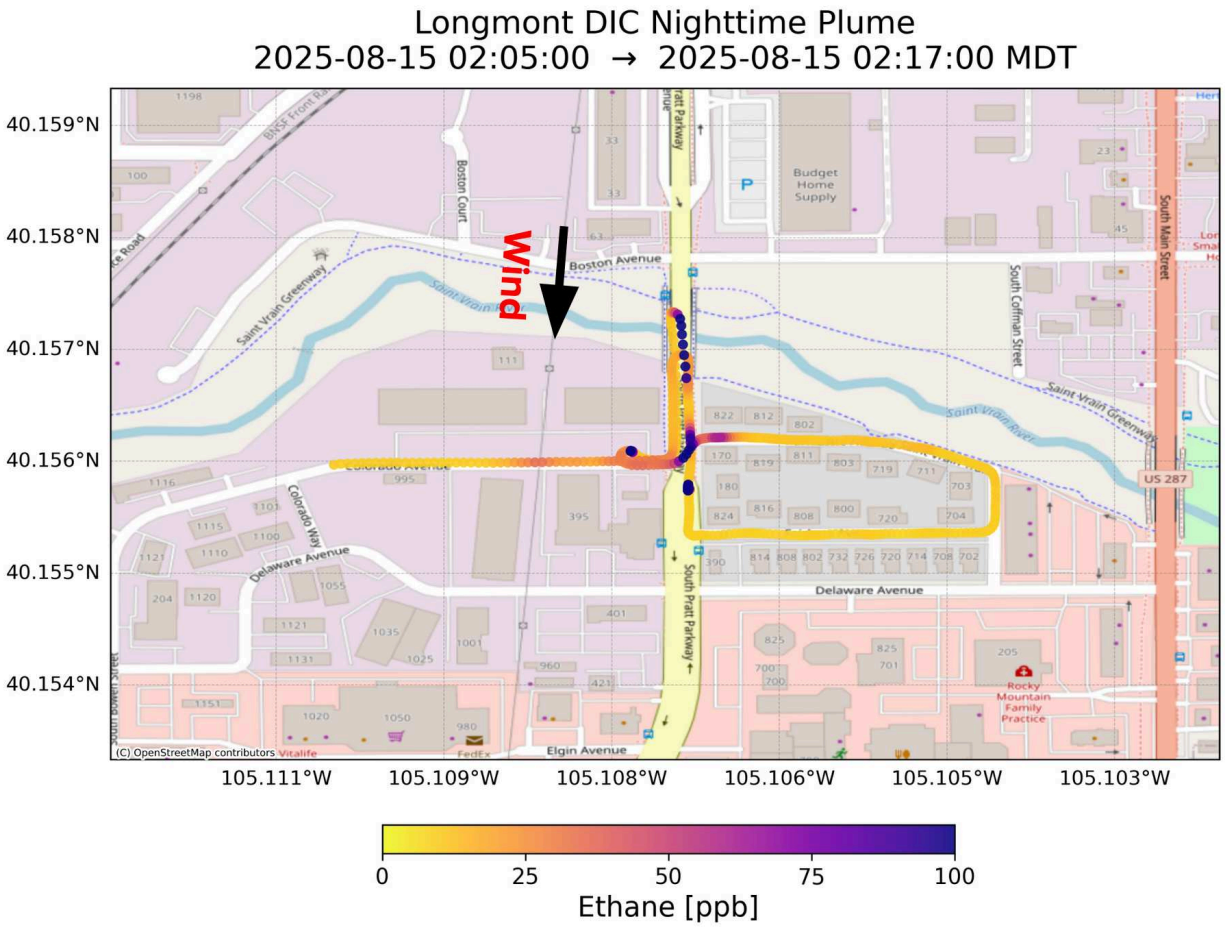
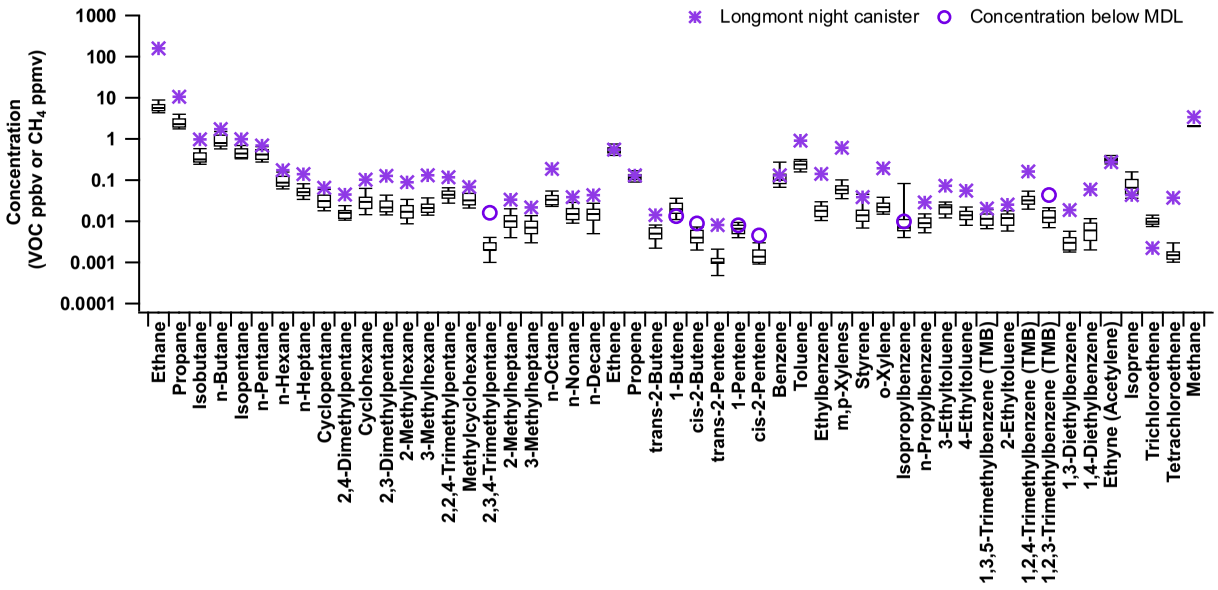


Figure 3.6: Map of ethane concentrations from the Longmont DIC plume on August 15, 2025. The black arrow depicts the wind vector at the time of sampling.



*The box plot summarize weekly observations from Jun to August (2025) from the Broomfield site as comparison.

Figure 3.7: Box and whisker plots of averaged concentrations over the study period (June 1-August 31, 2025) for 51 VOCs from several sites in Broomfield, CO. The purple stars plotted for each compound are the canister concentrations for each species from the Longmont DIC plume on August 15, 2025.

Another notable plume was detected in a DIC in Fort Lupton sampled during a nighttime drive on July 31-August 1, 2025. NO_2 measurements from the Teledyne CAPS revealed enhanced concentrations of NO_2 on U.S. Route 85, where there were a number of diesel trucks, while approaching Fort Lupton. Soon after DIC sampling began, it was clear that NO_2 concentrations were enhanced in the eastern side of the DIC, as shown in Figure 3.8. NO_2 concentrations ranged from ~7-11 ppbv in the eastern side of the DIC and decreased below 5 ppbv in the western section. As a result, NO_2 concentrations were nearly doubled in some parts of the community when compared to the background NO_2 concentration in the region. The wind was from the northwest during sampling, consistent with transport from U.S. 85. NO_2 concentration elevations were sustained over a broad region, suggesting they did not come from a single vehicle plume. The elevated NO_2 in this DIC appears to reflect transport of highway emissions into the adjacent residential area. The measured values of NO_2 in this DIC were below the 1-hour NO_2 NAAQS of 100 ppbv, but the presence of elevated NO_2 levels in a disadvantaged community remains concerning. While our measurements only constitute ~1 hour of sampling at night in this DIC, they again point to a need for longer-term monitoring in DICs. Fort Lupton currently has no air quality monitoring sites.

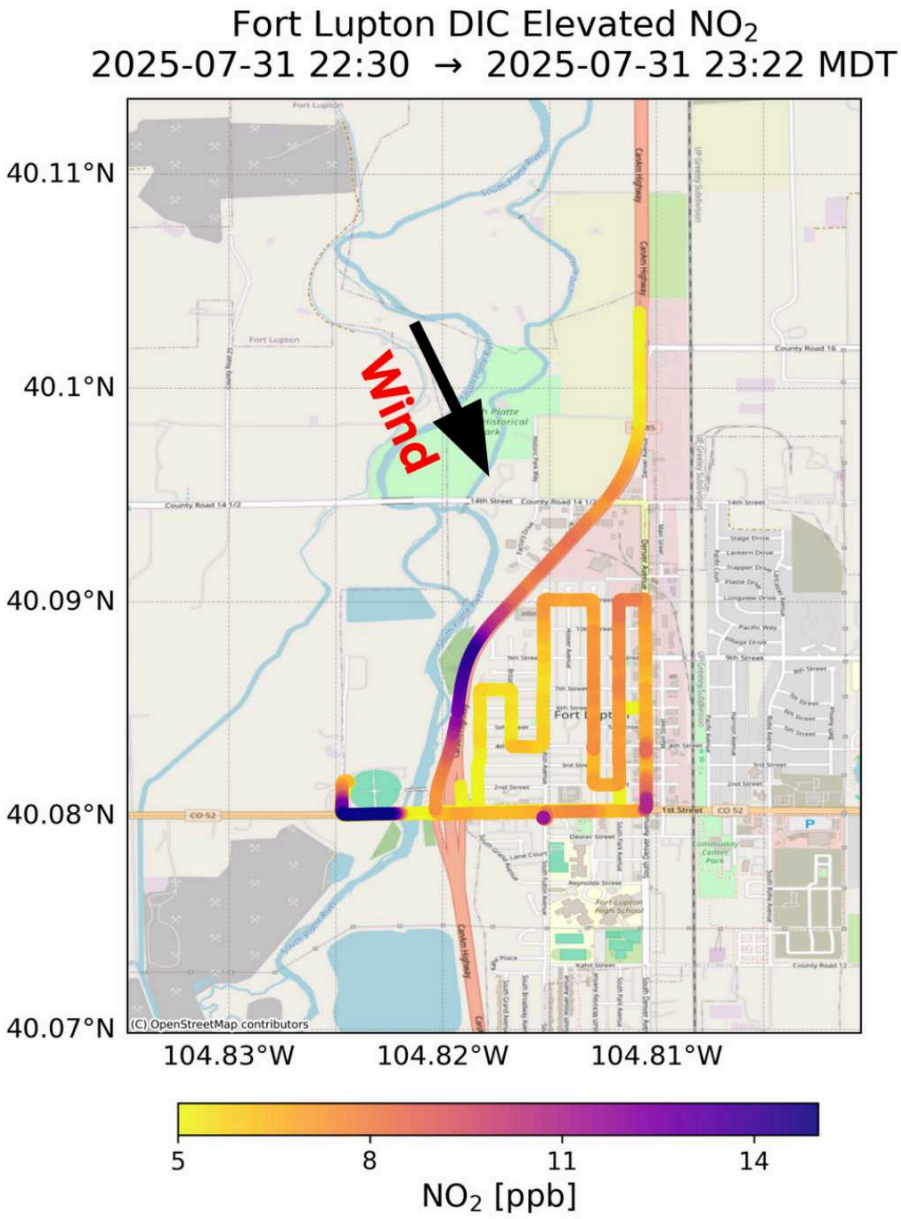


Figure 3.8: Map of NO_2 concentrations before, during, and after sampling a Fort Lupton DIC on July 31, 2025. The black arrow depicts the wind vector at the time of sampling.

A final notable plume case study is during a nighttime drive on July 31-August 1, 2025 of a gas leak from an O&G facility located next to County Road 31 in Weld County, CO, northwest of Greeley. While driving in a rural area after sampling a DIC in Greeley, ethane concentrations suddenly spiked to 950 ppb, and methane concentrations reached 23 ppm. A map of ethane concentrations associated with this plume can be seen in Figure 3.9. We spent nearly half an hour intercepting this plume multiple times, and found that it was consistently present in one location. Wind was directly from the north during sampling. Two O&G facilities were very close upwind of the plume on the side of the road. A canister was collected when intercepting the plume. After analysis, the canister was deemed rather "clean", except for a large presence of methane and ethane, suggesting that these O&G facilities may have been distribution centers for processed natural gas. We reported the gas leak to Weld County officials, who informed us that the operators were aware of the leak. This was a special case in which an observed natural gas leak was already identified but had not yet been addressed. There are many leaks that operators may not be aware of, especially in DICs (Weller et al., 2022). Mobile monitoring platforms, such as the Plume Tracker, are very important for quick identification of these leaks so that unintended greenhouse gas emissions can be reduced and residential exposure can be limited (von Fischer et al., 2017; Hendrick et al., 2016). No other natural gas leaks of this magnitude were identified during the FROZÉ campaign.

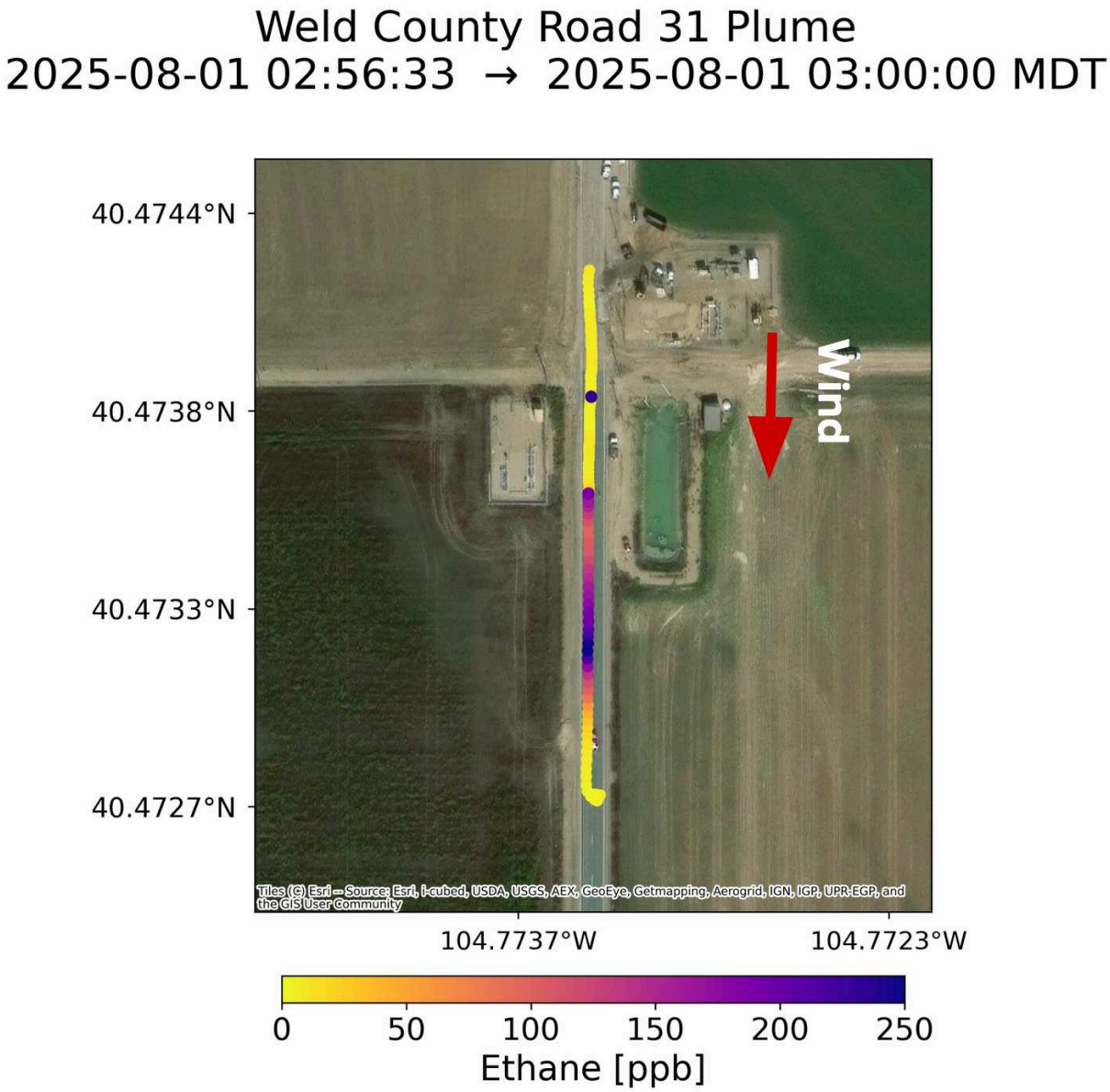


Figure 3.9: Map of ethane concentrations from a gas leak on County Road 31, northwest of Greeley, CO on August 1, 2025. The black arrow depicts the wind vector at the time of sampling.

3.2 Regional Scale Mobile Measurements

3.2.1 Mobile NO_2 Measurements in the Colorado Front Range

NO_2 measurements were taken every second for the duration of 11 driving intensives. Maps of filtered NO_2 concentrations during the day and night from the drives are shown in Figures 3.10 and 3.11, respectively. Regional NO_2 hotspots aligned with known combustion sources, such as traffic near population centers, during both daytime and nighttime sampling. NO_2 hotspots were most pronounced near Fort Collins, Greeley, and Denver. The highest sustained NO_2 concentration intercepted by the Plume Tracker was 15 ppbv on CO Highway 14, where there was traffic congestion entering Fort Collins. There were also a number of NO_2 hotspots on U.S. Route 85, where there were many diesel trucks present. These results are consistent with previous studies in both Colorado and Utah, which found increased NO_x near population centers and busy roads (Guevara Proaño, 2025; Wild et al., 2017).

It is important to note that we only had NO_2 measurements on-board the Plume Tracker. While NO_2 from fresh NO_x emissions is apparent in the data, NO_2 can also increase as NO_x emissions age. An interesting feature is elevated NO_2 levels in far northern Colorado, near Soapstone Prairie Natural Area. This area was sampled on July 14, a day with strong southerly flow, and will be discussed further in the O_3 case studies section. As such, the data in Figures 3.10 and 3.11 are not meant to be representative of the entire region in time nor space. Rather, they represent a series of snapshots of intercepted NO_2 on specific days that had varying meteorology and emissions. Consistent emission sources, such as those from traffic, however, may be gleaned in this analysis and highlight important sources of NO_2 in the Front Range.

Nighttime NO_2 levels were generally more concentrated and localized near sources than during the day. Nighttime NO_2 levels were higher (~10-15 ppbv) in the southern half of mobile sampling, closer to Denver. Conversely, NO_2 levels were lower (~2-8 ppbv) at night in the northwest section of mobile sampling, north of Longmont and west of Greeley. These spatial patterns in nighttime NO_2 are consistent with areas of heightened traffic (especially trucks). An additional NO_2 hotspot can be seen in Longmont at night that was not as pronounced during the day. While we only

performed two driving intensives at night, these observations seem to suggest less overall NO_2 levels at night, but more elevated levels nearer to sources. Plumes are easier to identify at night due to less dilution from atmospheric mixing due to a lower boundary layer, and this was consistent with our mobile NO_2 observations (David and Nair, 2011). Another factor in observing lower NO_2 concentrations at night could potentially be due to less NO to NO_2 conversion during night when there are lower O_3 and RO_2 radical concentrations.

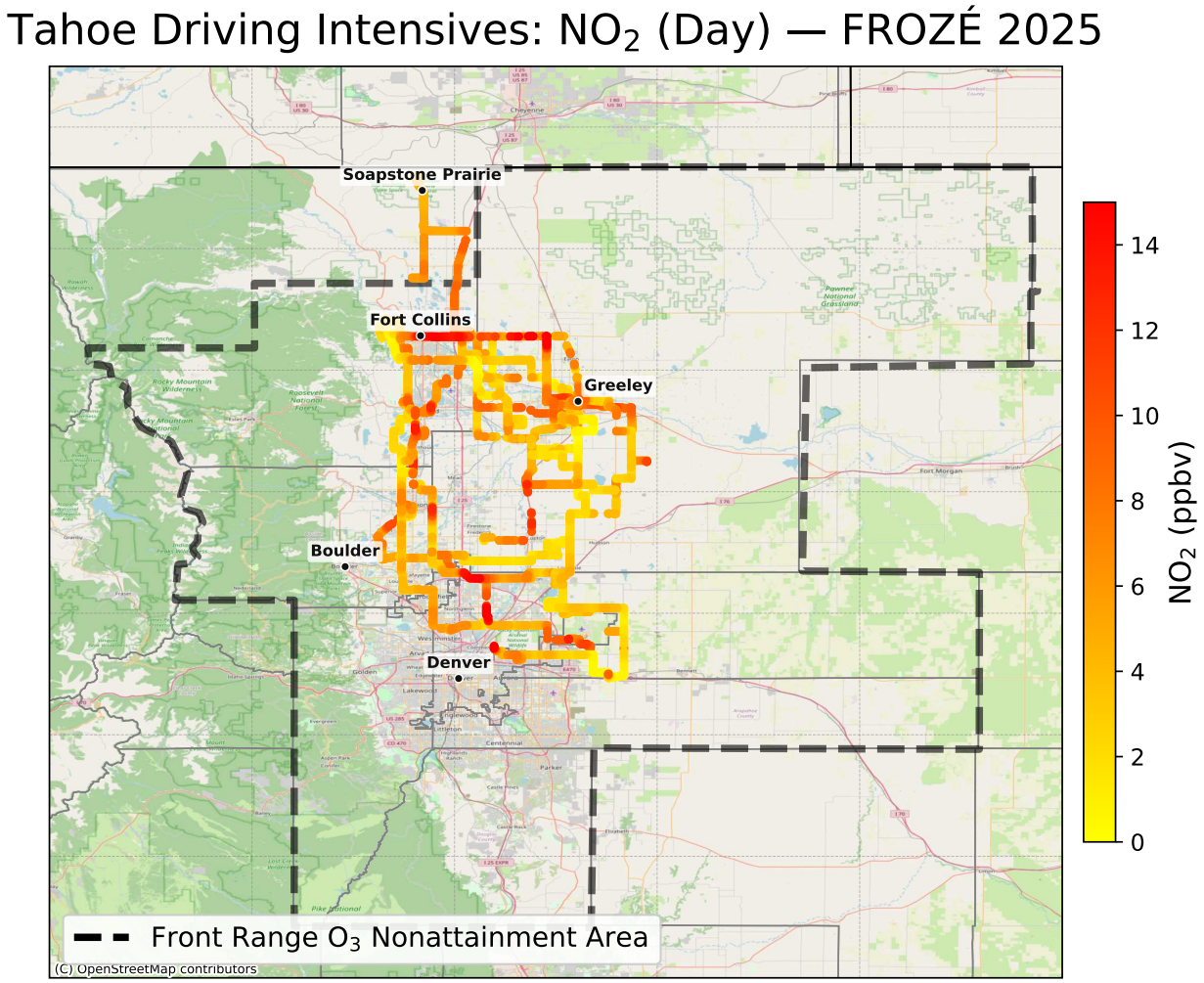


Figure 3.10: Map of filtered NO_2 concentrations measured by the Plume Tracker during daytime driving intensives. A 1-min rolling average was applied to the data to reduce instrument noise.

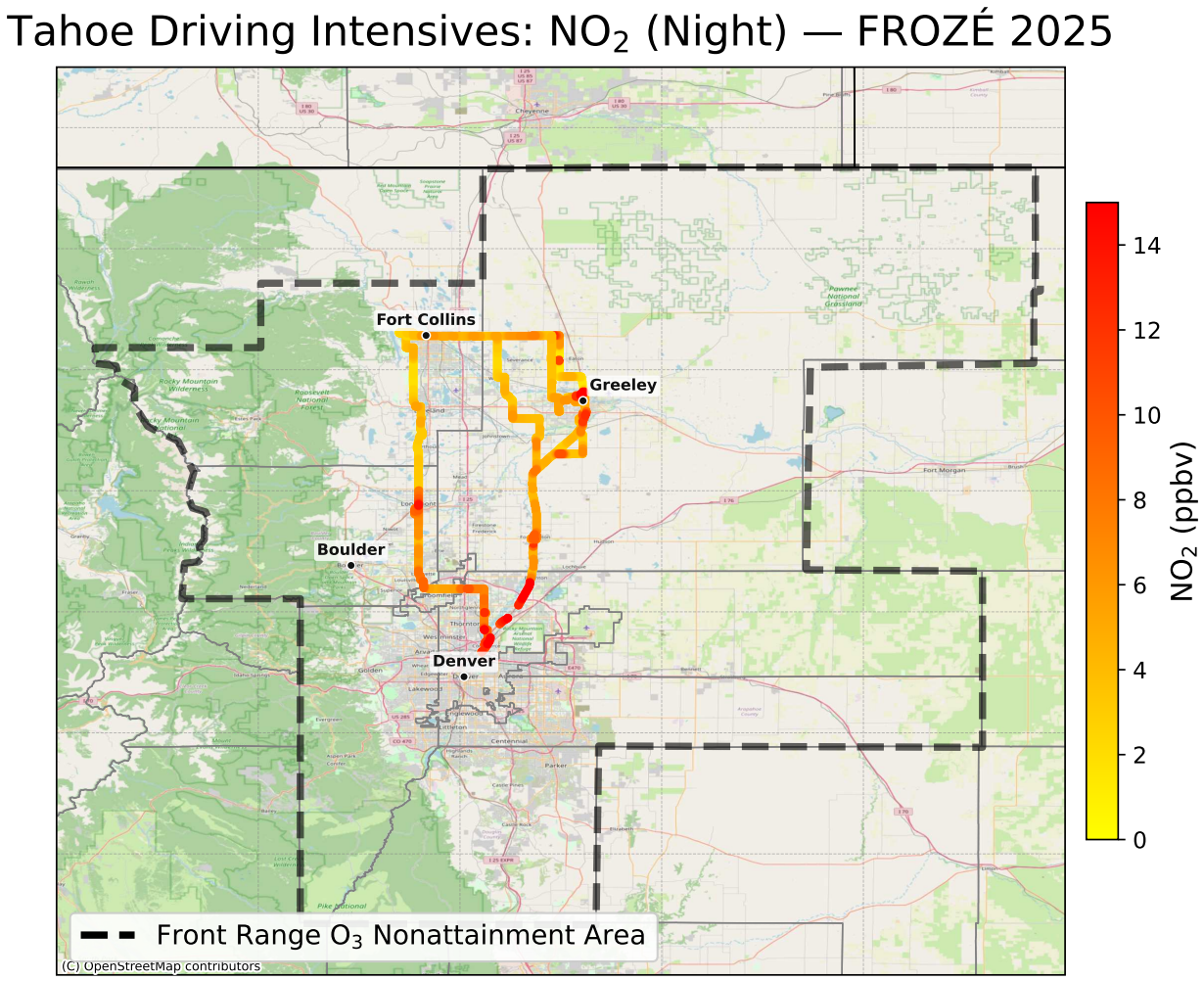


Figure 3.11: Map of filtered NO_2 concentrations measured by the Plume Tracker during nighttime driving intensives. A 1-min rolling average was applied to the data to reduce instrument noise.

To contextualize the mobile NO_2 measurements, TEMPO and stationary site NO_2 data were added. Plots of these comparisons for the nine daytime driving intensives are shown in Figure 3.12. The TEMPO instrument malfunctioned during the August 4 driving intensive, but stationary site data were still available. The spatial alignment of surface and TEMPO NO_2 data was quite variable. On the August 18 and 19 driving intensives, mobile NO_2 observations indicate a swath of high values (10-15 ppbv) in the Northern Front Range, especially on CO Highway 14. Stationary site data appear rather lower (~5-6 ppbv) on these two days, but are still elevated compared to other

days where TEMPO NO_2 is similarly low. Despite the indication of higher NO_2 values to the north, TEMPO NO_2 data seem to miss this apparent surface enhancement of NO_2. Similarly, on August 12, mobile NO_2 measurements increased to 11 ppbv in the vicinity of Denver International Airport, but TEMPO NO_2 data do not seem to pick up this increase. Disagreements might reflect differences in vertical distributions of NO_2; the drives and stationary sites sample surface NO_2 while TEMPO measures vertically-integrated NO_2 columns above the surface. Additionally, there are some TEMPO NO_2 column features that the surface measurements seem to miss. On the July 21 driving intensive, TEMPO shows a large swath of NO_2 extending from the Denver metro to central Weld County. Mobile NO_2 observations indicate enhancements near heavily-trafficked roads, but these values decrease within most of the TEMPO NO_2 swath. July 25 is another interesting example, as TEMPO NO_2 data once again show a large plume extending from the Denver metro to far northern Weld County. While mobile measurements seem to remain elevated near the foothills (~12 ppbv), the eastern portion of the mobile sampling route does not indicate enhanced NO_2 concentrations despite the indicated TEMPO NO_2 swath. Mobile and stationary site NO_2 measurements were generally more spatially consistent.

It is important to remember when interpreting these data that they are fundamentally different measurement techniques and are susceptible to their respective biases (Bechle et al., 2013; Mihaita et al., 2018). Also important to note is the different timescales of the measurement techniques. For this analysis, mobile NO_2 measurements had a 1-min rolling average applied to them, and these are compared to a mean of stationary and TEMPO NO_2 data over the full duration of the driving intensive. The utility of comparing surface data to TEMPO column observations remains uncertain, and our results here are meant to be more exploratory. While comparisons between mobile and stationary NO_2 measurements are understudied in the literature, our findings are consistent with those of Tessum et al. (2018), who also found moderate to strong agreement between the two. Additionally, the strong agreement between stationary and TEMPO NO_2 measurements in our analysis is consistent with previous studies (Acker et al., 2025).

Having mobile, stationary, and TEMPO NO_2 data also provided comprehensive insight into the behavior of NO_2 in the Front Range when emissions or transport patterns changed. One well-known

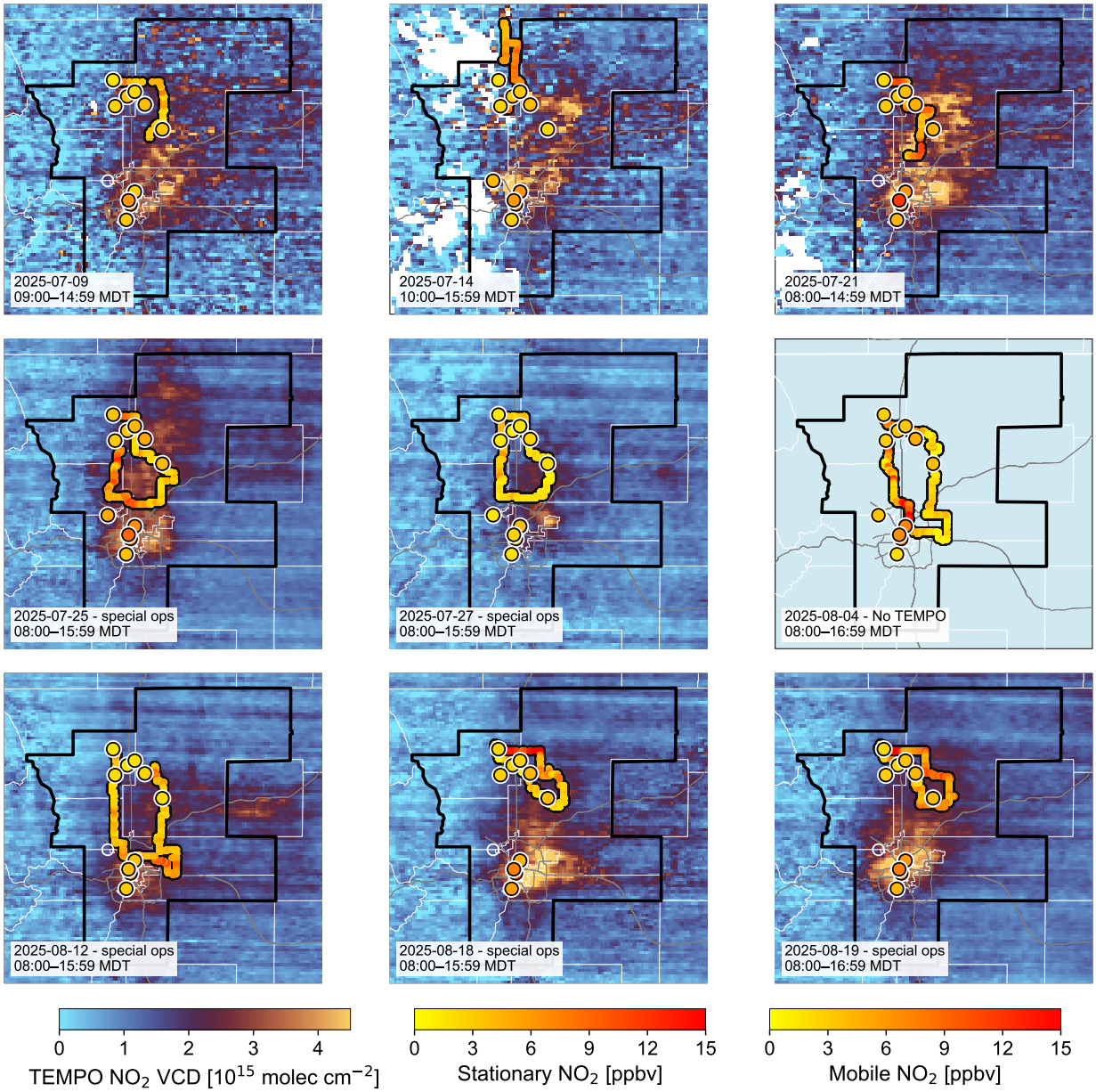


Figure 3.12: Plots of 1-min rolling-averaged, filtered mobile NO_2 data, as well as TEMPO and stationary site NO_2 data that have been averaged for the duration of each driving intensive. The color of the circles represents the stationary site NO_2 concentrations averaged over the duration of the sampling period. Driving intensives with TEMPO special operations are indicated next to the date.

phenomenon is the weekend-weekday effect, where emissions decrease on the weekends due to less (especially truck) traffic (Pollack et al., 2021b). The weekend-weekday effect was studied during FROZÉ on Friday, July 25 and Sunday, July 27. These days were both hot, sunny, and selected

for TEMPO special operations. The results of these driving intensives are shown in Figure 3.13. On Friday, TEMPO indicated a large swath of NO_2 extending from the Denver urban core to the far northern extent of the DMNFR O_3 NAA. Stationary and mobile NO_2 measurements generally agreed, though the Plume Tracker did not observe as much NO_2 in the eastern section of the TEMPO plume. When comparing these measurements to Sunday, a stark contrast was observed. TEMPO measured a clear NO_2 plume near Denver International Airport, but this was the only area with heightened levels. The Denver urban core had much lower (~1-4 ppbv) NO_2 concentrations according to all three measurement methods. While it is not unexpected for emissions, and therefore NO_2, to be lower on weekends than weekdays, the magnitude of difference between these two days was notable. One likely contributing factor to this difference was meteorological variability between the two days. The high for Friday was 88 degrees Fahrenheit, while on Sunday, it was 96. Winds were also notably higher on Sunday, gusting to over 20 mph. Increased atmospheric mixing due to diabatic heating and higher winds likely led to dilution of NO_2 and O_3 measured on Sunday. The spatial contrast in TEMPO NO_2 on the two days is consistent with sustained air traffic on Sunday when surface truck traffic was expected to decrease.

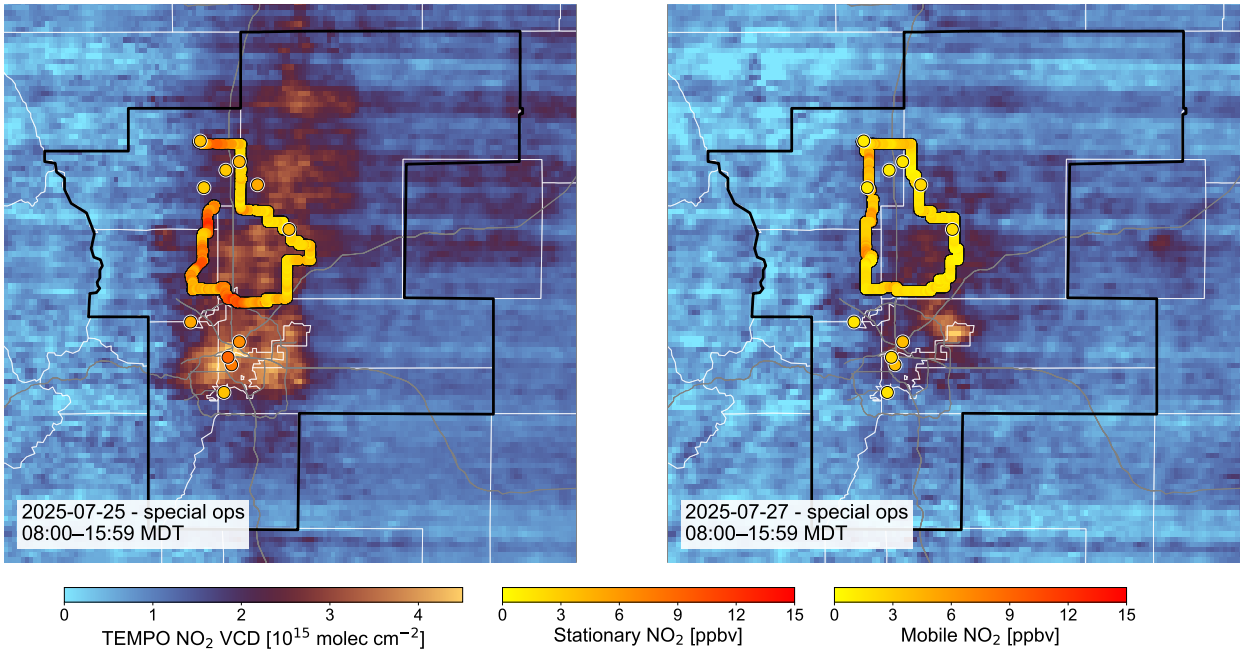


Figure 3.13: Plots of 1-min rolling-averaged, filtered mobile NO_2 data, as well as TEMPO and stationary site NO_2 data that have been averaged for the duration of the Friday, July 25 (left), and Sunday, July 27 (right) driving intensives, respectively. The color of the circles represents the stationary site NO_2 concentrations averaged over the duration of the sampling period.

3.2.2 Mobile O_3 Measurements in the Colorado Front Range

O_3 measurements were collected every 2 seconds during all 13 driving intensives. The driving intensives took place on different days, using different driving paths (except for August 18 and 19, which were the same), and had significant differences in meteorological conditions. Despite variations in driving routes, two clear regimes of O_3 behavior were observed for a majority of the driving intensives, as illustrated in Figure 3.14. For this analysis, we are only considering the 11 daytime driving intensives, as O_3 concentrations are typically highest during the day. The first category is what we identify as "regional O_3 formation," or ROF. ROF driving intensives featured a steady increase in O_3 throughout the day, with minimal deviation in slope. This type of O_3 behavior is in line with typical expectations, as O_3 is considered to be a regional pollutant (Chen et al., 2009). We observed O_3 to follow the ROF regime for three of 11 driving intensives, with O_3 levels climbing approximately 20-25 ppbv over a six-hour period. O_3 formation throughout the day did not follow this pattern on other days, often following into a second category that we

call "local O_3 modification," or LOM. These driving intensives featured large peaks and/or dips in O_3 throughout the drive, rather than exhibiting a consistent upward trend. LOM drives exhibited fast increases and decreases in O_3, climbing up 20 ppbv in less than two hours in some cases. Five of 11 drives were characterized as LOM events. Four of five of the LOM driving intensives exhibited a very large increase in O_3 in the afternoon, followed by a large decrease. The July 27 drive was clearly a LOM event but exhibited a different pattern with O_3 levels remaining suppressed throughout the day, with an interesting drop and subsequent increase in O_3 around 13:00 MDT. Two of the uncategorized drives were either a combination of ROF and LOM or did not fit into either of these categories. The last daytime drive was hard to analyze due to instrument malfunction.

Maps of ROF and LOM drive paths are shown in Figure 3.15. An interesting pattern can be seen when looking at these paths with time. For ROF cases, the drives begin by heading east towards Greeley, then driving back westward in the afternoon. As a result, the Plume Tracker was closer to the foothills towards the end of sampling. The opposite pattern is observed for most of the LOM driving intensives that begin by heading south, staying close to the foothills for several hours. In the afternoon hours, around peak O_3 formation, the vehicle was near Greeley, usually heading northwest afterward. However, there was one LOM driving intensive that began by heading east towards Greeley, following a similar path to the ROF driving intensives. The key difference in this LOM driving intensive is that it was later in the afternoon when the vehicle was heading northwest.

Of particular interest are the LOM drives, where the quick increases/decreases in O_3 concentrations are not immediately explainable from the time series alone. In order to better understand the O_3 changes during drives, we incorporate visible satellite data, HYSPLIT back trajectories, and TEMPO NO_2 data. Four LOM events are chosen as case studies, while a final case study features a ROF event with a unique feature.

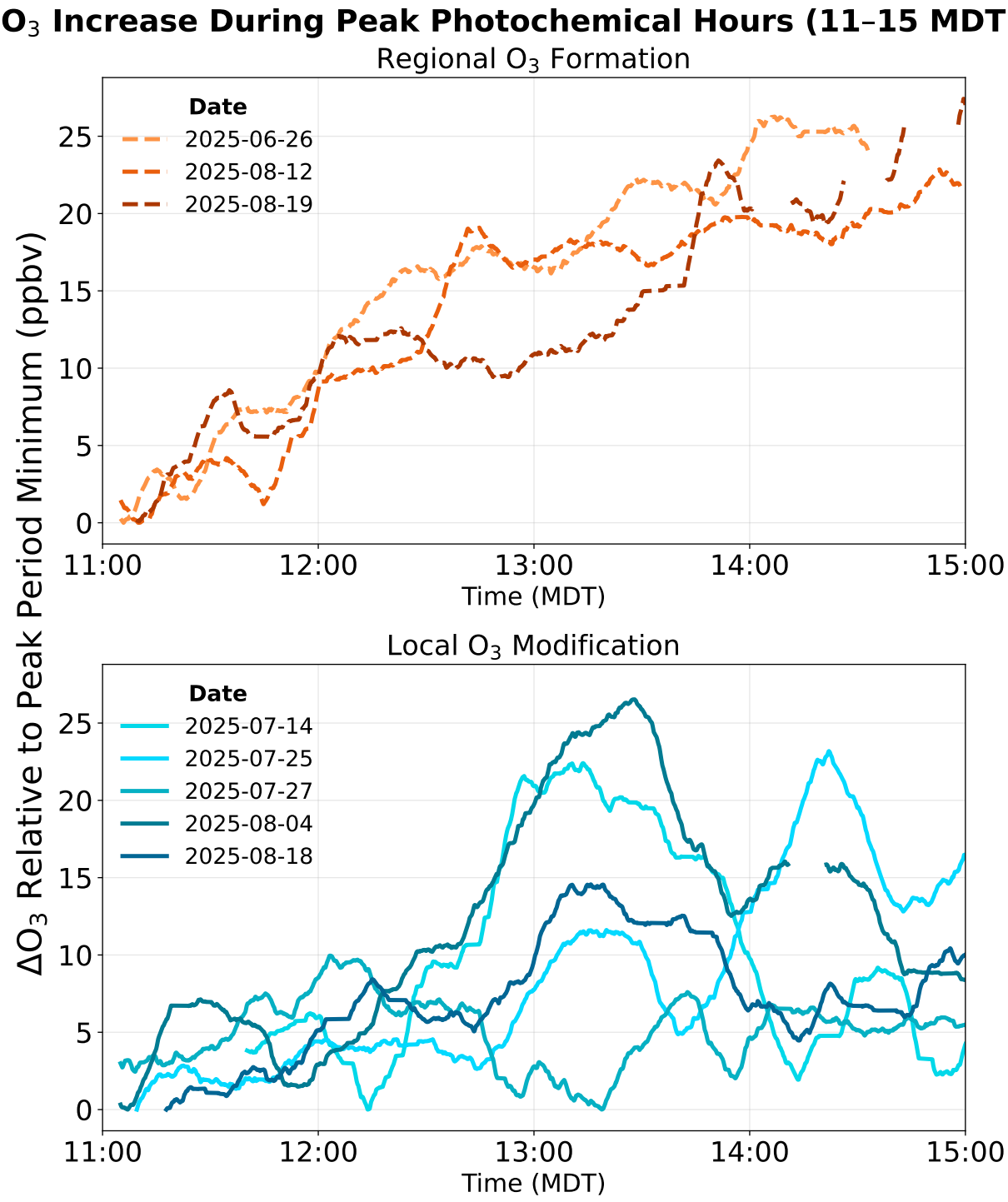


Figure 3.14: Plots of filtered, 10-min rolling-averaged mobile O_3 data for regional O_3 formation (top) and local O_3 modification (bottom) driving intensives during a defined peak photochemical period from 11:00-15:00 MDT. The minimum O_3 value during the peak photochemical period has been subtracted from each driving intensive to facilitate more direct comparison.

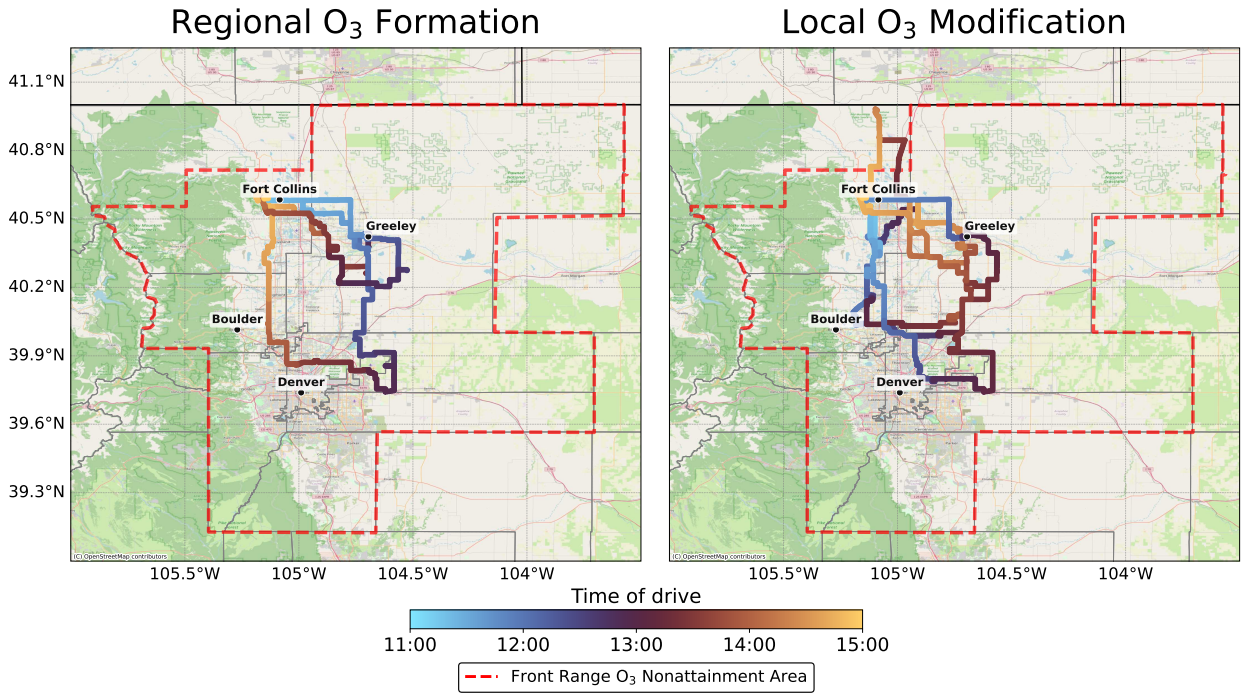


Figure 3.15: Maps of the drive paths for regional O_3 formation, or ROF (left), and local O_3 modification, or LOM (right) cases colored by time of day. Blue colors indicate earlier times during the peak photochemical period, and yellow colors indicate the end.

Case Study #1: July 14, 2025 (LOM)

The first case study is for July 14, 2025. On this day, the goal was to perform sampling in Soapstone Prairie Natural Area, which is located near the Colorado-Wyoming border and falls away from major sources, outside of the DMNFR O_3 NAA. This location was targeted to assess how O_3 behaves outside the DMNFR O_3 NAA. July 14 was designated as an Ozone Action Day by CDPHE. Time series of the O_3 and NO_2 measurements from this drive can be found in Figure 3.16, along with stationary O_3 site data and solar radiation data from the FTCW site. This drive saw among the highest O_3 levels of the field campaign, with mobile O_3 concentrations reaching a maximum of 85 ppbv around 13:00 MDT. O_3 on this day exhibited a very sudden increase just after noon, followed by a rather quick decrease after being sustained for around an hour. Due to high temperatures, ample moisture, and upslope flow, convection formed in the early afternoon due to orographically-induced lifting and cloud cover was present during afternoon sampling as illustrated by visible satellite imagery (Figure 3.17). After sampling in a Loveland DIC, cloud cover started

increasing around noon. The vehicle headed northeast in an attempt to outrun the cloud cover, but this was mostly unsuccessful. Despite the prevalence of widespread cloud cover, mobile O_3 concentrations stayed high (>80 ppbv). Examining HYSPLIT back trajectories (Figure 3.18), it is evident that there was a wind shift from northerly flow in the morning to strong southerly flow by the afternoon. This suggests that O_3 precursors from farther south in the NAA were advected north, contributing to elevated O_3. O_3 concentrations in Soapstone Prairie Natural Area support this hypothesis, as it is usually considered to be a "background" site, but on this day reached above 70 ppbv. Stationary measurements from FTCW, by contrast, indicate low O_3 concentrations for most of the day, likely due to cloud cover, as indicated by the relatively low values of solar radiation. Interestingly, measurements from the UM Van at Bethke Elementary farther to the east also indicate relatively low O_3 concentrations compared to the CSU Tahoe O_3, peaking at around only 70 ppbv. It is important to note that the UM Van was undergoing instrument calibrations for a significant part of the Plume Tracker drive period, so there are missing data.

While relatively noisy, the NO_2 data do not indicate any fresh plumes (identified by a large increase and subsequent decrease) at the time of CSU Tahoe O_3 concentrations decreasing around 13:45. The steady decrease in mobile O_3 levels is possibly correlated with the initiation of convection near Soapstone Prairie and its associated outflow. TEMPO NO_2 data were not useful for this analysis due to widespread cloud cover. Nevertheless, this case study exemplifies interesting behavior of high O_3 in a relatively narrow corridor that was only identified due to mobile O_3 measurements sampling an area without routine monitoring. Further, this case study is also unusual in the persistence of O_3 formation despite widespread cloud cover.

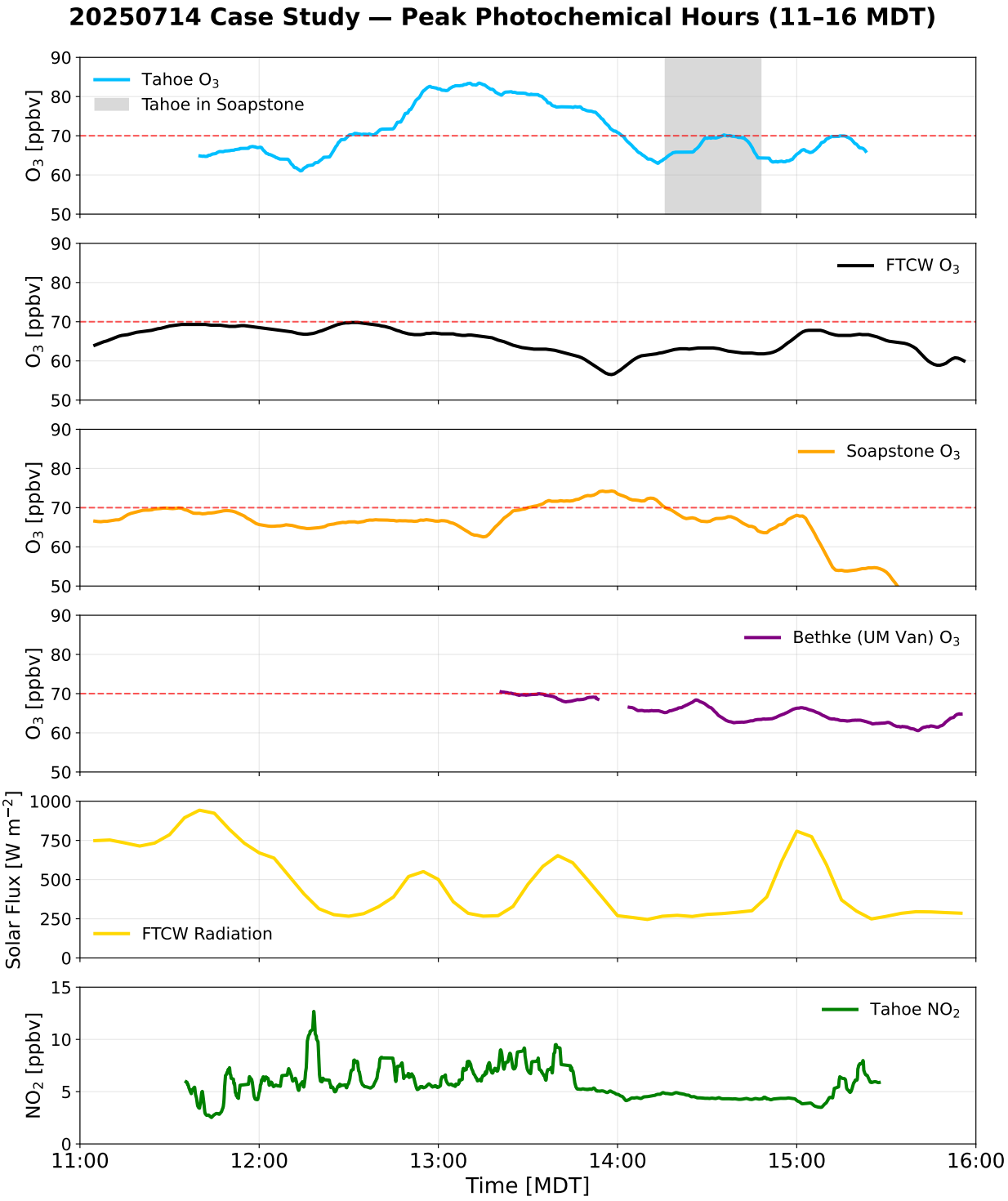


Figure 3.16: Time series of Plume Tracker/CSU Tahoe O_3, Fort Collins-West (FTCW) O_3, Soapstone Natural Prairie O_3, stationary UM Van O_3 measurements in Bethke, FTCW solar radiation measurements, and CSU Tahoe NO_2 measurements. All depicted measurements have a 10-min rolling average applied to them, except for the NO_2 measurements, which had a 1-min rolling average applied.

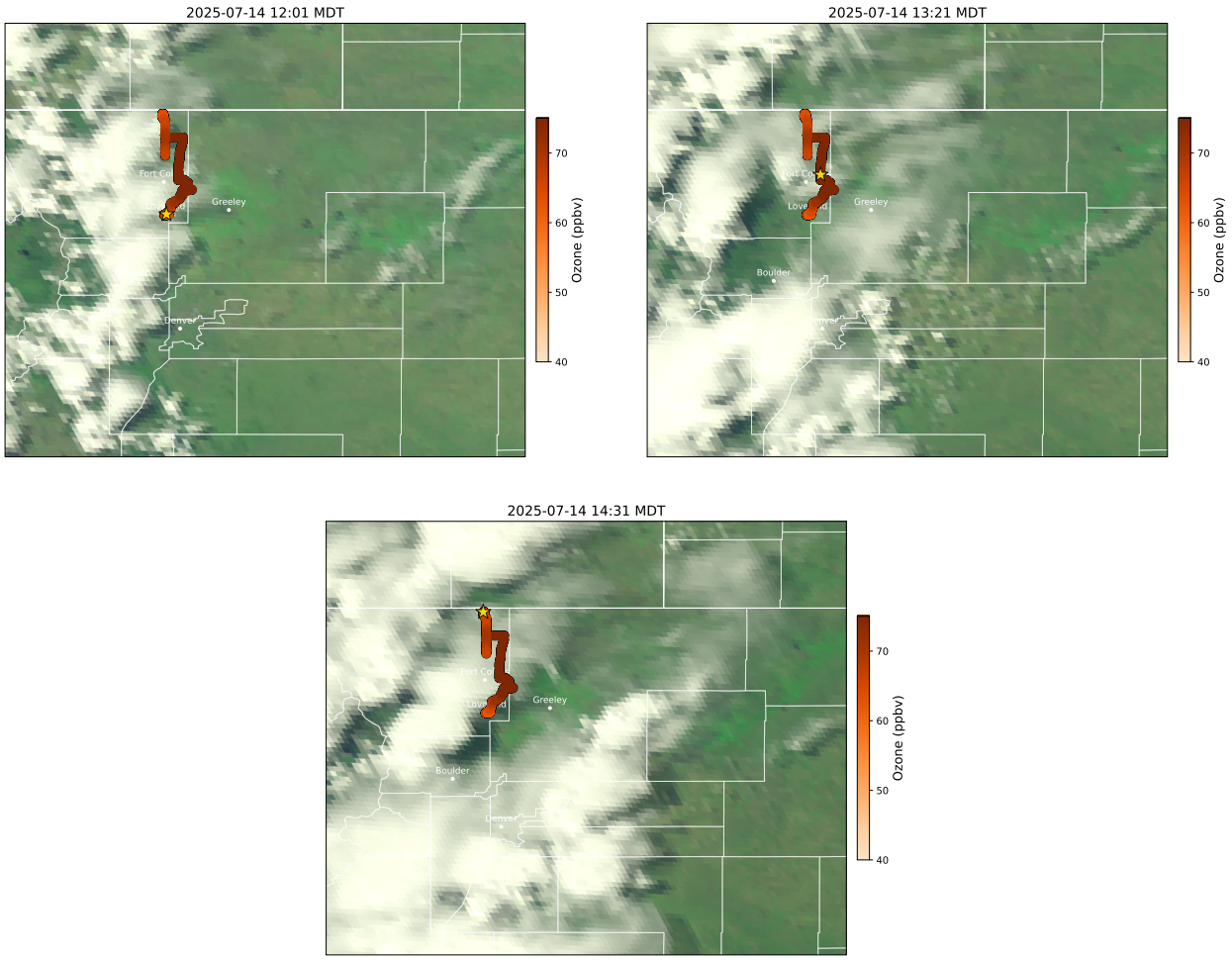


Figure 3.17: Visible GOES imagery from various times on July 14, 2025 overlaid with the CSU Tahoe O_3 concentrations. The yellow star indicates the vehicle's location at the time the satellite scan was taken.

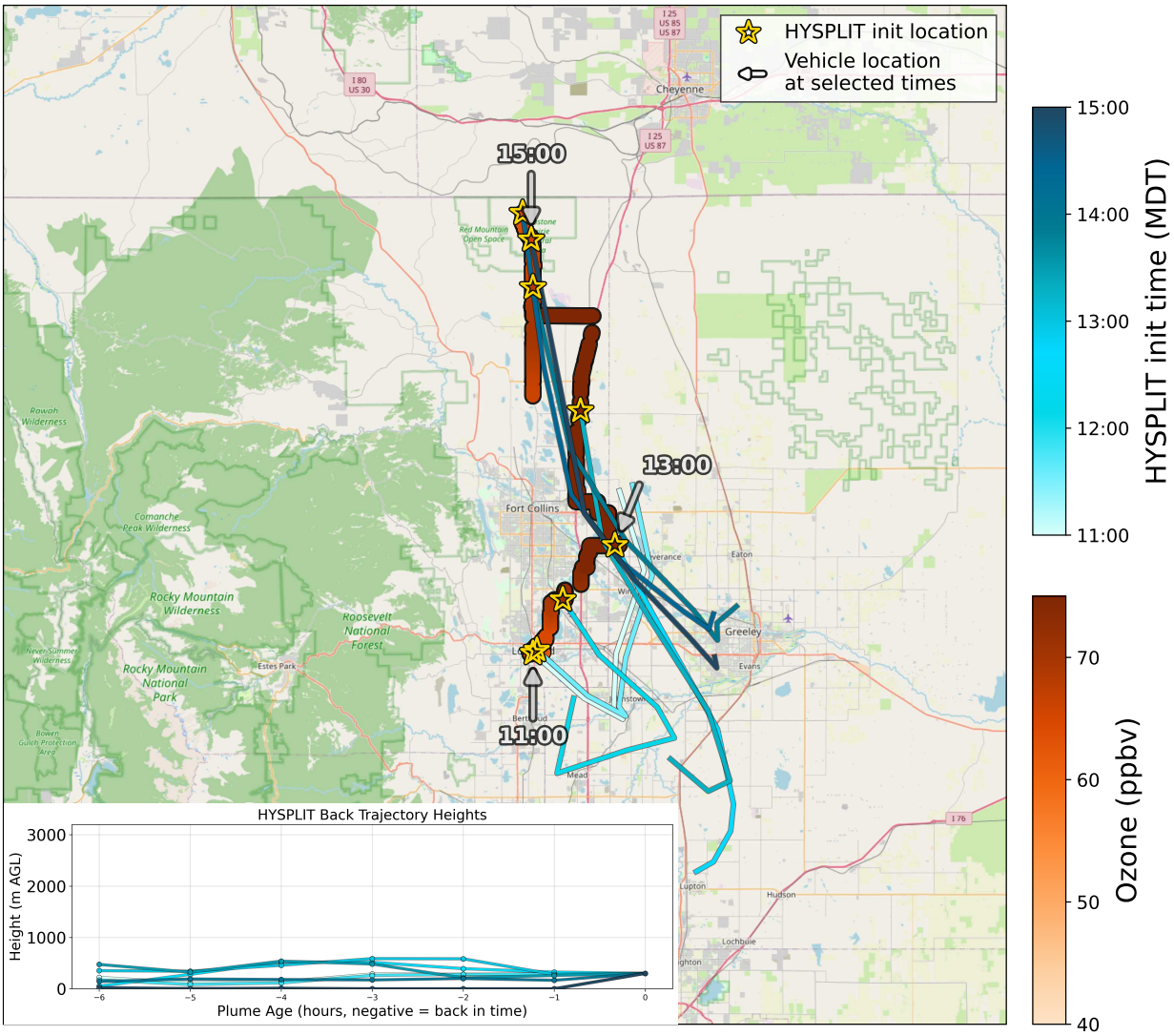


Figure 3.18: HYSPLIT back trajectories on July 14, 2025 initiated for 6 hours back in time every 30 minutes of the CSU Tahoe driving intensive overlaid with CSU Tahoe O_3 levels. The hollow yellow stars indicate the vehicle's location at the time of each trajectory initiation. The trajectories are colored by time, with darker colors being initiated later in the driving intensive. The heights of each trajectory along its path are shown in the bottom left.

Case Study #2: July 25, 2025 (LOM)

TEMPO special operations were requested for July 25, 2025, a CDPHE Ozone Action Day. The day's drive included east-west transects north of Denver to optimize measurements in tandem with TEMPO. In addition to being hot (highs in the upper 80s), there was dilute smoke present in the Front Range. Mobile O_3 and NO_2 measurements from the Plume Tracker can be seen in Figure 3.19. This day was of interest due to stable O_3 levels earlier in the day followed by two O_3 peaks and subsequent decreases during the afternoon. Visible satellite imagery in Figure 3.20 clearly indicates that cloud cover did not limit O_3 production in the morning or lead to the afternoon O_3 decreases. HYSPLIT back trajectories in Figure 3.21 show transport from the west and across the north Denver metro area until 11:00 MDT as we were sampling north of the city. O_3 levels increased around 11:00, during a period when back trajectories suggest greater transport from the urban core, then remained fairly steady for the next two hours as the vehicle headed northeast from the city. As the vehicle headed north, transport patterns changed to feature more recirculation around the O&G production region in Weld County and O_3 levels climbed starting shortly before 13:00. The first broad decrease in O_3 began around 13:30, when the Plume Tracker crossed U.S. Route 85. This highway had heavy traffic from diesel trucks. We don't see any substantial change in NO_2 at this time, but it is likely most local emissions were still present as NO which then titrated local O_3. O_3 levels reached a peak around 14:20 south of Windsor, coinciding with increasingly easterly flow from O&G-abundant areas south of Greeley. O_3 decreased again heading north of Windsor toward Bethke Elementary in Timnath. Transport during this period might include Greeley's urban emissions, but once again, this O_3 decrease does not seem to coincide with an increase in NO_2 measured by the Tahoe. NO_2 does increase again after 15:00, when the vehicle was likely sampling heavier traffic emissions from CO Highway 14, and O_3 climbs again as the vehicle moves west into Fort Collins. Looking at TEMPO NO_2 data in Figure 3.22 does not help much in interpreting the O_3 changes seen across the region between Greeley and Fort Collins, as the observations appear somewhat noisy, although a rather small plume of NO_2 can be made out to the west of Greeley at 14:37. While we do not have sufficient observations to completely understand O_3 variations during this case study, it is an important example of how O_3 levels can vary over

spatial scales of a few miles in the presence of spatially varying emission sources and temporally shifting wind patterns.

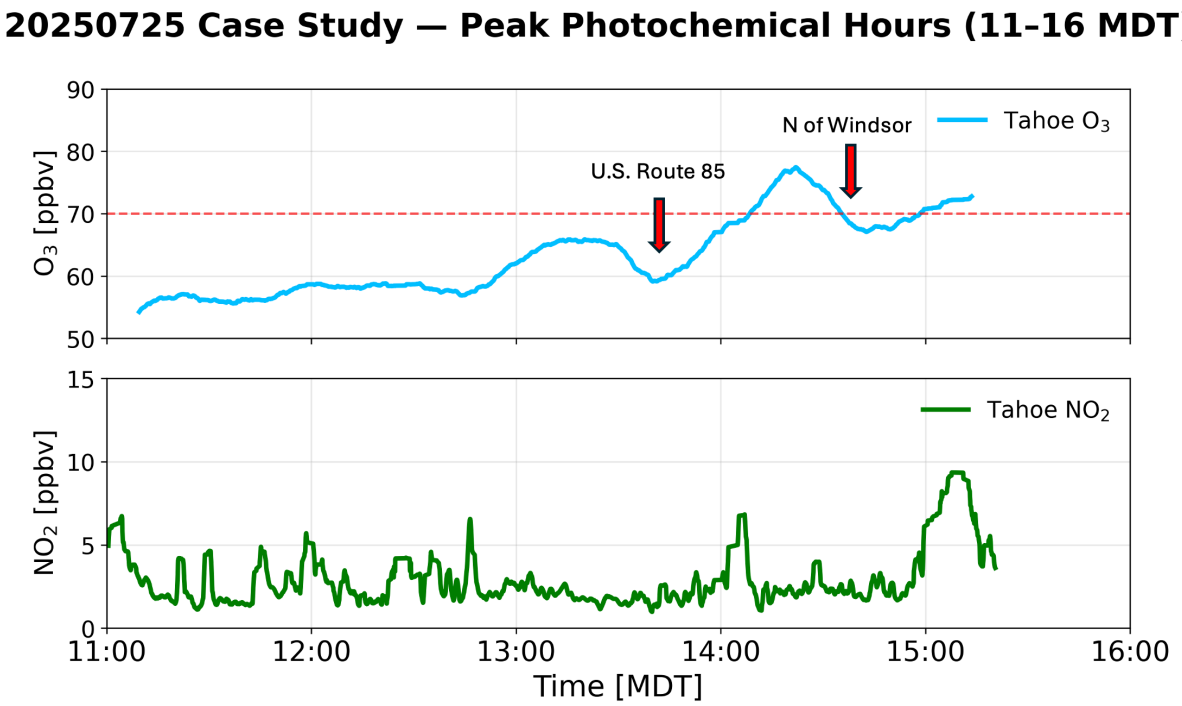


Figure 3.19: Time series of Plume Tracker/CSU Tahoe O_3 and NO_2 measurements on July 25, 2025. The O_3 data have a 10-min rolling average applied and the NO_2 data have a 1-min rolling average.

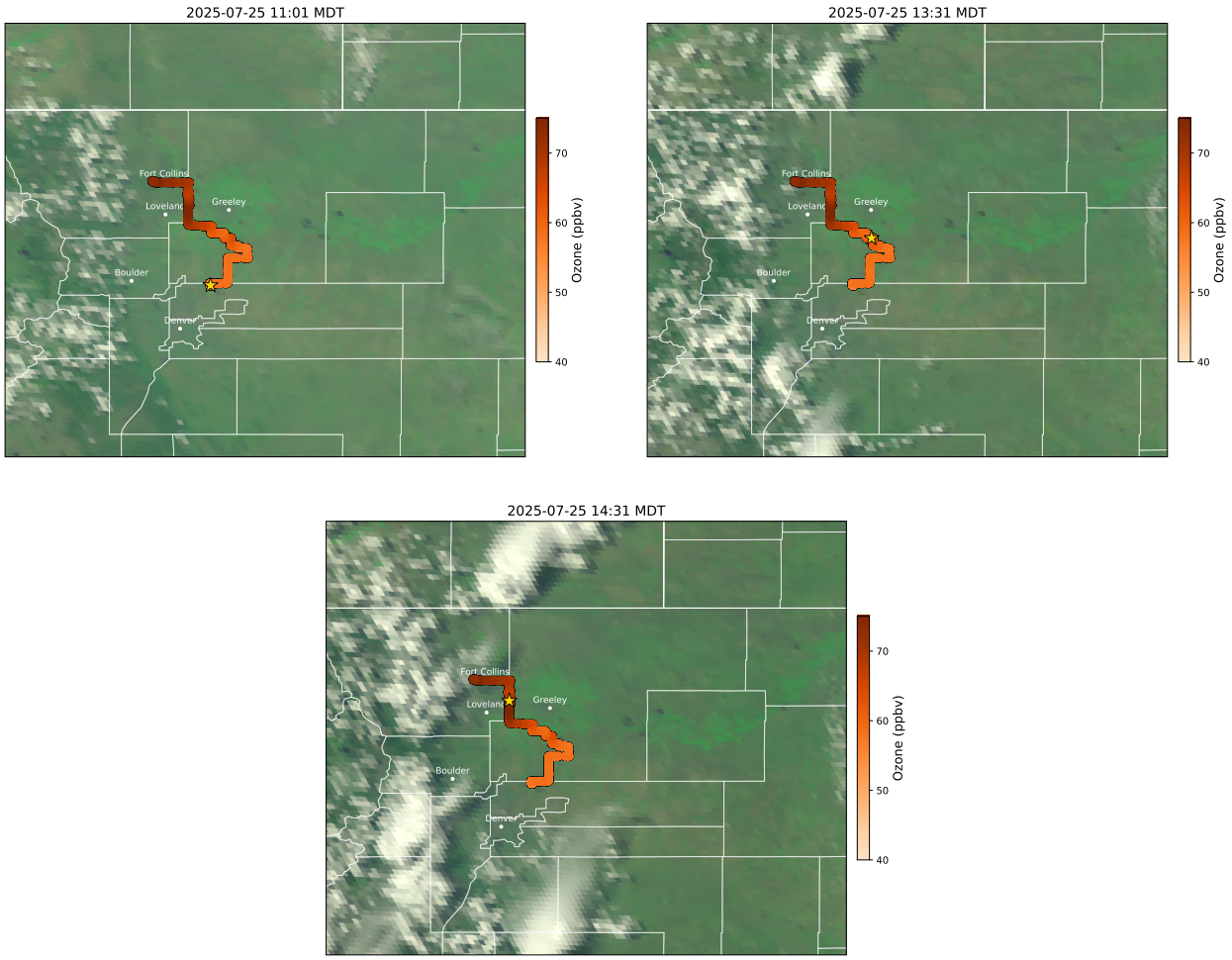


Figure 3.20: Visible GOES imagery from various times on July 25, 2025 overlaid with the CSU Tahoe O_3 concentrations. The yellow star indicates the vehicle's location at the time the satellite scan was taken.

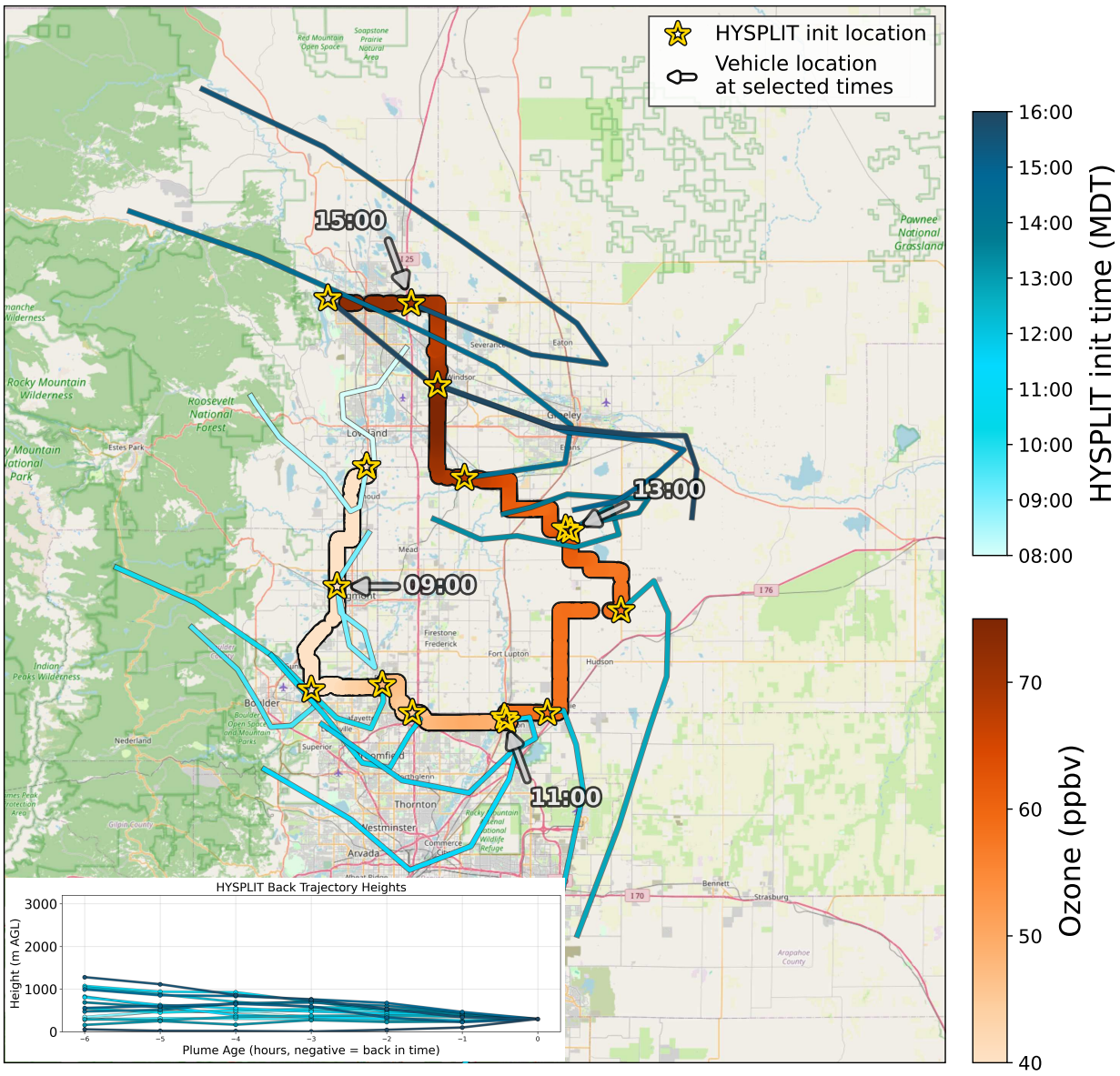


Figure 3.21: HYSPLIT back trajectories on July 25, 2025 initiated for 6 hours back in time every 30 minutes of the CSU Tahoe driving intensive overlaid with CSU Tahoe O_3 levels. The hollow yellow stars indicate the vehicle's location at the time of each trajectory initiation. The trajectories are colored by time, with darker colors being initiated later in the driving intensive. The heights of each trajectory along its path are shown in the bottom left.

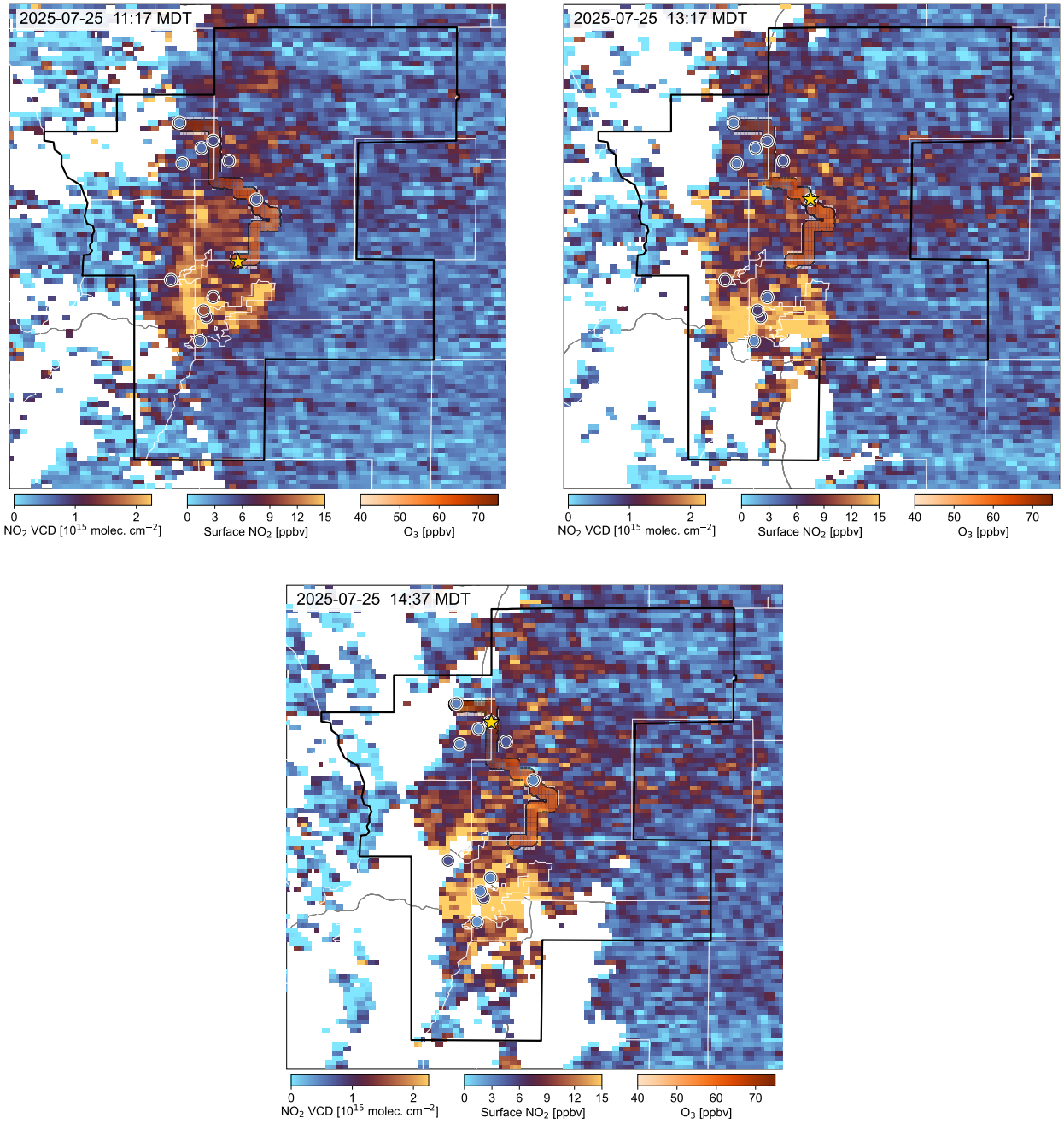
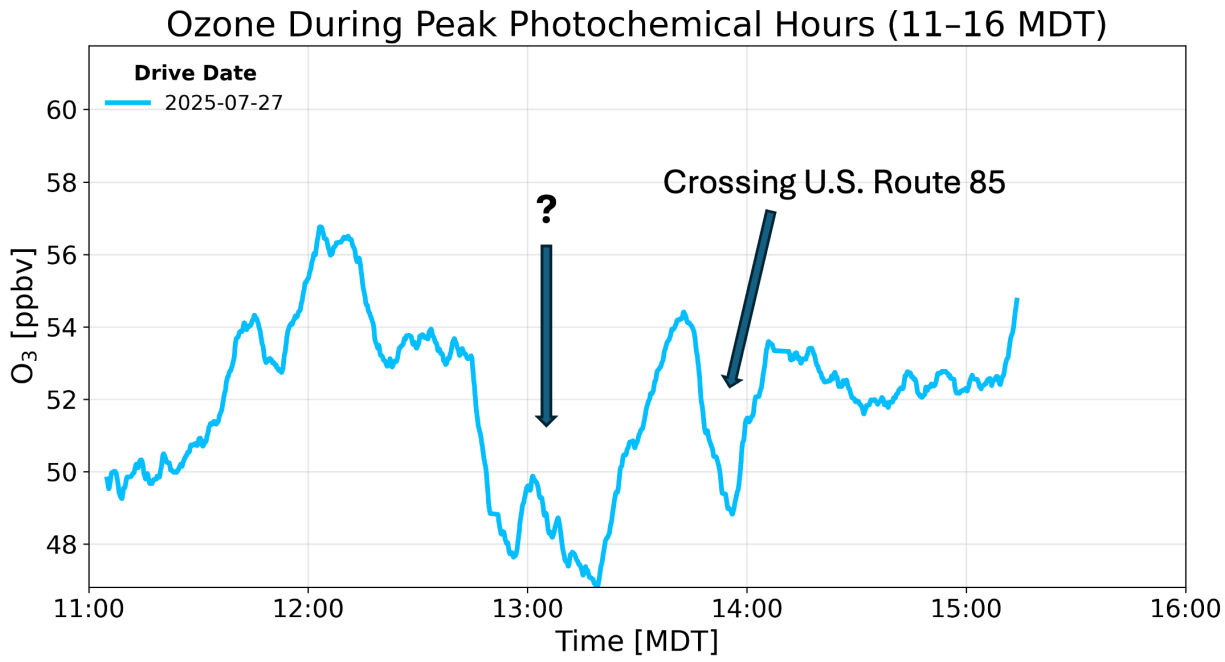


Figure 3.22: TEMPO NO_2 data scans at various times on July 25, 2025 overlaid with semi-transparent mobile O_3 concentrations and hourly NO_2 stationary site measurements (depicted as circles). The gold star represents the vehicle's location at the time of the TEMPO scan.

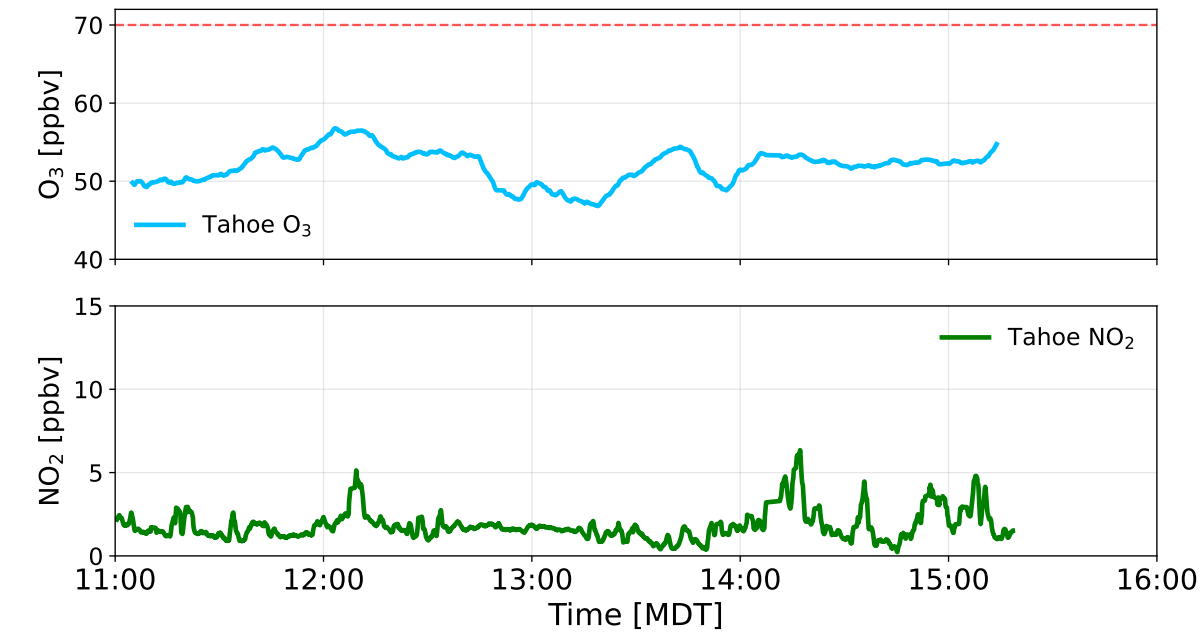
Case Study #3: July 27, 2025 (LOM)

The drive on July 27 was similar to the one on July 25, with a similar route and availability of TEMPO special operations. The major difference between these two days was that July 27 was a Sunday and was much hotter (highs in the upper 90s); this date was not designated as an Ozone Action Day by CDPHE due to the heat forecast. Due to the relatively low O_3 levels measured this day, a close-up annotated version of the data is shown in Figure 3.23. The maximum mobile O_3 concentration on this day was ~57 ppbv, much lower than on any of the other driving intensives. Two broad, sudden decreases in O_3 concentrations are evident. The second, narrower decrease just before 14:00 was readily identified as local O_3 titration while crossing U.S. Route 85. However, the first broader decrease in O_3, centered around 13:00, was not as easily explained. Looking at side-by-side comparisons of mobile O_3, mobile NO_2, and visible satellite imagery in Figure 3.24, it is clear this decrease was not due to cloud cover. HYSPLIT back trajectories in Figure 3.25 indicate strong westerly morning flow over the Rocky Mountains that slowly transitions to weak upslope flow around 12:30 MDT. This first decrease in mobile O_3 concentrations occurs shortly after the wind shift. When looking at TEMPO NO_2 data (Figure 3.26), it is clear that NO_2 overall across the region this Sunday was much less abundant, consistent with reduced traffic (especially truck) emissions. A large plume of NO_2 was, however, observed by TEMPO over the course of the day originating from the location of Denver International Airport. This plume remains largely stationary until the wind shift occurs and begins to advect NO_2 to the northwest. At 12:48, almost exactly at the time that mobile O_3 starts to decrease, the farthest reaches of the plume are seen intersecting with the location of the Plume Tracker. HYSPLIT back trajectory heights from the 12:30 and 13:00 initialization locations show ascent (likely from diabatic heating) in the hours before the wind shift. Just an hour before the plume was likely overhead of the Plume Tracker, the HYSPLIT parcels are seen to descend slightly to their initialization height of 300 m. While it is not possible to say with absolute certainty that fresh NO_x emissions from Denver International Airport titrated O_3 locally in the area that the Plume Tracker was sampling, it is certainly plausible. This case study is a fascinating example of how O_3 variability can occur regionally, even when

concentrations are relatively low and there are less emissions. It is also a clear example of the potential importance of airport NO_x emissions to regional air quality.



(a)



(b)

Figure 3.23: Top: Filtered mobile O_3 annotated with times of interest. Bottom: Filtered mobile O_3 and NO_2 concentrations from the July 27, 2025 driving intensive with a 10-min rolling average applied and the NO_2 data have a 1-min rolling average. Note that the y-axis scale is shifted for better visualization of O_3 decrease events.

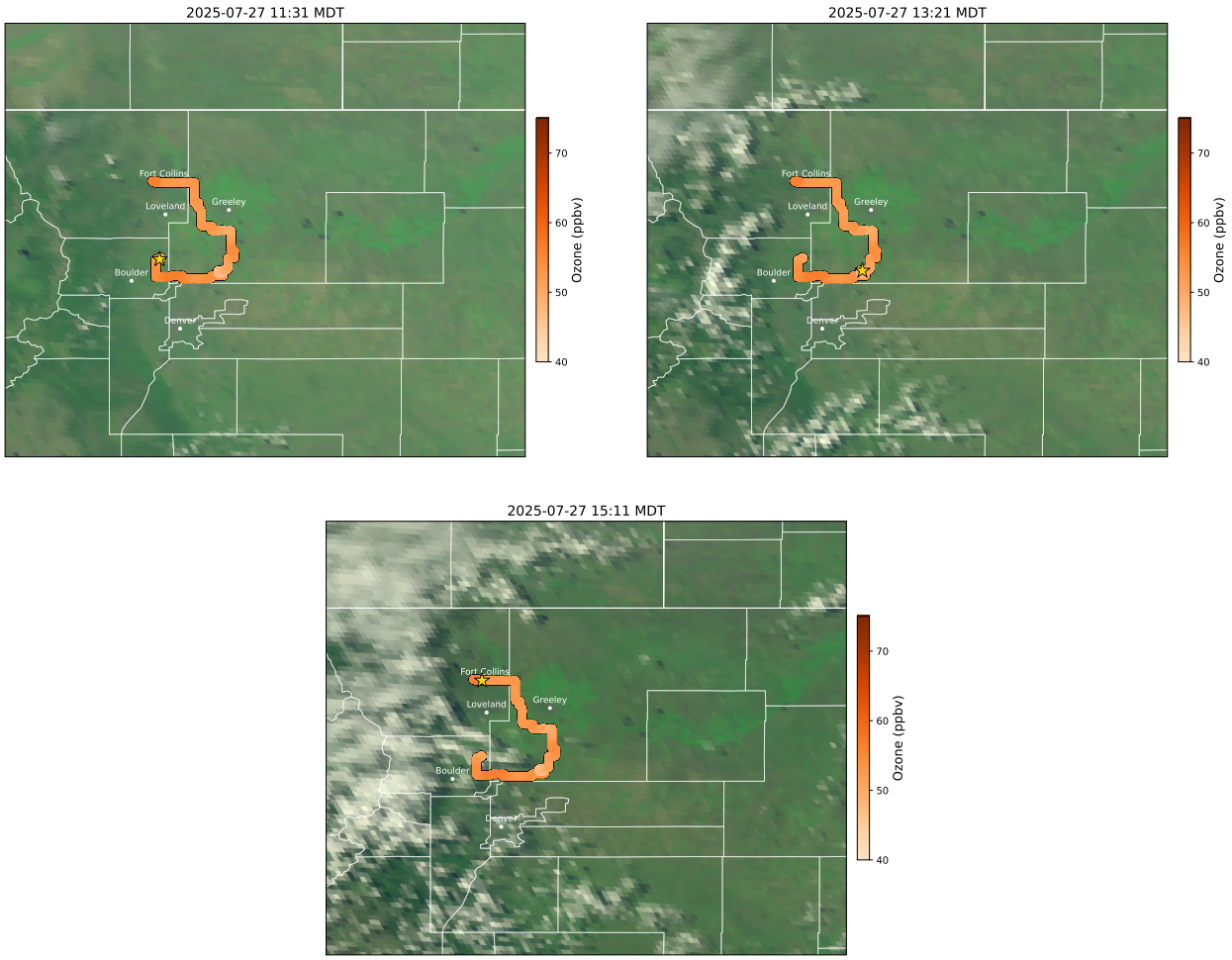


Figure 3.24: Visible GOES imagery from various times on July 27, 2025 overlaid with the CSU Tahoe O_3 concentrations. The yellow star indicates the vehicle's location at the time the satellite scan was taken.

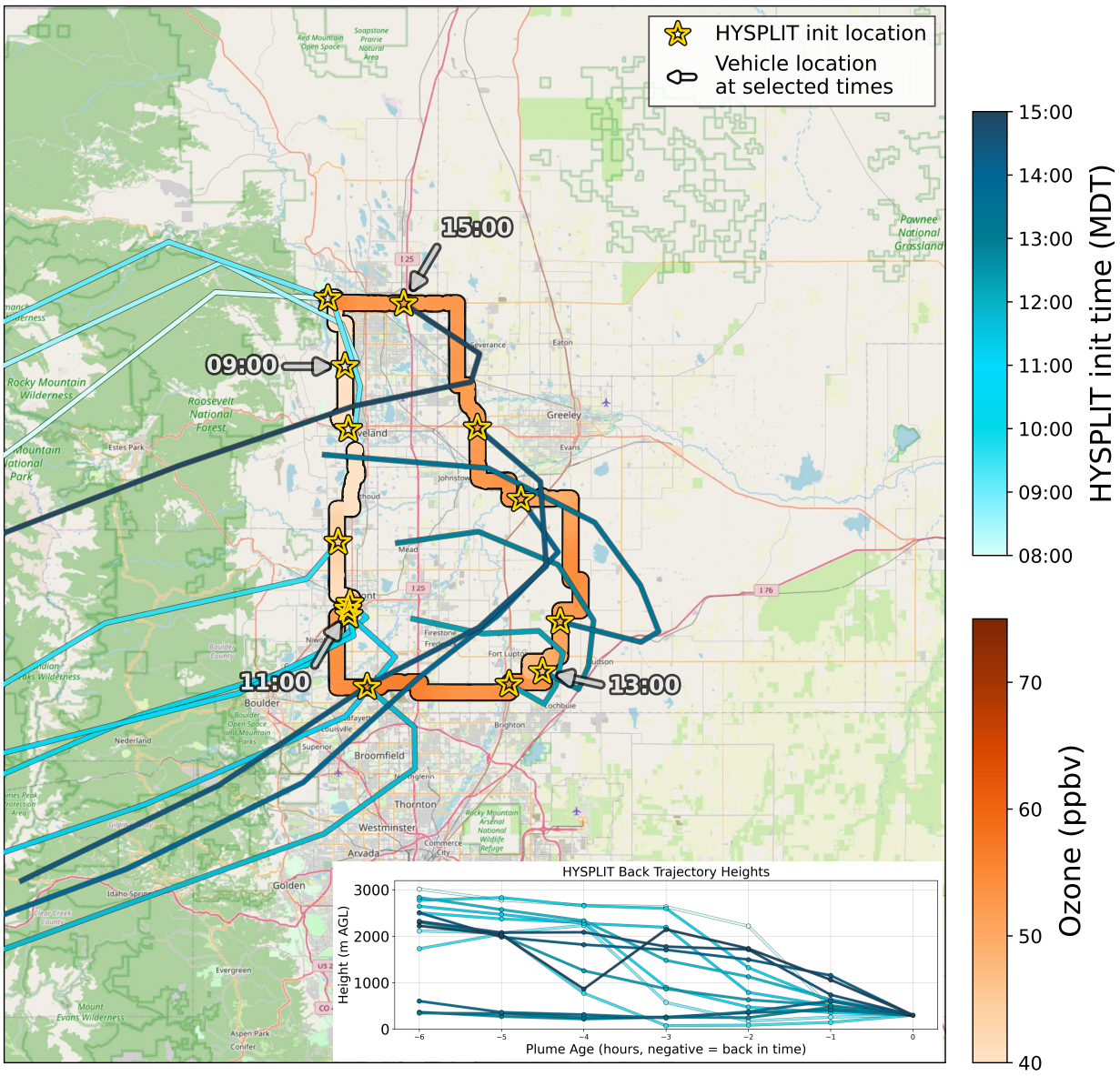


Figure 3.25: HYSPLIT back trajectories on July 27, 2025 initiated for 6 hours back in time every 30 minutes of the CSU Tahoe driving intensive overlaid with CSU Tahoe O_3 levels. The hollow yellow stars indicate the vehicle's location at the time of each trajectory initiation. The trajectories are colored by time, with darker colors being initiated later in the driving intensive. The heights of each trajectory along its path are shown in the bottom right.

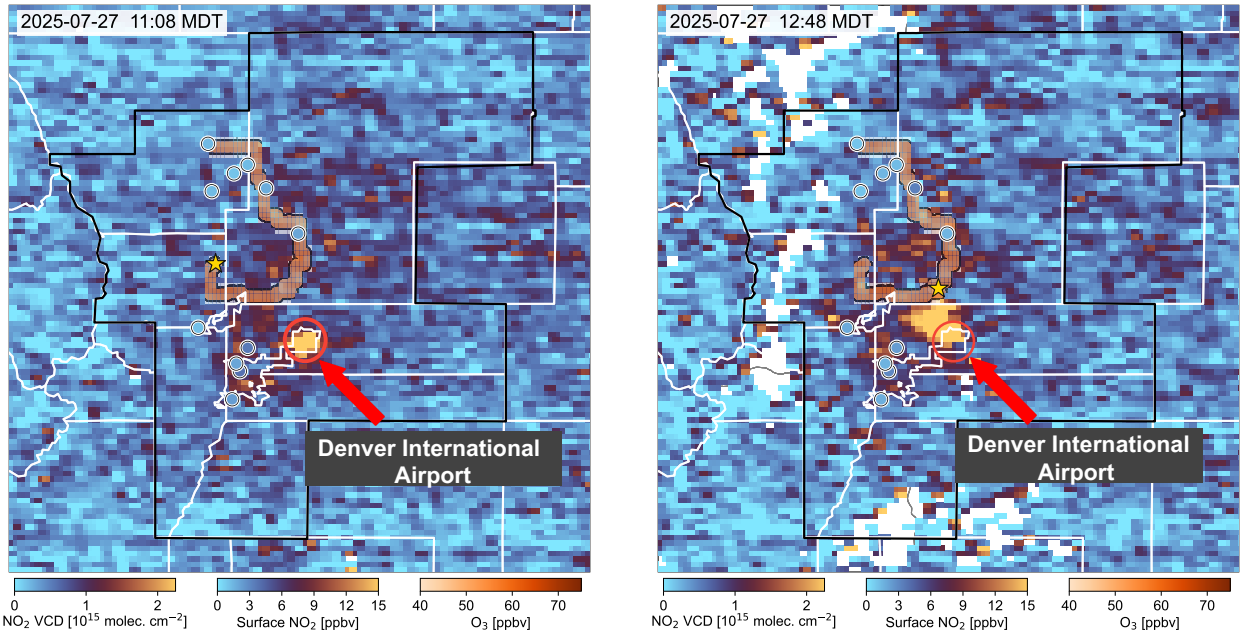


Figure 3.26: TEMPO NO_2 data scans at various times on July 27, 2025 overlaid with semi-transparent mobile O_3 concentrations and hourly NO_2 stationary site measurements (depicted as circles). The gold star represents the vehicle's location at the time of the TEMPO scan.

Case Study #4: August 4, 2025 (LOM)

August 4, 2025 was one of the most complex situations sampled during mobile sampling. It was a hot day with a forecast of upslope flow and was designated as an Ozone Action Day by CDPHE. In addition to the traditional high O_3 factors present, smoke, which can enhance O_3 formation (Lindaas et al., 2017), was present in the Front Range on this day. The sampling strategy was to have a long drive path with an emphasis on taking measurements around Denver International Airport, where stationary monitors are limited. TEMPO special operations were requested. Unfortunately, there was a technical malfunction with the instrument, so we do not have any TEMPO measurements on this day (not even the nominal operations hourly scans). This adds to the difficulty of analyzing O_3 behavior on this day. Mobile O_3 concentrations on this day were quite high (>80 ppbv) with notably sharp gradients, as shown in Figure 3.27. Mobile O_3 measurements compared to stationary measurements, as well as mobile NO_2, C_2H_6, and CH_4 measurements, are shown in Figure 3.28. The first interesting feature is a sudden decrease in mobile O_3 around 13:30 MDT. Visible satellite

imagery (Figure 3.29) suggests that this was not due to cloud cover. HYSPLIT back trajectories (Figure 3.30) indicate a quick initiation of relatively strong upslope flow starting around 14:00, just after the time of maximum mobile O_3 levels. After 14:00, the trajectories become long, suggesting stronger winds. Interestingly, the shortest HYSPLIT back trajectory is the one initiated at 13:30. This seems to suggest a stagnation in winds before upslope flow initiated. This area is in close proximity to O&G operations, and it is possible that the weak winds allowed O_3 precursors to pool. Mobile ethane and methane measurements support this hypothesis, with a steady increase as the vehicle entered the area. Ethane and methane start to decrease after 13:30, the same time as O_3 starts to decrease, consistent with increasing winds. Stationary O_3 measurements also agree, with WCT and LST showing maximum O_3 levels at 13:30 followed by a steady decrease. TIM, which lies downwind of WCT and LST, measured very high O_3 concentrations (>90 ppbv) starting after 14:00. Another factor that may have contributed to high O_3 at TIM in the afternoon was dilute smoke at the surface, which was indicated after 13:00 (Figure 3.31). Therefore, it would appear plausible that the reason for the decrease in mobile O_3 south of Greeley under clear skies was advection of O_3 precursors out of the area. The transport of photochemically-aged air to the west by upslope flow led to high O_3 levels downwind, but these were not intercepted by the Plume Tracker until 15:45. At this time, mobile O_3 suddenly increased by ~9 ppbv in just a few minutes. These observations are consistent with strengthening upslope flow that was likely transporting O_3 precursors into the area that the Plume Tracker was sampling as they photochemically-aged. Beyond data limitations, this case study shows there are large variations in O_3 within the Front Range that depend on wind direction and the photochemical age of air masses.

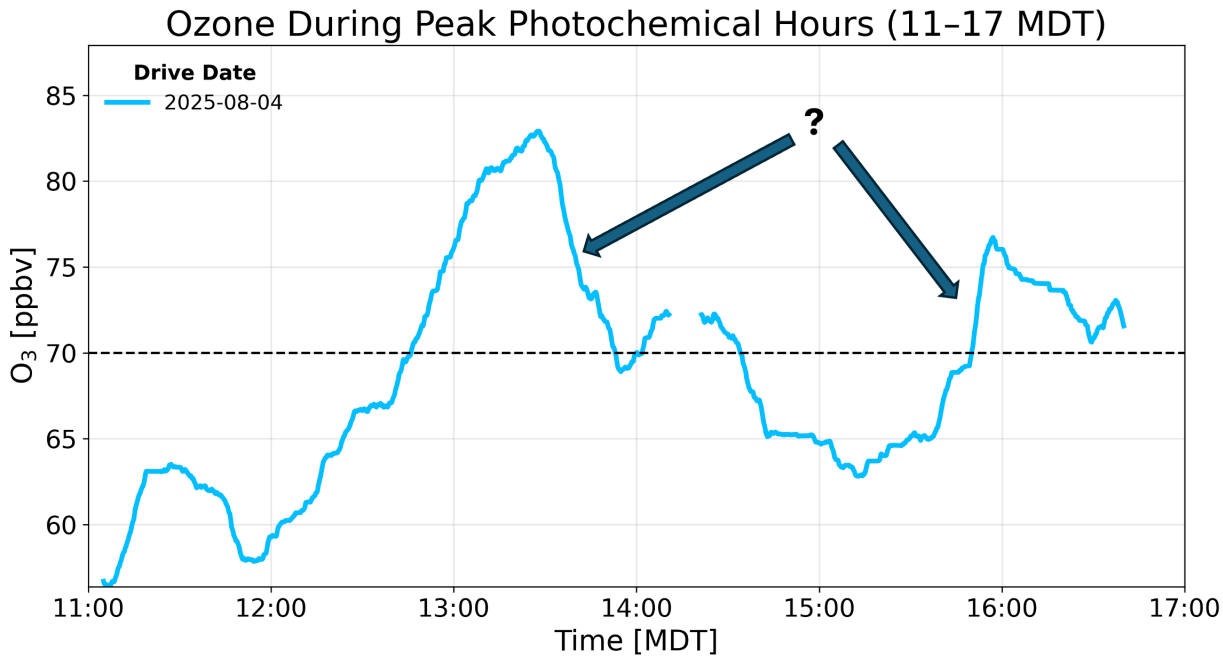


Figure 3.27: Filtered mobile O_3 concentrations from the August 4, 2025 driving intensive with a 10-min rolling average applied. The arrows indicate particular gradients of interest.

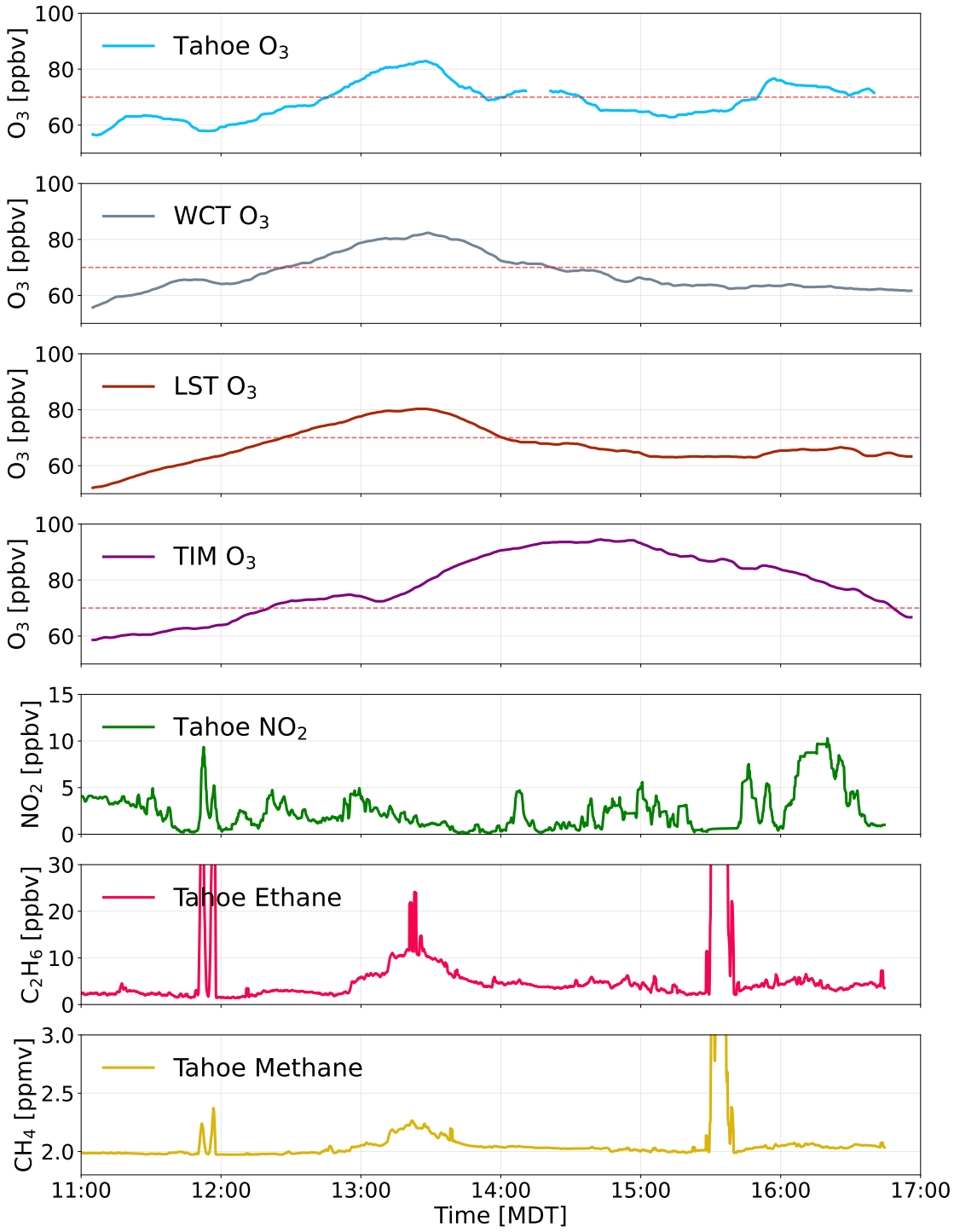


Figure 3.28: Time series of mobile O_3 and stationary O_3 measurements on August 4, 2025 from: Weld County Tower (WCT), La Salle Tower (LST), and Timnath - Bethke Elementary (TIM). Also shown are mobile NO_2, ethane (C_2H_6), and methane (CH_4) measurements. All depicted measurements have a 10-min rolling average applied to them, except for the NO_2 measurements, which had a 1-min rolling average applied.

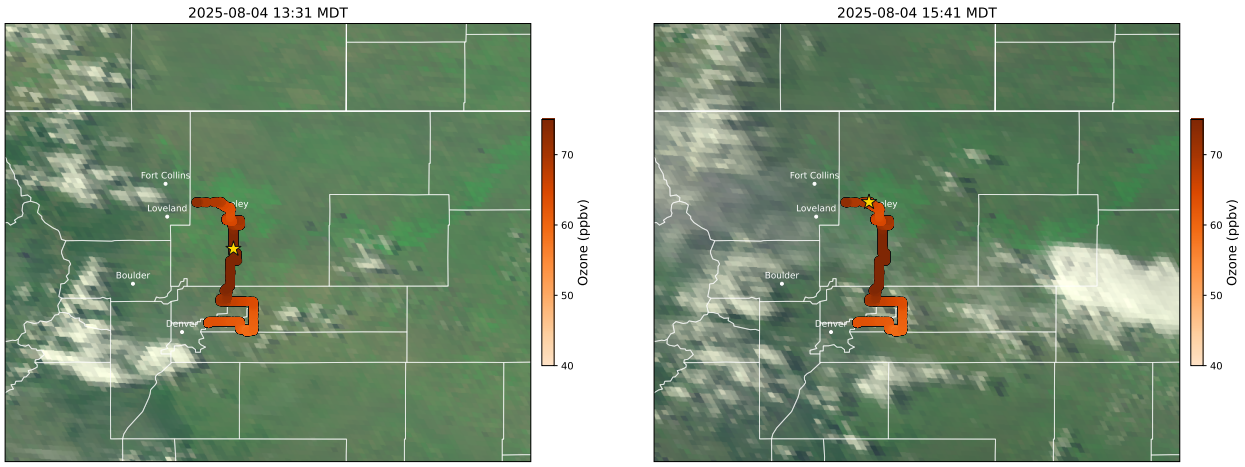


Figure 3.29: Visible GOES imagery from various times on August 4, 2025 overlaid with the CSU Tahoe O_3 concentrations. The yellow star indicates the vehicle's location at the time the satellite scan was taken.

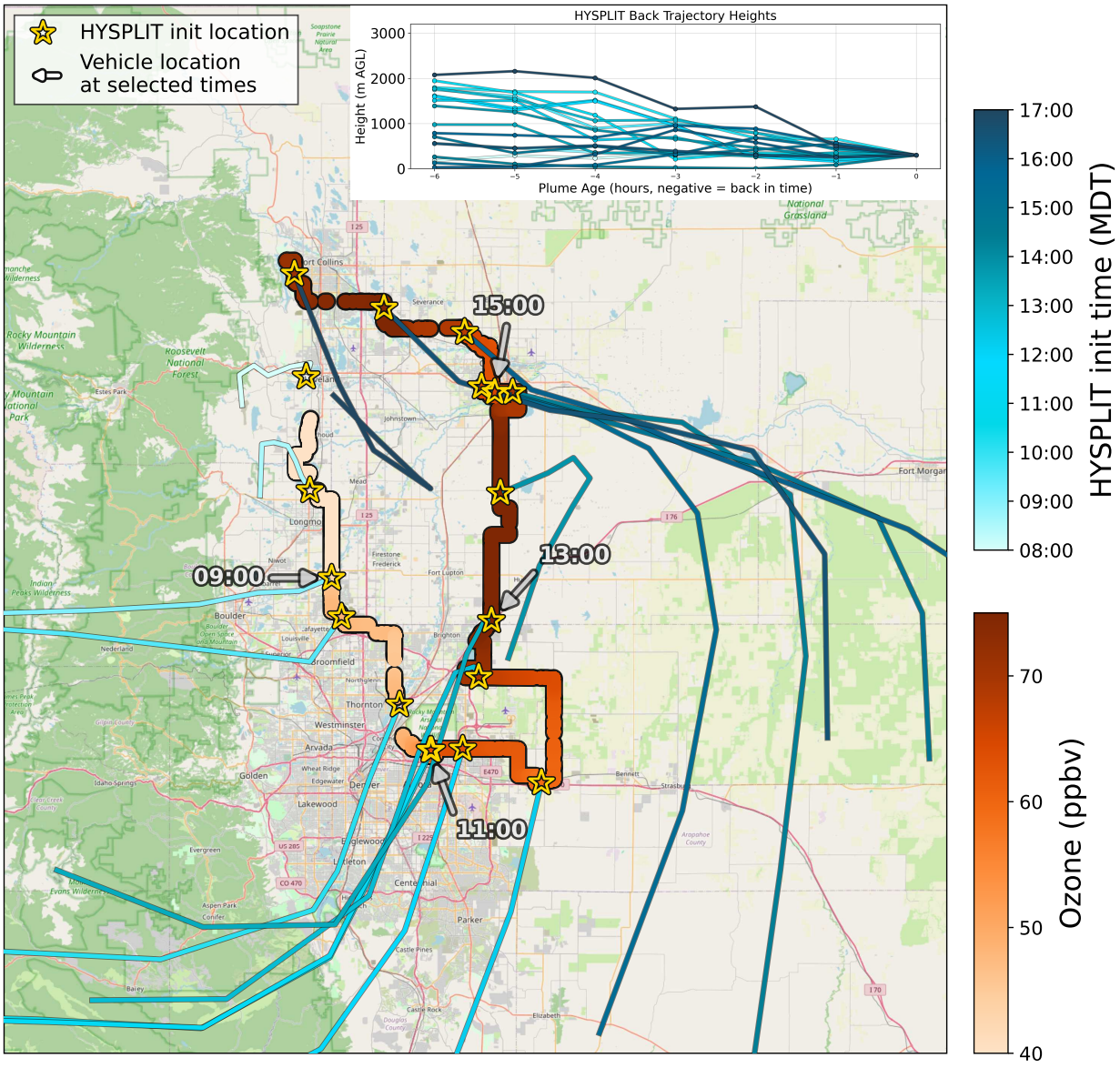


Figure 3.30: HYSPLIT back trajectories on August 4, 2025 initiated for 6 hours back in time every 30 minutes of the CSU Tahoe driving intensive overlaid with CSU Tahoe O_3 levels. The hollow yellow stars indicate the vehicle's location at the time of each trajectory initiation. The trajectories are colored by time, with darker colors being initiated later in the driving intensive. The heights of each trajectory along its path are shown in the upper right.

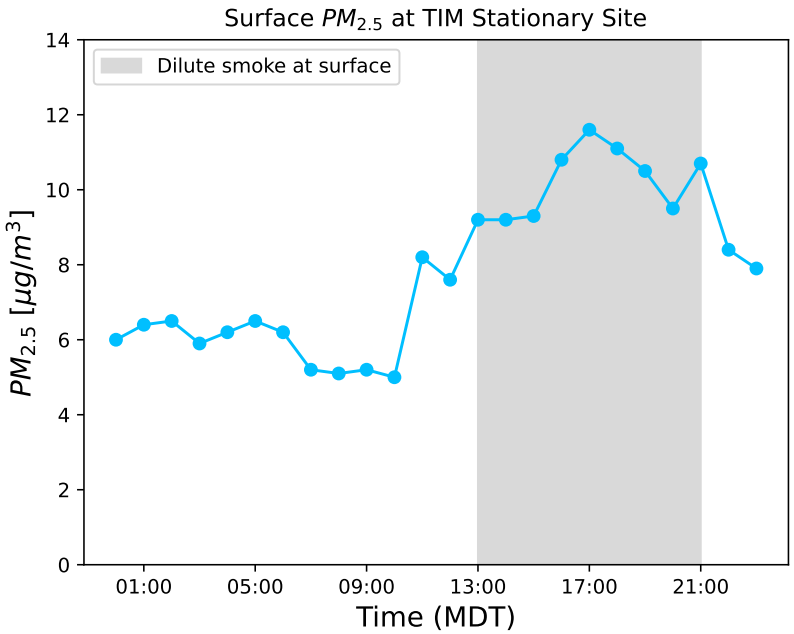


Figure 3.31: Hourly $PM_{2.5}$ data from the Timnath - Bethke Elementary (TIM) stationary site on August 4, 2025. The presence of dilute smoke at the surface is indicated in gray using Brandon McGuire's smoke identification algorithm, which is adapted from Brey et al. (2018).

Case Study #5: August 19, 2025 (ROF)

The August 19 drive is a ROF case, analyzed here to explore a relatively large increase in O_3 towards the end of the driving intensive when the vehicle drove up on top of the hogback ridge on the east side of Horsetooth Reservoir (Figure 3.32). There was also a notable decrease in O_3 after the vehicle left Horsetooth Reservoir and descended from the ridge at 15:00 MDT. The elevation of Fort Collins is 5004 ft, while the elevation of the ridge is around 5600 ft. There are quite a few gaps in the data when the POM was malfunctioning on the ridge. However, this increase was also observed each time we sampled Horsetooth Reservoir. Other than this feature, the rest of the mobile O_3 data earlier on this drive followed a typical slow, steady increase when following the upslope flow. The drive path for this day was designed to perform Lagrangian sampling with the upslope/easterly flow. TEMPO special operations were requested and available. This day was not designated an Ozone Action Day by CDPHE, likely due to the forecast calling for strong winds. Mobile O_3 and NO_2 data compared to stationary O_3 and NO_2 measurements are shown in Figure 3.33. O_3 concentrations

at FTCW start to steadily decrease just as mobile O_3 measured at Horsetooth Reservoir just to the west starts to climb. As seen in Figure 3.34, there was minimal cloud cover this day (other than some convection over the Rockies). HYSPLIT back trajectories in Figure 3.35 indicate initiation of strong upslope flow at 12:30 that persisted through the end of the drive. TEMPO NO_2 data (Figure 3.36) show a large swath of NO_2 extending from the Denver urban core to the far northern part of the DMNFR O_3 NAA in Weld County. These precursor emissions were likely advected to the west by the strong upslope flow that initiated just after noon. This is hard to fully confirm observationally because NO_2 was likely converted to more oxidized forms (e.g., nitric acid) as it was carried westward in the afternoon and because TEMPO coverage was incomplete due to a narrow corridor of cloud cover associated with convection on the foothills. However, Figure 3.33 does show NO_2 peaking later at FTCW (~12:45 MDT) than at TIM and Fossil Creek (FOS), which lie upwind, suggesting aged precursor emissions were indeed transported westward by strong upslope flow shortly after the time of its formation. It is likely that these photochemically-aging emissions contributed to O_3 formation in the region. We hypothesize that the increased O_3 measured by the Plume Tracker at Horsetooth Reservoir was due to formation and advection of O_3 from upwind precursor transport in the strong upslope flow. While we cannot confidently conclude that O_3 levels are consistently higher at Horsetooth Reservoir, its location further downwind of major precursor sources and increased O_3 above levels at FTCW suggest this is worth further exploration. There is currently no monitoring at Horsetooth Reservoir or elsewhere in the foothills just west of Fort Collins.

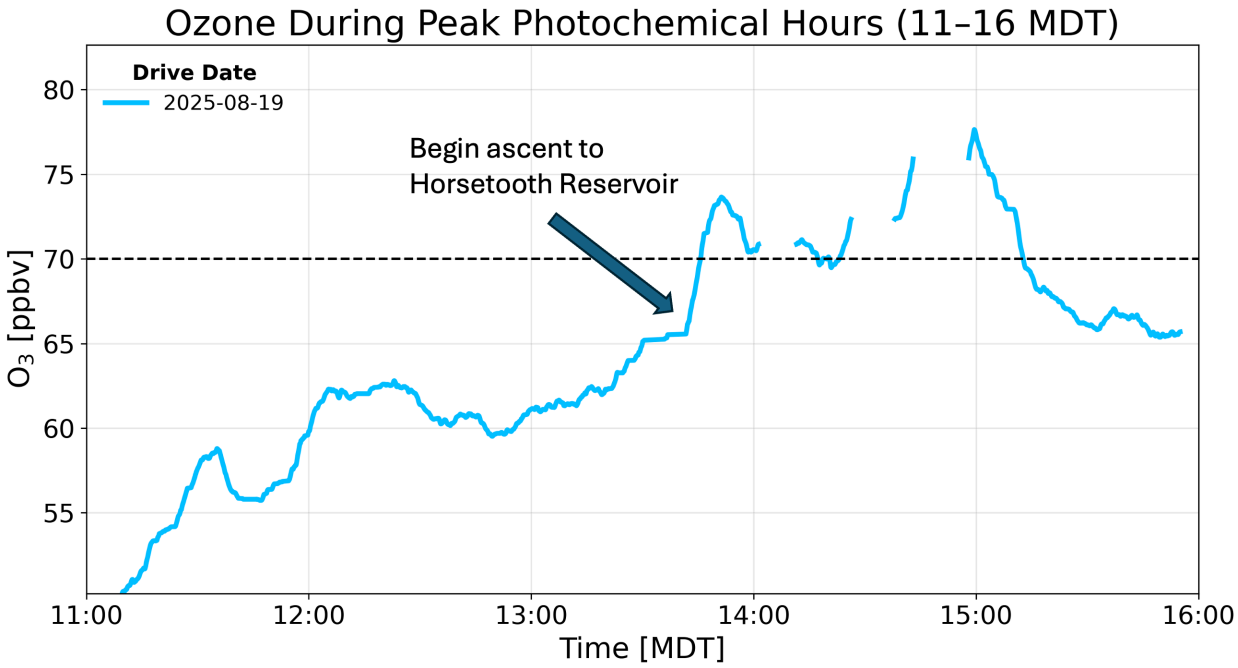


Figure 3.32: Filtered mobile O_3 concentrations from the August 19, 2025 driving intensive with a 10-min rolling average applied. The red arrow indicates when the Plume Tracker began sampling Horsetooth Reservoir. Gaps represent missing data from when the POM instrument malfunctioned.

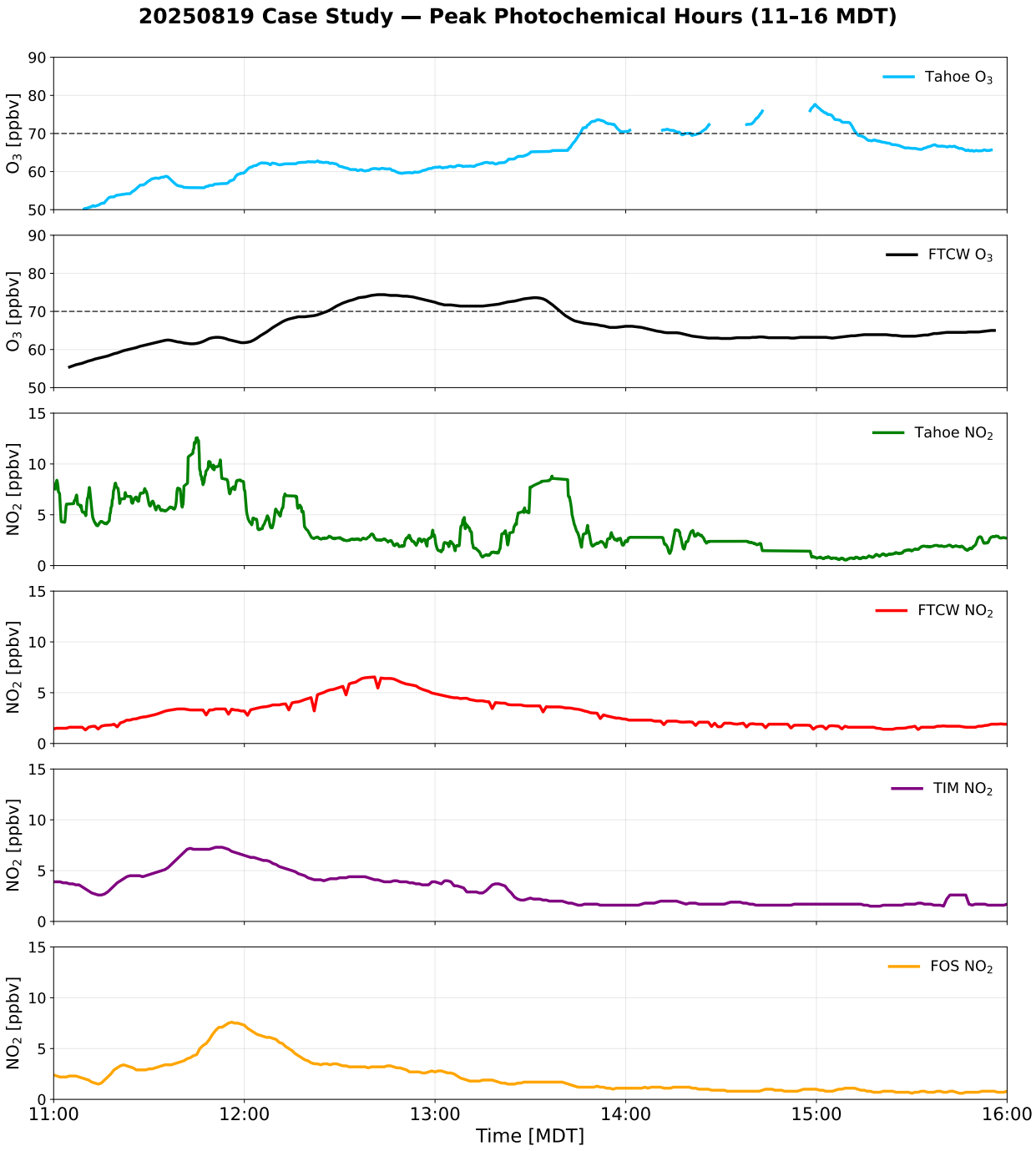


Figure 3.33: Time series of Plume Tracker O_3, stationary O_3 measurements on August 19, 2025 from the Fort Collins-West (FTCW) site, Plume Tracker NO_2 measurements, and stationary NO_2 measurements from the FCTW, Bethke Elementary (TIM), and Fossil Creek (FOS) sites. The O_3 data have a 10-min rolling average applied and the Plume Tracker NO_2 data have a 1-min rolling average.

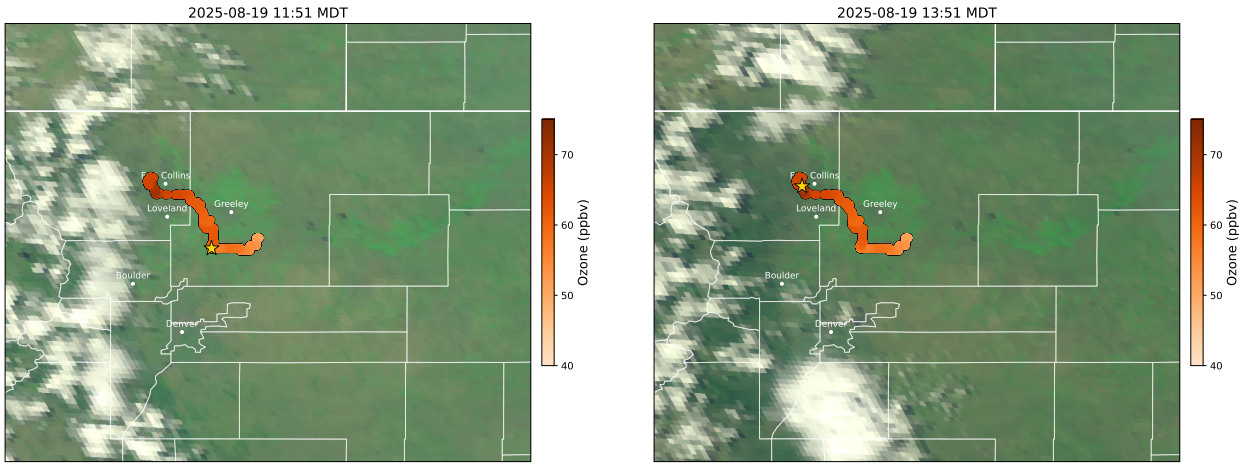


Figure 3.34: Visible GOES imagery from various times on August 19, 2025 overlaid with the CSU Tahoe O_3 concentrations. The yellow star indicates the vehicle's location at the time the satellite scan was taken.

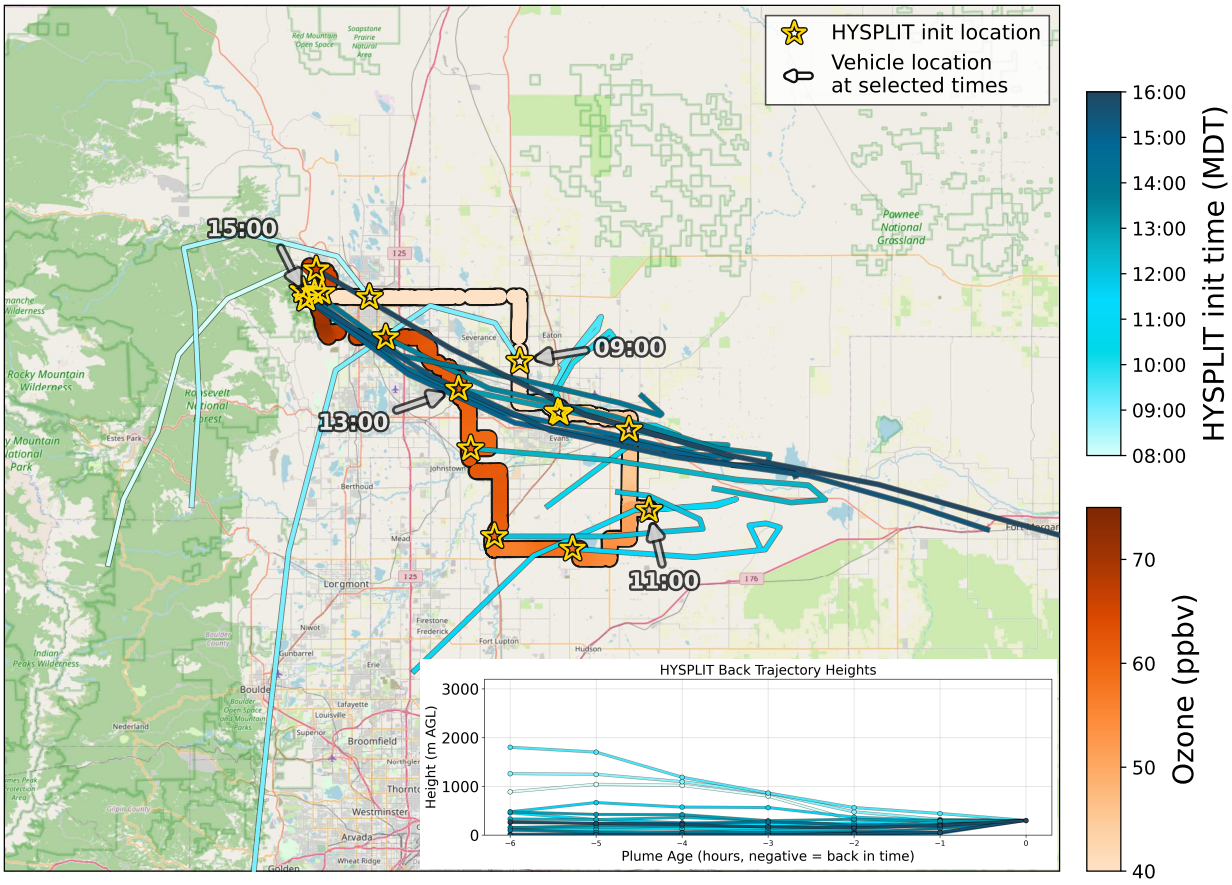


Figure 3.35: HYSPLIT back trajectories on August 19, 2025 initiated for 6 hours back in time every 30 minutes of the CSU Tahoe driving intensive overlaid with CSU Tahoe O_3 levels. The hollow yellow stars indicate the vehicle's location at the time of each trajectory initiation. The trajectories are colored by time, with darker colors being initiated later in the driving intensive. The heights of each trajectory along its path are shown in the bottom right.

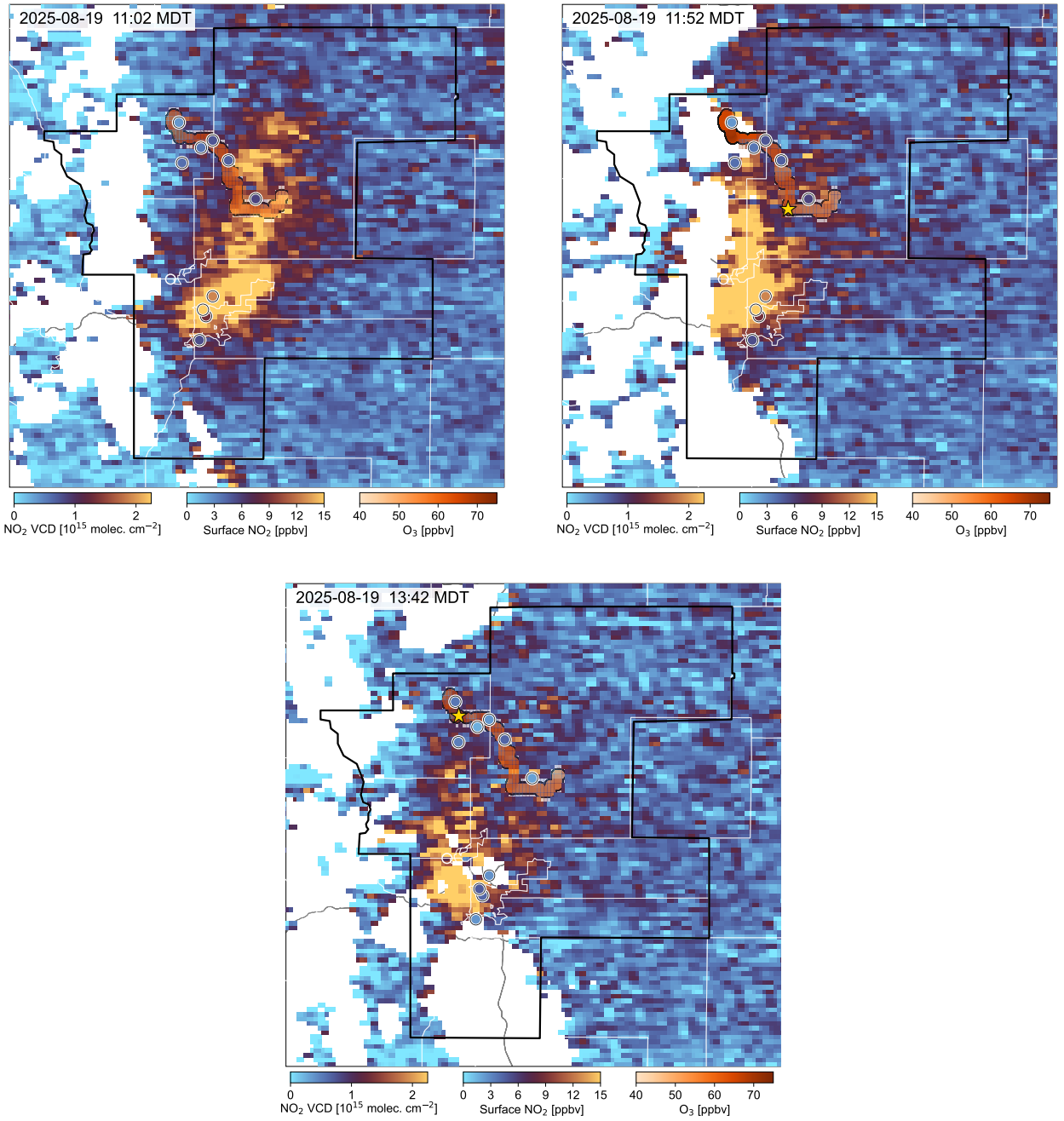


Figure 3.36: TEMPO NO_2 data scans at various times on August 19, 2025 overlaid with semi-transparent mobile O_3 concentrations and hourly NO_2 stationary site measurements (depicted as circles). The gold star represents the vehicle's location at the time of the TEMPO scan.

O_3 has long been thought of as a regional pollutant, as it exhibits less spatial variability than other pollutants, such as NO_2 and particulate matter (Chavez et al., 2025). Our analysis suggests that while this is true, substantial variability in O_3 still exists on relatively small spatial scales, and the plethora of contributing factors remain understudied. One better-known phenomenon contributing to O_3 variability is near-road O_3 titration due to fresh NO emissions from traffic (Riley et al., 2014; Solomon et al., 2020; Wild et al., 2017). This was frequently observed in our mobile data analysis, and remains an important factor to consider when O_3 variation was occurring. This effect is also commonly observed across urban areas where O_3 levels can decrease in an urban core and grow again as air is transported downwind of the city. Previous work has identified O_3 variability between the land-sea and urban-rural interfaces (Zhang et al., 2020a,b) using fixed-site measurements. This work adds to observations of such phenomena by employing both mobile and stationary measurements. Previous work has also shown the importance of O&G-related O_3 precursors in enhancing mobile O_3 measurements in rural areas in the DMNFR O_3 NAA (Cheadle et al., 2017b). Our data seem to support this conclusion, as mobile O_3 measurements were often elevated in the vicinity of or downwind of widespread O&G operations (e.g., Case Study #4).

In many cases, however, our ability to attribute O_3 variations to specific source emissions or other factors remains challenging. For a more comprehensive analysis, it would be useful to have both NO and NO_2 measurements, as opposed to solely NO_2, along with online measurements of multiple VOCs that can serve as source tracers. Despite these limitations, the mobile observations and case studies considered here clearly reveal important variations in O_3 levels over relatively short distances and help provide better understanding of O_3 formation and behavior across the DMNFR O_3 NAA.

4. CONCLUSION

Applying mobile measurement and whole air grab canister techniques, this work assessed the presence of air toxics, O&G-related tracer compounds, and criteria air pollutants in 12 DICs in the Northern Colorado Front Range during the summer of 2025 as a part of the FROZÉ field campaign. Mobile, stationary, and satellite measurements were also utilized to assess spatiotemporal distributions of O_3 and O_3 precursors across the DMNFR O_3 NAA.

The DICs chosen for sampling in this field campaign were among the most environmentally-burdened communities in Colorado, as indicated by CO Enviroscreen 2.0 scores. By performing zigzag sampling patterns in these DICs at a slow vehicle speed (~10 mph), we attempted to obtain representative data for the time period sampled. Whole air grab canister samples were analyzed for 51 different VOCs to quantify the concentrations of air toxics and other VOCs in these communities. Continuous, on-board measurements of NO_2 and O_3 allowed us to observe spatial gradients in these criteria pollutant concentrations in DICs.

Measured VOC, NO_2 and O_3 concentrations were compared to simultaneous measurements from several stationary air quality monitoring sites across the Front Range. We find that while the concentrations of air toxics in DICs were always below acute ATSDR/EPA HGVs during the time of sampling, air toxics and O&G tracers were elevated in some DICs compared to the mean value obtained from non-DIC stationary monitoring sites. For BTEX, toluene was significantly elevated in two and ethylbenzene and xylene (m+p+o) were significantly elevated in three of 15 DIC sampling periods. Among O&G tracers, hexane was significantly elevated in five of 15 DIC sampling periods and ethane was significantly elevated in 10 of 15. The i/n-pentane ratio was significantly higher or lower than the stationary sites in 12 of 15 DIC sampling periods, reflecting typical differences in local contributions from O&G emissions. For criteria air pollutants, we find that daytime O_3 was relatively low in DICs when compared to non-DIC stationary monitoring sites. NO_2 was significantly elevated in at least two of 15 DIC sampling periods (more if NO_2 data were not filtered for local plume removal) due to our filtering method. Most of the DICs we sampled did

not have existing air quality monitoring and our findings suggest a need to increase especially air toxics and NO_2 monitoring in Front Range DICs.

Thirteen mobile drives were conducted across the DMNFR O_3 NAA, with 11 during the day and two at night. The drive paths were designed with a range of objectives and often included an attempt to follow upslope flow, avoid cloud cover, and incorporate DIC sampling. We attempted to include regional transects between areas of interest, such as east-west transects north of the Denver metropolitan area. For NO_2, we find that regional hotspots often aligned with combustion sources, especially traffic near population centers around Fort Collins, Greeley, and Denver. When comparing mobile, stationary, and TEMPO NO_2 data, we find that spatial patterns observed show broad spatial agreement and that utilizing all three measurement sources increased our ability to observe spatial gradients across the region and assess weekend-weekday differences in NO_x emissions.

Mobile driving intensives revealed important spatial and temporal differences in O_3 concentrations across the DMNFR O_3 NAA. O_3 variations in individual drives often fell into one of two categories. The first type was a slow, steady increase in O_3 concentrations with time as the vehicle followed upslope flow, which we term "regional O_3 formation", or ROF, events. The second type was "local O_3 modification", or LOM, which featured substantial increases and/or decreases in O_3 concentrations over short time periods. We find that although O_3 is often considered to be a regional pollutant due to its slow photochemical formation from a variety of precursor NO_x and VOC emissions, our observations suggest considerable variability in O_3 concentrations, and associated exposures, at the local scale. While we lack sufficient observations to quantitatively attribute local O_3 variability to particular causes in all case studies we examined, we can conclude that LOM events are likely often associated with wind shifts that alter advection of precursor emissions, changes in the age and types/sources of precursor emissions, and titration of O_3 from fresh NO_x plumes on highways and denser urban settings. These results underscore the degree to which O_3 can vary spatiotemporally due to changes in meteorology and precursor emission sources, and represent a crucial step in better understanding O_3 formation and resulting exposure in the DMNFR O_3 NAA.

4.1 Future Work

The Colorado Front Range remains a complex landscape with respect to air quality in which regions of distinct emission sources interact. Given the spatial variability of these sources and the complexity of local meteorological patterns, mobile measurement platforms are a useful way to identify how O_3, its precursors, and air toxics are changing in real time. Our observations in DICs were short-term in nature due to other demands of the field campaign, and subsequent studies should establish longer-term or repeated monitoring in Front Range DIC communities. Adding longer-term mobile or fixed-site measurements in DICs would provide a more complete picture of the environmental burden placed on DICs by air toxics and criteria air pollutants. Future work could, for example, focus on populated areas (e.g., Greeley) that have little or no prior monitoring and are in closer proximity to O&G operations than most Front Range air quality monitors. While some wealthier Front Range communities (e.g., Broomfield, Erie, Longmont) have chosen to support their own monitoring of air toxics and criteria air pollutants, DICs in the Front Range remain understudied and under-resourced.

Mobile NO_2 measurements remain challenging to leverage due to the need for effective filtering of plumes from nearby vehicles. For our measurements, a great amount of effort was put into filtering the data. Despite this, our filtering method was still imperfect. Subsequent studies could benefit from having a more efficient filtering method that is less dependent on manually-selected thresholds. Better filtering of NO_2 would allow for a more direct comparison of measurements to existing datasets, as well as represent gradients in NO_2 in the DMNFR O_3 NAA more accurately. While our analysis included only NO_2, a more comprehensive measurement of both NO and NO_2 (NO_x) could better distinguish fresh and aged emissions. Future work should also include additional NO_x sampling in the Northern Colorado Front Range, which has historically less measurements than areas such as Denver. Recent CDPHE NO_x monitor additions in Loveland, Fort Collins, and Timnath are, fortunately, already helping to address this critical data gap. Additionally, this work represents a novel combination of mobile and TEMPO NO_2 data. Future studies should further utilize surface observations and vertical profiles (e.g., from aircraft measurements) of NO_2 (and

formaldehyde, HCHO) with TEMPO observations to assess the accuracy of TEMPO data and its utility for assessing temporospatial variability across the region.

There is still much that we do not understand about O_3 formation in the DMNFR O_3 NAA. Specifically, our LOM event results suggest a need to better contextualize the factors that control O_3 formation at the local scale, especially as it relates to precursor emissions and, ultimately, to human exposure. Given the inhomogeneity of emission sources across the DMNFR O_3 NAA, subsequent studies should leverage multiple mobile measurement platforms (including those from FROZÉ) to increase spatiotemporal coverage. This would allow for better examination of how emissions are photochemically aging and respond to local additions from different emission sources. A particularly valuable scenario would involve one vehicle sampling along the foothills, while another vehicle performs north-south transects further east in the DMNFR O_3 NAA, a strategy that could provide valuable insight into how emissions photochemically react while being advected westward in afternoon upslope flow. Additionally, analyzing mobile O_3 data in the context of TEMPO O_3 data was not possible during our study, as the TEMPO team is still working on finishing its O_3 data product. When it is available, future studies should prioritize contextualizing mobile O_3 measurements with TEMPO O_3 data. The better we understand these challenges to having clean air, the more these results will inform policies to implement changes that reduce people's exposure to harmful pollutants.

REFERENCES

Acker, S., T. Holloway, and M. Harkey, 2025: Satellite detection of NO_2 distributions using TROPOMI and TEMPO and comparison with ground-based concentration measurements. *Atmospheric Chemistry and Physics*, **25 (14)**, 8271–8288, doi: 10.5194/acp-25-8271-2025, URL https://acp.copernicus.org/articles/25/8271/2025/.

Actkinson, B., K. Ensor, and R. J. Griffin, 2021: SIBaR: a new method for background quantification and removal from mobile air pollution measurements. *Atmospheric Measurement Techniques*, **14 (8)**, 5809–5821, doi: 10.5194/amt-14-5809-2021, URL https://amt.copernicus.org/articles/14/5809/2021/.

Andersen, P. C., C. J. Williford, and J. W. Birks, 2010: Miniature Personal Ozone Monitor Based on UV Absorbance. *Analytical Chemistry*, **82 (19)**, 7924–7928, doi: 10.1021/ac1013578, URL https://pubs.acs.org/doi/10.1021/ac1013578.

Ash, M., J. K. Boyce, G. Chang, M. Pastor, and J. Scoggins, 2009: Justice in the Air: Tracking Toxic Pollution from America's Industries and Companies to our States, Cities and Neighborhoods.

Bechle, M. J., D. B. Millet, and J. D. Marshall, 2013: Remote sensing of exposure to NO2: Satellite versus ground-based measurement in a large urban area. *Atmospheric Environment*, **69**, 345–353, doi: 10.1016/j.atmosenv.2012.11.046, URL https://www.sciencedirect.com/science/article/pii/S1352231012011144.

Benedict, K. B., et al., 2019: Volatile organic compounds and ozone in Rocky Mountain National Park during FRAPPÉ. *Atmospheric Chemistry and Physics*, **19 (1)**, 499–521, doi: 10.5194/acp-19-499-2019, URL https://acp.copernicus.org/articles/19/499/2019/.

Birks, J. W., P. C. Andersen, C. J. Williford, A. A. Turnipseed, S. E. Strunk, C. A. Ennis, and E. Mattson, 2018: Folded tubular photometer for atmospheric measurements of NO_2 and NO. *Atmospheric Measurement Techniques*, **11 (5)**, 2821–2835, doi: 10.5194/amt-11-2821-2018, URL https://amt.copernicus.org/articles/11/2821/2018/.

Bravo, M. A., R. Anthopolos, M. L. Bell, and M. L. Miranda, 2016: Racial isolation and exposure to airborne particulate matter and ozone in understudied US populations: Environmental justice applications of downscaled numerical model output. *Environment International*, **92-93**, 247–255, doi: 10.1016/j.envint.2016.04.008, URL https://www.sciencedirect.com/science/article/pii/S0160412016301386.

Brey, S. J., M. Ruminski, S. A. Atwood, and E. V. Fischer, 2018: Connecting smoke plumes to sources using Hazard Mapping System (HMS) smoke and fire location data over North America. *Atmospheric Chemistry and Physics*, **18 (3)**, 1745–1761, doi: 10.5194/acp-18-1745-2018, URL https://acp.copernicus.org/articles/18/1745/2018/.

Cardoso-Saldaña, F. J., Y. Kimura, P. Stanley, G. McGaughey, S. C. Herndon, J. R. Roscioli, T. I. Yacovitch, and D. T. Allen, 2019: Use of Light Alkane Fingerprints in Attributing Emissions

from Oil and Gas Production. *Environmental Science & Technology*, **53 (9)**, 5483–5492, doi: 10.1021/acs.est.8b05828, URL https://doi.org/10.1021/acs.est.8b05828.

Chavez, M., L. Vazquez-Raygoza, E. Williams, and W.-W. Li, 2025: Spatial-Temporal Assessment of Traffic-Related Pollutants Using Mobile and Stationary Monitoring in an Urban Environment. *Air*, **3 (2)**, 18, doi: 10.3390/air3020018, URL https://www.mdpi.com/2813-4168/3/2/18.

Cheadle, L., L. Deanes, K. Sadighi, J. Gordon Casey, A. Collier-Oxandale, and M. Hannigan, 2017a: Quantifying Neighborhood-Scale Spatial Variations of Ozone at Open Space and Urban Sites in Boulder, Colorado Using Low-Cost Sensor Technology. *Sensors (Basel, Switzerland)*, **17 (9)**, 2072, doi: 10.3390/s17092072, URL https://pmc.ncbi.nlm.nih.gov/articles/PMC5620960/.

Cheadle, L. C., et al., 2017b: Surface ozone in the Colorado northern Front Range and the influence of oil and gas development during FRAPPE/DISCOVER-AQ in summer 2014. *Elementa: Science of the Anthropocene*, **5**, 61, doi: 10.1525/elementa.254, URL https://doi.org/10.1525/elementa.254.

Chen, J., et al., 2009: The effects of global changes upon regional ozone pollution in the United States. *Atmospheric Chemistry and Physics*, **9 (4)**, 1125–1141, doi: 10.5194/acp-9-1125-2009, URL https://acp.copernicus.org/articles/9/1125/2009/.

Chiavarini, M., P. Rosignoli, B. Sorbara, I. Giacchetta, and R. Fabiani, 2024: Benzene Exposure and Lung Cancer Risk: A Systematic Review and Meta-Analysis of Human Studies. *International Journal of Environmental Research and Public Health*, **21 (2)**, 205, doi: 10.3390/ijerph21020205, URL https://www.mdpi.com/1660-4601/21/2/205.

Cohr, K.-H. and J. Stokholm, 1979: Toluene: A toxicologic review. *Scandinavian Journal of Work, Environment & Health*, **5 (2)**, 71–90, URL https://www.jstor.org/stable/40964761.

Crutzen, P. J., 1988: Tropospheric Ozone: An Overview. *Tropospheric Ozone: Regional and Global Scale Interactions*, I. S. A. Isaksen, Ed., Springer Netherlands, Dordrecht, 3–32, doi: 10.1007/978-94-009-2913-5˙1, URL https://doi.org/10.1007/978-94-009-2913-5_1.

Currit, E., 2022: Disproportionate Exposure to Air Pollution for Low-Income Communities in the United States. *Ballard Brief*, **2022 (2)**, URL https://scholarsarchive.byu.edu/ballardbrief/vol2022/iss2/6.

Das, A., B. S. Giri, and R. Manjunatha, 2025: Systematic review on benzene, toluene, ethylbenzene, and xylene (BTEX) emissions; health impact assessment; and detection techniques in oil and natural gas operations. *Environmental Science and Pollution Research*, **32 (1)**, 1–22, doi: 10.1007/s11356-024-35698-1, URL https://doi.org/10.1007/s11356-024-35698-1.

David, L. M. and P. R. Nair, 2011: Diurnal and seasonal variability of surface ozone and NOx at a tropical coastal site: Association with mesoscale and synoptic meteorological conditions. *Journal of Geophysical Research: Atmospheres*, **116 (D10)**, doi: 10.1029/2010JD015076, URL https://onlinelibrary.wiley.com/doi/abs/10.1029/2010JD015076, _eprint:

https://agupubs.onlinelibrary.wiley.com/doi/pdf/10.1029/2010JD015076.

Di Virgilio, G., J. P. Evans, S. A. P. Blake, M. Armstrong, A. J. Dowdy, J. Sharples, and R. McRae, 2019: Climate Change Increases the Potential for Extreme Wildfires. *Geophysical Research Letters*, **46 (14)**, 8517–8526, doi: 10.1029/2019GL083699, URL https://onlinelibrary.wiley.com/doi/abs/10.1029/2019GL083699, _eprint: https://agupubs.onlinelibrary.wiley.com/doi/pdf/10.1029/2019GL083699.

Donzelli, G. and M. M. Suarez-Varela, 2024: Tropospheric Ozone: A Critical Review of the Literature on Emissions, Exposure, and Health Effects. *Atmosphere*, **15 (7)**, 779, doi: 10.3390/atmos15070779, URL https://www.mdpi.com/2073-4433/15/7/779.

Dummer, N., C. Leoni, E. Saldaña, C. Villa, S. Guerra, C. Schroeder, M. D'agostino, and B. González, 2025: Air permitting for Colorado stationary sources in disproportionately impacted communities. *Journal of the Air & Waste Management Association*, **75 (8)**, 615–623, doi: 10.1080/10962247.2025.2502501, URL https://doi.org/10.1080/10962247.2025.2502501, _eprint: https://doi.org/10.1080/10962247.2025.2502501.

Evans, J. M. and D. Helmig, 2017: Investigation of the influence of transport from oil and natural gas regions on elevated ozone levels in the northern Colorado front range. *Journal of the Air & Waste Management Association*, **67 (2)**, 196–211, doi: 10.1080/10962247.2016.1226989, URL https://doi.org/10.1080/10962247.2016.1226989, _eprint: https://doi.org/10.1080/10962247.2016.1226989.

Fishbein, L., 1985a: An overview of environmental and toxicological aspects of aromatic hydrocarbons II. Toluene. *Science of The Total Environment*, **42 (3)**, 267–288, doi: 10.1016/0048-9697(85)90062-2, URL https://www.sciencedirect.com/science/article/pii/0048969785900622.

Fishbein, L., 1985b: An overview of environmental and toxicological aspects of aromatic hydrocarbons IV. Ethylbenzene. *Science of The Total Environment*, **44 (3)**, 269–287, doi: 10.1016/0048-9697(85)90100-7, URL https://www.sciencedirect.com/science/article/pii/0048969785901007.

Flocke, F., G. Pfister, J. H. Crawford, K. E. Pickering, G. Pierce, D. Bon, and P. Reddy, 2020: Air Quality in the Northern Colorado Front Range Metro Area: The Front Range Air Pollution and Photochemistry Éxperiment (FRAPPÉ). *Journal of Geophysical Research: Atmospheres*, **125 (2)**, e2019JD031 197, doi: 10.1029/2019JD031197, URL https://onlinelibrary.wiley.com/doi/abs/10.1029/2019JD031197, _eprint: https://agupubs.onlinelibrary.wiley.com/doi/pdf/10.1029/2019JD031197.

Foley, K. M., et al., 2023: 2002–2017 anthropogenic emissions data for air quality modeling over the United States. *Data in Brief*, **47**, 109 022, doi: 10.1016/j.dib.2023.109022, URL https://www.sciencedirect.com/science/article/pii/S2352340923001403.

Gelencsér, A., K. Siszler, and J. Hlavay, 1997: TolueneBenzene Concentration

Ratio as a Tool for Characterizing the Distance from Vehicular Emission Sources. *Environmental Science & Technology*, **31 (10)**, 2869–2872, doi: 10.1021/es970004c, URL https://doi.org/10.1021/es970004c.

Gilman, J. B., B. M. Lerner, W. C. Kuster, and J. A. de Gouw, 2013: Source Signature of Volatile Organic Compounds from Oil and Natural Gas Operations in Northeastern Colorado. *Environmental Science & Technology*, **47 (3)**, 1297–1305, doi: 10.1021/es304119a, URL https://doi.org/10.1021/es304119a.

Guevara Proaño, D. C., 2025: Summertime Spatiotemporal Patterns of Nitrogen Oxides (NOx) in Salt Lake City. M.S. thesis, Colorado State University, United States – Colorado, URL https://www.proquest.com/docview/3291098410/abstract/5814B286493040C3PQ/1.

Hamilton, R. J. and D. H. Schaffer, 2026: n-hexane Toxicity. *StatPearls*, StatPearls Publishing, Treasure Island (FL), URL http://www.ncbi.nlm.nih.gov/books/NBK609093/.

Hecobian, A., et al., 2019: Air Toxics and Other Volatile Organic Compound Emissions from Unconventional Oil and Gas Development. *Environmental Science & Technology Letters*, **6 (12)**, 720–726, doi: 10.1021/acs.estlett.9b00591, URL https://doi.org/10.1021/acs.estlett.9b00591.

Helmig, D., 2020: Air quality impacts from oil and natural gas development in Colorado. *Elementa: Science of the Anthropocene*, **8**, 4, doi: 10.1525/elementa.398, URL https://doi.org/10.1525/elementa.398.

Hendrick, M. F., R. Ackley, B. Sanaie-Movahed, X. Tang, and N. G. Phillips, 2016: Fugitive methane emissions from leak-prone natural gas distribution infrastructure in urban environments. *Environmental Pollution*, **213**, 710–716, doi: 10.1016/j.envpol.2016.01.094, URL https://www.sciencedirect.com/science/article/pii/S0269749116300938.

Houston, D., J. Wu, P. Ong, and A. Winer, 2004: Structural Disparities of Urban Traffic in Southern California: Implications for Vehicle-Related Air Pollution Exposure in Minority and High-Poverty Neighborhoods. *Journal of Urban Affairs*, **26 (5)**, 565–592, doi: 10.1111/j.0735-2166.2004.00215.x, URL https://doi.org/10.1111/j.0735-2166.2004.00215.x, _eprint: https://doi.org/10.1111/j.0735-2166.2004.00215.x.

Irie, H., M. Nomoto, Y. Kamiya, and Y. Terao, 2026: Simultaneous measurements of near-surface CO_2 and NO_2 to monitor the fossil-fuel combustion-derived CO_2 in the Greater Tokyo Area. *Atmospheric Measurement Techniques*, **19 (7)**, 2369–2378, doi: 10.5194/amt-19-2369-2026, URL https://amt.copernicus.org/articles/19/2369/2026/.

Johnston, J. E., K. Okorn, Y. O. V. Horne, and A. Jimenez, 2021: Changes in neighborhood air quality after idling of an urban oil production site. *Environmental Science: Processes & Impacts*, **23 (7)**, 967–980, doi: 10.1039/D1EM00048A, URL https://pubs.rsc.org/en/content/articlelanding/2021/em/d1em00048a.

Katz, D., 2015: The Interstate Highway System and Environmental Justice: Disproportionate

Environmental Impacts on Low Income and Minority Communities. *Student Theses 2015-Present*, URL https://research.library.fordham.edu/environ_2015/6.

Kim, S.-J., I.-T. Ku, Y. Zhou, D. Pan, L. Low, M. Frazier, B. Buck, and J. L. Collett, 2026: Long-term community monitoring of volatile organic compounds and methane in Erie, Colorado: sources and health risks. *Science of The Total Environment*, **1010**, 181 100, doi: 10.1016/j.scitotenv.2025.181100, URL https://www.sciencedirect.com/science/article/pii/S0048969725027408.

Kim, S.-Y., E. Kim, and W. J. Kim, 2020: Health Effects of Ozone on Respiratory Diseases. *Tuberculosis and Respiratory Diseases*, **83 (Supple 1)**, S6–S11, doi: 10.4046/trd.2020.0154, URL https://pmc.ncbi.nlm.nih.gov/articles/PMC7837374/.

Ku, I.-T., et al., 2024: Air quality impacts from the development of unconventional oil and gas well pads: Air toxics and other volatile organic compounds. *Atmospheric Environment*, **317**, 120 187, doi: 10.1016/j.atmosenv.2023.120187, URL https://www.sciencedirect.com/science/article/pii/S1352231023006131.

Levy, I., C. Mihele, G. Lu, J. Narayan, N. Hilker, and J. R. Brook, 2014: Elucidating multipollutant exposure across a complex metropolitan area by systematic deployment of a mobile laboratory. *Atmospheric Chemistry and Physics*, **14 (14)**, 7173–7193, doi: 10.5194/acp-14-7173-2014, URL https://acp.copernicus.org/articles/14/7173/2014/.

Li, S., Z. Li, and X. Sun, 2017: Effect of flue gas and *n*-hexane on heavy oil properties in steam flooding process. *Fuel*, **187**, 84–93, doi: 10.1016/j.fuel.2016.09.050, URL https://www.sciencedirect.com/science/article/pii/S0016236116309073.

Lindaas, J., D. K. Farmer, I. B. Pollack, A. Abeleira, F. Flocke, R. Roscioli, S. Herndon, and E. V. Fischer, 2017: Changes in ozone and precursors during two aged wildfire smoke events in the Colorado Front Range in summer 2015. *Atmospheric Chemistry and Physics*, **17 (17)**, 10 691–10 707, doi: 10.5194/acp-17-10691-2017, URL https://acp.copernicus.org/articles/17/10691/2017/.

Lippmann, M., 1989: HEALTH EFFECTS OF OZONE A Critical Review. *JAPCA*, **39 (5)**, 672–695, doi: 10.1080/08940630.1989.10466554, URL https://doi.org/10.1080/08940630.1989.10466554, _eprint: https://doi.org/10.1080/08940630.1989.10466554.

Liu, Y., et al., 2026: Laboratory and field assessment of mid-infrared absorption (MIRA) instrument performance for methane and ethane dry mole fractions. *Atmospheric Measurement Techniques*, **19 (3)**, 965–981, doi: 10.5194/amt-19-965-2026, URL https://amt.copernicus.org/articles/19/965/2026/.

Low, L., 2025: Volatile Organic Compounds and Air Toxics in Northern Colorado. M.S. thesis, Colorado State University, United States – Colorado, URL https://www.proquest.com/docview/3291414358/abstract/A12617A447ED4B59PQ/1.

Low, L., et al., 2026: (in review) spatiotemporal variations and source apportionment of volatile organic compounds and air toxics in northern colorado. *Journal of Geophysical Research: Atmospheres*.

Macey, G. P., R. Breech, M. Chernaik, C. Cox, D. Larson, D. Thomas, and D. O. Carpenter, 2014: Air concentrations of volatile compounds near oil and gas production: a community-based exploratory study. *Environmental Health: A Global Access Science Source*, **13**, 82, doi: 10.1186/1476-069X-13-82.

Malin, S. A., I. Luxton, K. Hulama, and R. Beltrán, 2025: "We go to the hospital everyday": The Suncor oil refinery, environmental injustice, and contested illness. *Health & Place*, **95**, 103 525, doi: 10.1016/j.healthplace.2025.103525, URL https://www.sciencedirect.com/science/article/pii/S1353829225001157.

McDuffie, E. E., et al., 2016: Influence of oil and gas emissions on summertime ozone in the Colorado Northern Front Range. *Journal of Geophysical Research: Atmospheres*, **121 (14)**, 8712–8729, doi: 10.1002/2016JD025265, URL https://onlinelibrary.wiley.com/doi/abs/10.1002/2016JD025265, _eprint: https://agupubs.onlinelibrary.wiley.com/doi/pdf/10.1002/2016JD025265.

McKenzie, L. M., et al., 2018: Ambient Nonmethane Hydrocarbon Levels Along Colorado's Northern Front Range: Acute and Chronic Health Risks. *Environmental Science & Technology*, **52 (8)**, 4514–4525, doi: 10.1021/acs.est.7b05983, URL https://doi.org/10.1021/acs.est.7b05983.

Mihaita, A.-S., L. Dupont, O. Cherry, M. Camargo, and C. Cai, 2018: Air quality monitoring using stationary versus mobile sensing units: a case study from Lorraine, France.

Morgan, B., R. Hansgen, W. Hawthorne, and S. L. Miller, 2015: Industrial odor sources and air pollutant concentrations in Globeville, a Denver, Colorado neighborhood. *Journal of the Air & Waste Management Association*, **65 (9)**, 1127–1140, doi: 10.1080/10962247.2015.1064833, URL https://doi.org/10.1080/10962247.2015.1064833, _eprint: https://doi.org/10.1080/10962247.2015.1064833.

Muzio, L. J. and G. C. Quartucy, 1997: Implementing NOx control: Research to application. *Progress in Energy and Combustion Science*, **23 (3)**, 233–266, doi: 10.1016/S0360-1285(97)00002-6, URL https://www.sciencedirect.com/science/article/pii/S0360128597000026.

Nawaz, M. O., D. E. Huber, G. H. Kerr, L. M. Judd, S. J. Acker, and D. L. Goldberg, 2025: A Comparative Analysis of TEMPO NO2 Remote Sensing With Surface-Level Monitoring Through Diurnal and Seasonal Trends, Meteorology, and Monitor Characteristics. *Journal of Geophysical Research: Atmospheres*, **130 (20)**, e2025JD043 923, doi: 10.1029/2025JD043923, URL https://onlinelibrary.wiley.com/doi/abs/10.1029/2025JD043923, _eprint: https://agupubs.onlinelibrary.wiley.com/doi/pdf/10.1029/2025JD043923.

Niaz, K., H. Bahadar, F. Maqbool, and M. Abdollahi, 2015: A review of environmental and

occupational exposure to xylene and its health concerns. *EXCLI Journal*, **14**, 1167–1186, doi: 10.17179/excli2015-623, URL https://pmc.ncbi.nlm.nih.gov/articles/PMC4743476/.

Nitschke, M., 1999: Respiratory health effects of nitrogen dioxide exposure and current guidelines. *International Journal of Environmental Health Research*, **9 (1)**, 39–53, doi: 10.1080/09603129973344, URL https://doi.org/10.1080/09603129973344, _eprint: https://doi.org/10.1080/09603129973344.

Niu, Y., et al., 2018: Estimation of personal ozone exposure using ambient concentrations and influencing factors. *Environment International*, **117**, 237–242, doi: 10.1016/j.envint.2018.05.017, URL https://www.sciencedirect.com/science/article/pii/S0160412018304021.

Nowlan, C. R., G. G. Abad, X. Liu, Huiqun Wang, and K. Chance, 2025: TEMPO Nitrogen Dioxide Retrieval Algorithm Theoretical Basis Document. doi: 10.5067/WX026254FI2U, URL https://www.earthdata.nasa.gov/apt/documents/tempo-nitrogen-dioxide-retrieval/v1.0.

Oltmans, S. J., et al., 2019: Boundary layer ozone in the Northern Colorado Front Range in July–August 2014 during FRAPPE and DISCOVER-AQ from vertical profile measurements. *Elementa: Science of the Anthropocene*, **7**, 6, doi: 10.1525/elementa.345, URL https://online.ucpress.edu/elementa/article/doi/10.1525/elementa.345/112474/Boundary-layer-ozone-in-the-Northern-Colorado.

Pandey, S. K. and J. Singh, 2021: Nitrogen dioxide: Risk assessment, environmental, and health hazard. *Hazardous Gases*, Elsevier, 273–288, doi: 10.1016/B978-0-323-89857-7.00001-3, URL https://linkinghub.elsevier.com/retrieve/pii/B9780323898577000013.

Pfister, G., C.-T. Wang, M. Barth, F. Flocke, W. Vizuete, and S. Walters, 2019: Chemical Characteristics and Ozone Production in the Northern Colorado Front Range. *Journal of Geophysical Research: Atmospheres*, **124 (23)**, 13 397–13 419, doi: 10.1029/2019JD030544, URL https://onlinelibrary.wiley.com/doi/abs/10.1029/2019JD030544, _eprint: https://agupubs.onlinelibrary.wiley.com/doi/pdf/10.1029/2019JD030544.

Pollack, I. B., D. Helmig, K. O'Dell, and E. V. Fischer, 2021a: Seasonality and Source Apportionment of Nonmethane Volatile Organic Compounds at Boulder Reservoir, Colorado, Between 2017 and 2019. *Journal of Geophysical Research: Atmospheres*, **126 (9)**, e2020JD034 234, doi: 10.1029/2020JD034234, URL https://onlinelibrary.wiley.com/doi/abs/10.1029/2020JD034234, _eprint: https://agupubs.onlinelibrary.wiley.com/doi/pdf/10.1029/2020JD034234.

Pollack, I. B., D. Helmig, K. O'Dell, and E. V. Fischer, 2021b: Weekend-Weekday Implications and the Impact of Wildfire Smoke on Ozone and Its Precursors at Boulder Reservoir, Colorado Between 2017 and 2019. *Journal of Geophysical Research: Atmospheres*, **126 (17)**, e2021JD035 221, doi: 10.1029/2021JD035221, URL https://onlinelibrary.wiley.com/doi/abs/10.1029/2021JD035221, _eprint: https://agupubs.onlinelibrary.wiley.com/doi/pdf/10.1029/2021JD035221.

Pusker, S. M., K. A. DeBie, M. L. Clark, A. M. Neophytou, K. P. Keller, M. J. Gutilla, and D. Rojas-Rueda, 2024: Environmental Justice and Sustainable Development: Cumulative Environmental Exposures and All-Cause Mortality in Colorado Counties. *Sustainability*, **16 (21)**, 9147, doi: 10.3390/su16219147, URL https://www.mdpi.com/2071-1050/16/21/9147.

Pétron, G., et al., 2012: Hydrocarbon emissions characterization in the Colorado Front Range: A pilot study. *Journal of Geophysical Research: Atmospheres*, **117 (D4)**, doi: 10.1029/2011JD016360, URL https://onlinelibrary.wiley.com/doi/abs/10.1029/2011JD016360, _eprint: https://agupubs.onlinelibrary.wiley.com/doi/pdf/10.1029/2011JD016360.

Reddy, P. J. and G. G. Pfister, 2016: Meteorological factors contributing to the interannual variability of midsummer surface ozone in Colorado, Utah, and other western U.S. states. *Journal of Geophysical Research: Atmospheres*, **121 (5)**, 2434–2456, doi: 10.1002/2015JD023840, URL https://onlinelibrary.wiley.com/doi/abs/10.1002/2015JD023840, _eprint: https://agupubs.onlinelibrary.wiley.com/doi/pdf/10.1002/2015JD023840.

Riley, E. A., et al., 2014: Multi-pollutant mobile platform measurements of air pollutants adjacent to a major roadway. *Atmospheric environment (Oxford, England : 1994)*, **98**, 492–499, doi: 10.1016/j.atmosenv.2014.09.018, URL https://pmc.ncbi.nlm.nih.gov/articles/PMC4212219/.

Rolph, G., A. Stein, and B. Stunder, 2017: Real-time Environmental Applications and Display sYstem: READY. *Environmental Modelling & Software*, **95**, 210–228, doi: 10.1016/j.envsoft.2017.06.025, URL https://www.sciencedirect.com/science/article/pii/S1364815217302360.

Rossabi, S. and D. Helmig, 2018: Changes in Atmospheric Butanes and Pentanes and Their Isomeric Ratios in the Continental United States. *Journal of Geophysical Research: Atmospheres*, **123 (7)**, 3772–3790, doi: 10.1002/2017JD027709, URL https://onlinelibrary.wiley.com/doi/abs/10.1002/2017JD027709, _eprint: https://agupubs.onlinelibrary.wiley.com/doi/pdf/10.1002/2017JD027709.

Rossabi, S., J. Hueber, W. Wang, P. Milmoe, and D. Helmig, 2021: Spatial distribution of atmospheric oil and natural gas volatile organic compounds in the Northern Colorado Front Range. *Elementa: Science of the Anthropocene*, **9 (1)**, 00036, doi: 10.1525/elementa.2019.00036, URL https://doi.org/10.1525/elementa.2019.00036.

Russo, R. S., Y. Zhou, M. L. White, H. Mao, R. Talbot, and B. C. Sive, 2010: Multi-year (2004–2008) record of nonmethane hydrocarbons and halocarbons in New England: seasonal variations and regional sources. *Atmospheric Chemistry and Physics*, **10 (10)**, 4909–4929, doi: 10.5194/acp-10-4909-2010, URL https://acp.copernicus.org/articles/10/4909/2010/.

Ryder, S. S., 2017: A Bridge to Challenging Environmental Inequality: Intersectionality, Environmental Justice, and Disaster Vulnerability. *Social Thought & Research*, **34**, 85–115, URL https://www.jstor.org/stable/44807699.

Saeedi, M., B. Malekmohammadi, and S. Tajalli, 2024: Interaction of benzene, toluene, ethylbenzene, and xylene with human's body: Insights into characteristics, sources and health risks. *Journal of Hazardous Materials Advances*, **16**, 100 459, doi: 10.1016/j.hazadv.2024.100459, URL https://www.sciencedirect.com/science/article/pii/S2772416624000603.

Sexton, K., H. GongJr., J. C. Bailar, J. G. Ford, D. R. Gold, W. E. Lambert, and M. J. Utell, 1993: Air Pollution Health Risks: Do Class and Race Matter? *Toxicology and Industrial Health*, **9 (5)**, 843–878, doi: 10.1177/074823379300900509, URL https://doi.org/10.1177/074823379300900509.

Smith, M. L., E. A. Kort, A. Karion, C. Sweeney, S. C. Herndon, and T. I. Yacovitch, 2015: Airborne Ethane Observations in the Barnett Shale: Quantification of Ethane Flux and Attribution of Methane Emissions. *Environmental Science & Technology*, **49 (13)**, 8158–8166, doi: 10.1021/acs.est.5b00219, URL https://doi.org/10.1021/acs.est.5b00219.

Solomon, P. A., D. Vallano, M. Lunden, B. LaFranchi, C. L. Blanchard, and S. L. Shaw, 2020: Mobile-Platform Measurement of Air Pollutant Concentrations in California: Performance Assessment, Statistical Methods for Evaluating Spatial Variations, and Spatial Representativeness. *Atmospheric measurement techniques*, **13 (6)**, 10.5194/amt–13–3277–2020, doi: 10.5194/amt-13-3277-2020, URL https://pmc.ncbi.nlm.nih.gov/articles/PMC8422882/.

Stein, A. F., R. R. Draxler, G. D. Rolph, B. J. B. Stunder, M. D. Cohen, and F. Ngan, 2015: NOAA's HYSPLIT Atmospheric Transport and Dispersion Modeling System. *Bulletin of the American Meteorological Society*, **96 (12)**, 2059–2077, doi: 10.1175/BAMS-D-14-00110.1, URL https://journals.ametsoc.org/view/journals/bams/96/12/bams-d-14-00110.1.xml.

Su, J. G., M. Jerrett, A. de Nazelle, and J. Wolch, 2011: Does exposure to air pollution in urban parks have socioeconomic, racial or ethnic gradients? *Environmental Research*, **111 (3)**, 319–328, doi: 10.1016/j.envres.2011.01.002, URL https://www.sciencedirect.com/science/article/pii/S001393511100003X.

Su, J. G., et al., 2024: Examining air pollution exposure dynamics in disadvantaged communities through high-resolution mapping. *Science Advances*, **10 (32)**, eadm9986, doi: 10.1126/sciadv.adm9986, URL https://www.science.org/doi/full/10.1126/sciadv.adm9986.

Sullivan, J. T., et al., 2016: Quantifying the contribution of thermally driven recirculation to a high-ozone event along the Colorado Front Range using lidar. *Journal of Geophysical Research: Atmospheres*, **121 (17)**, 10,377–10,390, doi: 10.1002/2016JD025229, URL https://onlinelibrary.wiley.com/doi/abs/10.1002/2016JD025229, _eprint: https://agupubs.onlinelibrary.wiley.com/doi/pdf/10.1002/2016JD025229.

Swarthout, R. F., R. S. Russo, Y. Zhou, A. H. Hart, and B. C. Sive, 2013: Volatile organic compound distributions during the NACHTT campaign at the Boulder Atmospheric Observatory: Influence of urban and natural gas sources. *Journal of Geophysical Research: Atmospheres*, **118 (18)**, 10,614–10,637, doi: 10.1002/jgrd.50722,

URL https://onlinelibrary.wiley.com/doi/abs/10.1002/jgrd.50722, _eprint: https://agupubs.onlinelibrary.wiley.com/doi/pdf/10.1002/jgrd.50722.

T. Rajan, S. and N. Malathi, 2014: Health Hazards of Xylene: A Literature Review. *Journal of Clinical and Diagnostic Research : JCDR*, **8 (2)**, 271–274, doi: 10.7860/JCDR/2014/7544.4079, URL https://pmc.ncbi.nlm.nih.gov/articles/PMC3972585/.

Tessum, C. W., et al., 2019: Inequity in consumption of goods and services adds to racial-ethnic disparities in air pollution exposure. *Proceedings of the National Academy of Sciences of the United States of America*, **116 (13)**, 6001–6006, doi: 10.1073/pnas.1818859116.

Tessum, M. W., T. Larson, T. R. Gould, C. D. Simpson, M. G. Yost, and S. Vedal, 2018: Mobile and Fixed-Site Measurements To Identify Spatial Distributions of Traffic-Related Pollution Sources in Los Angeles. *Environmental Science & Technology*, **52 (5)**, 2844–2853, doi: 10.1021/acs.est.7b04889, URL https://doi.org/10.1021/acs.est.7b04889.

Thompson, C. R., J. Hueber, and D. Helmig, 2014: Influence of oil and gas emissions on ambient atmospheric non-methane hydrocarbons in residential areas of Northeastern Colorado. *Elementa: Science of the Anthropocene*, **3**, 000 035, doi: 10.12952/journal.elementa.000035, URL https://doi.org/10.12952/journal.elementa.000035.

von Fischer, J. C., et al., 2017: Rapid, Vehicle-Based Identification of Location and Magnitude of Urban Natural Gas Pipeline Leaks. *Environmental Science & Technology*, **51 (7)**, 4091–4099, doi: 10.1021/acs.est.6b06095, URL https://doi.org/10.1021/acs.est.6b06095.

Vu, K. T., et al., 2016: Impacts of the Denver Cyclone on regional air quality and aerosol formation in the Colorado Front Range during FRAPPÉ 2014. *Atmospheric Chemistry and Physics*, **16 (18)**, 12 039–12 058, doi: 10.5194/acp-16-12039-2016, URL https://acp.copernicus.org/articles/16/12039/2016/.

Wang, W., et al., 2024: Ozone pollution mitigation strategy informed by long-term trends of atmospheric oxidation capacity. *Nature Geoscience*, **17 (1)**, 20–25, doi: 10.1038/s41561-023-01334-9, URL https://www.nature.com/articles/s41561-023-01334-9.

Weber, D. T., J. L. Collett, E. V. Fischer, S. H. Jathar, and A. Hecobian, 2018: Volatile organic compound concentrations and the impacts of future oil and natural gas development in the Colorado Northern Front Range. URL https://hdl.handle.net/10217/189283.

Weisel, C. P., 2010: Benzene exposure: An overview of monitoring methods and their findings. *Chemico-Biological Interactions*, **184 (1)**, 58–66, doi: 10.1016/j.cbi.2009.12.030, URL https://www.sciencedirect.com/science/article/pii/S0009279709005754.

Weisner, M. L., P. M. Varner, I.-T. Ku, J. L. Collett, B. Buck, and L. M. McKenzie, 2025: Cumulative Human Health Risk Assessment of Regional Ozone and Volatile Organic Compounds from Unconventional Oil and Gas Sites in Colorado's Front Range. *Environmental Health Perspectives*, **133 (5)**, 057 025, doi: 10.1289/EHP16272, URL

https://pmc.ncbi.nlm.nih.gov/articles/PMC12120841/.

Weller, Z. D., S. Im, V. Palacios, E. Stuchiner, and J. C. von Fischer, 2022: Environmental Injustices of Leaks from Urban Natural Gas Distribution Systems: Patterns among and within 13 U.S. Metro Areas. *Environmental Science & Technology*, **56 (12)**, 8599–8609, doi: 10.1021/acs.est.2c00097, URL https://doi.org/10.1021/acs.est.2c00097.

Whitehill, A. R., M. Lunden, S. Kaushik, and P. Solomon, 2020: Uncertainty in collocated mobile measurements of air quality. *Atmospheric Environment: X*, **7**, 100 080, doi: 10.1016/j.aeaoa.2020.100080, URL https://www.sciencedirect.com/science/article/pii/S2590162120300198.

Wilczak, J. M. and T. W. Christian, 1990: Case Study of an Orographically Induced Mesoscale Vortex (Denver Cyclone). *Monthly Weather Review*, **118 (5)**, 1082–1102, doi: 10.1175/1520-0493(1990)118¡1082:CSOAOI¿2.0.CO;2, URL https://journals.ametsoc.org/view/journals/mwre/118/5/1520-0493_1990_118_1082_csoaoi_2_0_co_2.xml.

Wild, R. J., W. P. Dubé, K. C. Aikin, S. J. Eilerman, J. A. Neuman, J. Peischl, T. B. Ryerson, and S. S. Brown, 2017: On-road measurements of vehicle NO2/NOx emission ratios in Denver, Colorado, USA. *Atmospheric Environment*, **148**, 182–189, doi: 10.1016/j.atmosenv.2016.10.039, URL https://www.sciencedirect.com/science/article/pii/S1352231016308469.

Winter, P. L., P. E. Padgett, L.-A. S. Milburn, and W. Li, 2019: Neighborhood Parks and Recreationists' Exposure to Ozone: A Comparison of Disadvantaged and Affluent Communities in Los Angeles, California. *Environmental Management*, **63 (3)**, 379–395, doi: 10.1007/s00267-019-01140-3, URL https://doi.org/10.1007/s00267-019-01140-3.

Woo, S.-H., et al., 2016: Overestimation of on-road air quality surveying data measured with a mobile laboratory caused by exhaust plumes of a vehicle ahead in dense traffic areas. *Environmental Pollution*, **218**, 1116–1127, doi: 10.1016/j.envpol.2016.08.065, URL https://www.sciencedirect.com/science/article/pii/S026974911630985X.

Xu, R., et al., 2020: Wildfires, Global Climate Change, and Human Health. *New England Journal of Medicine*, **383 (22)**, 2173–2181, doi: 10.1056/NEJMsr2028985, URL https://www.nejm.org/doi/full/10.1056/NEJMsr2028985, _eprint: https://www.nejm.org/doi/pdf/10.1056/NEJMsr2028985.

Yang, B., et al., 2018: On-Road Chemical Transformation as an Important Mechanism of NO2Formation. *Environmental science & technology*, **52 (8)**, 4574–4582, doi: 10.1021/acs.est.7b05648, URL https://pmc.ncbi.nlm.nih.gov/articles/PMC6463298/.

Zhang, J., M. Ninneman, E. Joseph, M. J. Schwab, B. Shrestha, and J. J. Schwab, 2020a: Mobile Laboratory Measurements of High Surface Ozone Levels and Spatial Heterogeneity During LISTOS 2018: Evidence for Sea Breeze Influence. *Journal of Geophysical Research: Atmospheres*, **125 (11)**, e2019JD031 961, doi: 10.1029/2019JD031961, URL https://onlinelibrary.wiley.com/doi/abs/10.1029/2019JD031961, _eprint:

https://agupubs.onlinelibrary.wiley.com/doi/pdf/10.1029/2019JD031961.

Zhang, W., J. L. Collett, D. Pan, J. R. Pierce, and J. M. Ham, 2024: Quantification of volatile organic compound emissions from unconventional oil and gas development. URL https://hdl.handle.net/10217/239761.

Zhang, X., L. Zhao, M. Cheng, X. Wu, and D. Chen, 2020b: Urban ozone sink inferred from surface measurements in China. *Journal of Cleaner Production*, **253**, 119 881, doi: 10.1016/j.jclepro.2019.119881, URL https://www.sciencedirect.com/science/article/pii/S0959652619347511.

Zhao, Y., Y. Li, A. Kumar, Q. Ying, F. Vandenberghe, and M. J. Kleeman, 2022: Separately resolving NOx and VOC contributions to ozone formation. *Atmospheric Environment*, **285**, 119 224, doi: 10.1016/j.atmosenv.2022.119224, URL https://www.sciencedirect.com/science/article/pii/S1352231022002898.

Zuraski, K., et al., 2025: On-Road Measurements of Nitrogen Oxides, CO, CO2, and VOC Emissions in Two Southwestern U.S. Cities. *ACS ES&T Air*, **2 (4)**, 589–598, doi: 10.1021/acsestair.4c00316, URL https://doi.org/10.1021/acsestair.4c00316.

APPENDIX

A.1 GC VOC Method Detection Limits

The method detection limits (MDLs) for all 51 VOCs can be found in Table A.1. For this analysis, we did not replace any values that were below detection. This is because we did not use these concentrations for any averaging. Rather, the concentrations reported are plotted independently as "snapshots" in time, which is why we chose not to replace any of the values below the respective MDL. Species that were measured below the MDL at the time of sampling are indicated with a special symbol on all figures.

Table A.1: Table of the method detection limits (MDLs) for all 51 VOCs analyzed in the GC from October 2024. MDLs represent the mixing ratio required for a peak with a signal-to-noise ratio of 3 from replicate whole air standard analyses, where noise is defined as the standard deviation of the chromatograph baseline adjacent to the peak (Low, 2025).

Compound	**MDL (ppbv, CH_4 is in ppmv)**
ethane	0.208199944
ethene	0.022792432
propane	0.04185276
propene	0.016954968
i-butane	0.014680423
n-butane	0.021613523
ethyne	0.019388524
t-2-butene	0.005586485
1-butene	0.015944446
c-2-butene	0.011476796
cyclopentane	0.009786227

Table A.1: Table of the method detection limits (MDLs) for all 51 VOCs analyzed in the GC from October 2024. MDLs represent the mixing ratio required for a peak with a signal-to-noise ratio of 3 from replicate whole air standard analyses, where noise is defined as the standard deviation of the chromatograph baseline adjacent to the peak (Low, 2025).

Compound	**MDL (ppbv, CH_4 is in ppmv)**
i-pentane	0.016705559
n-pentane	0.005369615
t-2-pentene	0.007898604
1-pentene	0.03609565
cis-2-pentene	0.013851161
n-hexane	0.022156821
isoprene	0.003004094
2,4-dimethylpentane	0.024078522
n-heptane	0.017276135
benzene	0.016012723
cyclohexane	0.038014983
2,3-dmp	0.031986874
2-methylhexane	0.009963565
3-methylhexane	0.018943878
2,2,4-trimethylpentane	0.023793666
methylcyclohexane	0.041361456
2,3,4-trimethylpentane	0.021091348
toluene	0.017681654
2-methylheptane	0.028432988
3-methylheptane	0.009079251
n-octane	0.012145197
ethylbenzene	0.00845751

Table A.1: Table of the method detection limits (MDLs) for all 51 VOCs analyzed in the GC from October 2024. MDLs represent the mixing ratio required for a peak with a signal-to-noise ratio of 3 from replicate whole air standard analyses, where noise is defined as the standard deviation of the chromatograph baseline adjacent to the peak (Low, 2025).

Compound	**MDL (ppbv, CH_4 is in ppmv)**
m+p-xylene	0.020703931
styrene	0.015289749
o-xylene	0.022992354
n-nonane	0.022087447
I-propylbenzene	0.018390998
n-propylbenzene	0.024719011
3-ethyltoluene	0.00675909
4-ethyltoluene	0.030645498
1,3,5-trimethylbenzene	0.010112599
2-ethyltoluene	0.018404264
1,2,4-trimethylbenzene	0.00956222
n-decane	0.026175101
1,2,3-trimethylbenzene	0.155012012
1,3-diethylbenzene	0.022603457
1,4-diethylbenzene	0.013367086
trichloroethene_C2HCl3	0.001
tetrachloroethylene_C2Cl4	8.97559E-05
acetonitrile	N/A
methane	0.05

A.2 POM and EPA O_3 Regulatory Monitor Agreement

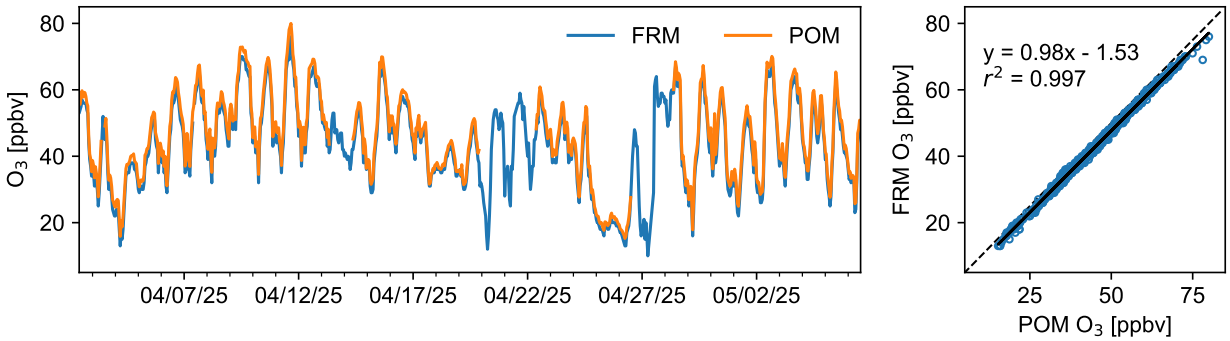


Figure A.1: Left: Time series from April 3 - May 7, 2025 of O_3 concentrations from the POM instrument (orange) and EPA O_3 Regulatory Monitor (blue), also referred to as Federal Reference Method (FRM). Right: Comparison of POM and FRM O_3 concentrations during the time of collocation.

A.3 Filtered & Unfiltered NO_2 Data for DIC Comparison

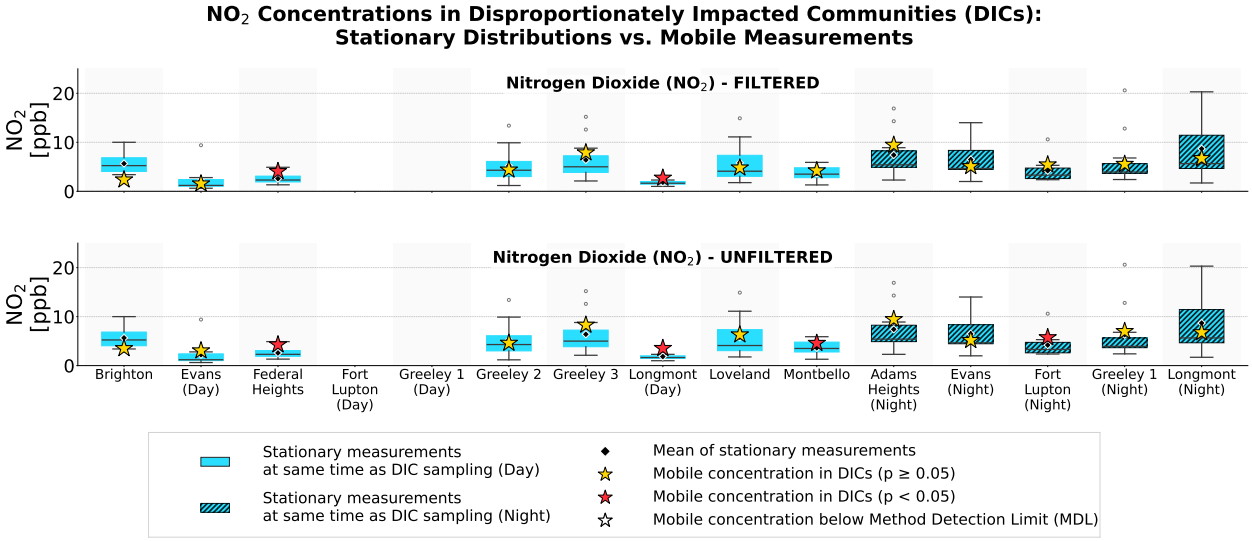


Figure A.2: Comparison of the mean of filtered (top) vs unfiltered (bottom) NO_2 data in DICs compared to the mean concentration of stationary measurements taken at the same hour. Red (yellow) stars indicate a statistically (in)significant difference between the stationary measurements and DIC canister. The small diamond shape inside the boxes indicates the mean of the stationary sites, while the horizontal line is the median. The whiskers indicate 1.5*IQR.